Assessment of Cell Type Specific Gene Expression Regulation

in Proneural Glioma and Response to Therapy

by

John J. Halliday

A Dissertation

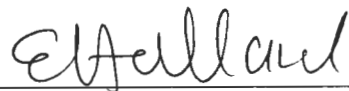Presented to the Faculty of the Louis V. Gerstner, Jr.

Graduate School of Biomedical Sciences,

Memorial Sloan-Kettering Cancer Center

in Partial Fulfillment of the Requirements for the Degree of
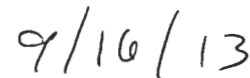
Doctor of Philosophy

New York, NY

September, 2013

Eric C. Holland, MD, PhD
Dissertation Mentor

9/16/13
Date

ABSTRACT

Glioblastoma is the most common primary adult brain tumor and has a dismal median survival of only 15 months. Therapeutic progress has been slow, with the introduction of radiation representing the last large improvement in survival. Understanding the biology and response to therapy of this disease is critical to developing improved therapeutic strategies.

Glioblastomas are highly heterogenous tumors comprised of a variety of stromal cell types in addition to tumor cells. The importance of the in vivo microenvironment in modulating tumor growth and response to treatment is becoming increasingly evident. It has also become clear that glioblastomas comprise 3-4 distinct subtypes, each characterized by particular genomic and signaling alterations. Additionally, in vitro work from our lab and others has indicated that translational regulation is a large component of the glioblastoma response to treatment.

We developed a system that utilizes Translating Ribosome Affinity Purification (TRAP) technology to allow genome wide assessment in a specific cell type of in vivo expression changes at the level of translational regulation and total mRNA. We combined this approach with an RCAS-PDGF driven model of glioblastoma that expresses markers characteristic of the proneural subset of glioblastomas, including Olig2. Olig2+ tumor cells in this model have gene expression profiles similar to that of human proneural glioblastomas. By generating PDGF tumors in transgenic mice that express the TRAP transgene from an Olig2 promoter, we are able to study global

transcriptional and translational regulation in a defined cell type in a model of a specific subtype of glioblastoma.

We used this system to study translational regulation differences between transformed PDGF driven tumor cells and their untransformed oligodendrocyte precursor cell counterparts, and found that genes associated with cell division and biosynthetic pathways were translated with increased efficiency in transformed cells. We then compared PDGF tumors with intact and deleted PTEN. PTEN is a regulator of the PI3K/Akt/mTOR pathway, which is a known regulator of the Warburg effect. We found that PTEN deletion resulted in a loss of translation efficiency of transcripts associated with oxidative phosphorylation, suggesting a possible translation component to the Warburg effect.

We next performed a study of the in vivo radiation response of proneural glioma, using our PDGF model and TRAP reporter system. Radiation induced transient cell cycle arrest and asynchronous apoptosis. Radiation response differed by cell type, with apoptosis largely restricted to the Olig2+ tumor cells. We used TRAP to study expression changes specifically in Olig2+ tumor cells. In agreement with histological data, gene expression programs for apoptosis and cell cycle arrest were up within 6hrs of radiation, while cell cycle progession related genes were depressed. Surprisingly and in contrast with previous work, we found that translational regulation is a small overall contributor to gene expression changes after irradiation in vivo. Most gene expression changes occurred at the total transcript level, and p53 and E2F appear to drive the largest expression changes.

The original work on glioma subtypes suggested that some proneural tumors became mesenchymal upon recurrence. We found that radiation induces a proneural-to-mesenchymal shift in PDGF driven tumors. CEBPB and Stat3 targets were amongst the most induced by radiation in our data, and previously it had been reported that CEBPB and Stat3 may act as master regulators of a mesenchymal shift. The shift we observed occurred within 6 hours in tumors on a variety of genetic backgrounds, and does not appear to be sensitive to p53 knockdown. The rapidity of the shift in tumor type was unexpected, and suggests a plasticity of subtype that has important implications for ongoing efforts to develop targeted treatment strategies based on subtype.

Finally, we have also been working to extend the TRAP system to the stromal cells of proneural gliomas. The stromal compartment of these tumors includes endothelial cells, smooth muscle cells, astrocytes, and microglia, each of which have been shown to have important effects on tumor progression. We have developed TRAP mice to target each of these cell types to allow such studies as we have performed on the Olig2+ tumor cell population. Expression in each of these lines has been validated in the cell type of interest. We focused more attention on the VE-Cadherin promoter driven endothelial targeted line. These mice express the TRAP transgene in a highly specific fashion in endothelial cells of various organs, including brain, lung, kidney, and intestine. RNase expression varies widely across tissues and poses a technical problem in some organs, but high quality RNA has been isolated via TRAP from brain, lung, kidney, and tumor endothelia. Going forwards, these lines should provide useful tools for studying expression and translation in a wide variety of in vivo contexts.

ACKNOWLEDGMENTS

Finally, I would like to thank Erin Perzov for her support, friendship, and love, for which I am eternally grateful.

TABLE OF CONTENTS

LIST OF TABLES

LIST OF FIGURES

LIST OF ABBREVIATIONS

BBB: Blood brain barrier

EGF: Epidermal growth factor

eGFP: Enhanced green fluorescent protein

EGFR: Epidermal growth factor receptor

eIF: Eukaryotic initiation factor

FDR: False discovery rate

FGF: Fibroblast growth factor

GBM: Glioblastoma Multiforme

GEMM: Genetically engineered mouse model

GFAP: Glial fibrillary acidic protein

GFP: Green fluorescent protein

GSEA: Geneset enrichment analysis

IP: Immunoprecipitation

L10a: Large ribosomal subunit 10a

mTOR: Mammaliam target of rapamycin

MVP: Microvascular Proliferation

OPC: Oligodendrocyte precursor cell

PDGF: Platelet derived growth factor

PDGFR: Platelet derived growth factor receptor

PI3K: Phosphoinositide 3-kinase

PTEN: Phosphatase and tensin homolog

PVN: Perivascular niche

RCAS: Replication-competent ALV splice acceptor

RPGFP: Ribosomal protein green fluorescent protein (eGFP-L10a fusion protein)

RTK: Receptor tyrosine kinase

SHH: Sonic hedgehog

SMA: Smooth muscle actin

SMMHC: Smooth muscle myosin heavy chain

TCGA: The Cancer Genome Atlas

TE: Translation efficiency

TRAP: Translating Ribosome Affinity Purification

TUNEL: Terminal deoxynucleotidyl transferase dUTP nick end labeling

UTR: Untranslated region

VECad: Vascular endothelial cadherin

VEGF: Vascular endothelial growth factor

vSMC: Vascular smooth muscle cell.

INTRODUCTION

Gliomas

High grade gliomas comprise 70% of primary malignant brain tumors, representing ~14,000 cases in adults annually in the US (1). Standard of care is resection combined with followed by as schedule of radiation and temozolomide. Unfortunately, gliomas are highly invasive tumors, rendering complete resection a near impossibility. They are radioresistant, and the presence of the blood-brain-barrier limits the effectiveness of chemotherapeutics. Partly for these reasons, high grade gliomas are essentially incurable, with a median survival of only 15 months.

Gliomas are so named due to their histological similarities to normal glial cells. They are classified as astrocytomas, oligodendrogliomas, or mixed oligoastrocytomas according to the presence of cells with astrocytic or oligodendroglial characteristics (2). Gliomas are graded by a WHO classification scheme (3), ranging from Grade I to Grade IV according to features such as cellularity, proliferative index and nuclear atypia. High grade gliomas also exhibit one or both of the histological hallmarks microvascular proliferation and pseudopalisading necrosis (1, 2). High grade, or malignant, gliomas are comprised of grade III tumors (anaplastic astrocytoma, anaplastic oligodendroglioma, and anaplastic oligoastrocytoma) and grade IV tumors (glioblastoma multiforme or GBM), with glioblastoma accounting for 60-70% of high grade tumors (1). Median survival for anaplastic gliomas is 2-5 years, while median survival for GBMs is only 15 months (1). The acquisition of GBM characteristics, including pseudopalisading necrosis and microvascular proliferation, is accompanied by a dramatic increase in radial growth and altered imaging properties (4). GBMs are also classified as primary or secondary.

Secondary gliomas are rarer and first present as lower grade gliomas in younger patients before progressing to GBM over a period of years. Primary gliomas exhibit grade IV histology at first detection and are typically found in older patients (1).

Genomic Alterations of Glioma

Some specific genomic alterations have long been known to occur frequently in gliomas. For instance, p53 mutations were known to be common in secondary GBMs, while EGFR amplifications and mutations were associated with primary GBMs (2). Recent large scale genomic and expression profiling efforts (5, 6) of GBMs have greatly expanded our understanding of the molecular underpinnings of high grade glioma. From these much more comprehensive datasets it has become clear that a handful of cellular signaling pathways are aberrantly altered at the genomic level in the majority GBMs.

Alterations resulting in the overactivation of receptor tyrosine kinase (RTK) signaling or their downstream effector pathways seem a near-ubiquitous feature of GBMs, with 88% of GBMs exhibiting genomic alterations in a component of these signaling pathways (Fig. 1A). RTKs are a class of receptors for various secreted signaling molecules and growth factors. Upon dimerization and ligand binding, RTKs cross-phosphorylate themselves and subsequently activate downstream signaling pathways, including Ras and phosphatidyl inositol kinase 3 (PI3K) which activate pro-growth and survival programs. The RTKs most commonly altered in GBMs were epidermal growth factor receptor (EGFR) and platelet derived growth factor receptor alpha (PDGFRA). Activating amplifications or mutations of EGFR were found in 45% of GBMs, while amplification of PDGFRA was seen in 13% of tumors. Activating mutations of Ras were seen in 2% of GBMs, and mutations or homozygous deletion of

the Ras inhibitor NF1 were seen in 18% of GBMs. 15% of GBMs had tumors with activating mutations in PI3K, and the phosphatase PTEN, which counteracts PI3K, was mutated or homozygously deleted in 36% of GBMs (5).
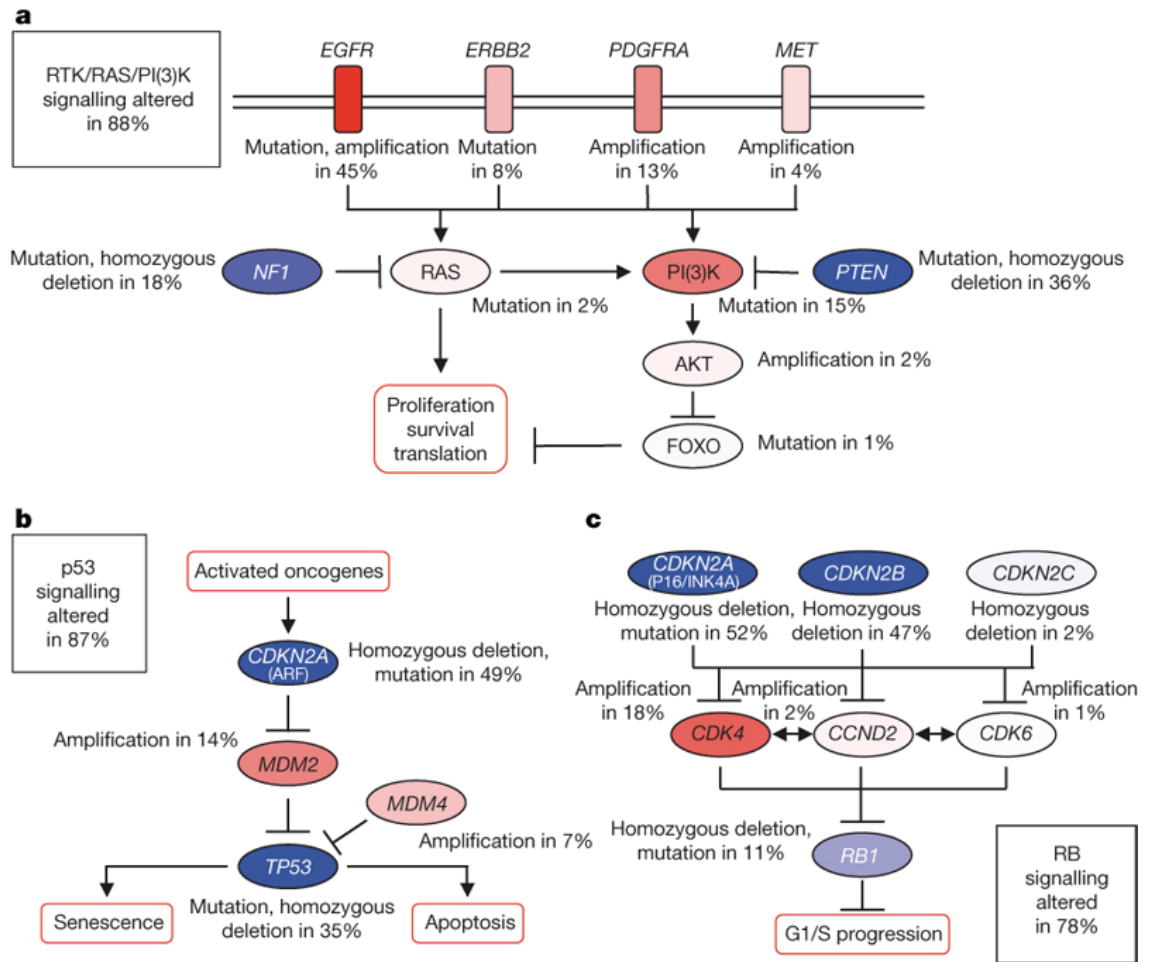
Figure 1. Frequent genetic alterations in three critical signalling pathways in GBM
The large majority of GBMs contain genomic alterations in each of (A) the receptor tyrosine kinase (RTK) pathway or downstream effectors, (B) p53 or its associated modifiers, and (C) RB or its upstream regulators. Red colors represent activating alterations, blue colors inactivating alterations, all shaded for prevalence. Cancer Genome Atlas Research Network. Comprehensive genomic characterization defines human glioblastoma genes and core pathways. Nature 2013 Jul 4;499(7456):43-9.

Signaling through the tumor suppressor p53 is compromised in approximately 87% of GBMs (Fig. 1B). p53 is activated in response to oncogenic stresses, including DNA damage and oncogenic signaling, and can trigger apoptosis or senescence (7). The gene encoding p53 is mutated or homozygously deleted in 35% of GBMs. MDM2 and MDM4, ubiquitin proteases which mediate the degradation of p53 (8), are amplified in 14% and 7% of GBMs, respectively. Arf, encoded in the CDNK2A locus, inhibits MDM2 in the event of oncogenic stresses (7), and is homozygously in deleted in 49% of GBMs (5).

Finally, the cell cycle inhibitor RB1, which prevents G1/S cell cycle progression, and its upstream modulators, were found to be altered at the genomic level in 78% of GBMs (Fig 1C). RB1 itself is deleted in 11% of GBMs, while cyclin dependent kinases (CDK4, CCND2, and CDK6) that inhibit RB1 were amplified, most notably CDK4 which was amplified in 18% of GBMs. Loci encoding inhibitors of these CDKs were homozygously deleted in a large fraction of GBMs, with the loci encoding Ink4a and p21 being deleted in 52% and 47% of GBMs (5). p21 is a well known effector of p53 signaling, illustrating some possible functional overlap of these pathways (8).

Most of the genomic alterations discovered by these large scale efforts were already known, albeit with incompletely defined patterns of co-occurrence. One notable exception was the discovery of recurrent mutations of isocitrate dehydrogenase 1 (IDH1) (5). IDH1 catalyzes the NADP+ dependent oxidative carboxylation of isocitrate into α-ketoglutarate. Mutations in the active site of the enzyme were present in over 70% of secondary GBMs, as well as the large majority of Grade II and Grade III gliomas, while being largely absent from primary gliomas (5, 9). IDH1 mutation was primarily

associated with younger patients, consistent with its prevalence in secondary gliomas, and is a positive prognostic indicator (5). IDH1 mutants have a novel gain of function mutation that results in the production of the metabolite 2-hydroxyglutarate (10). IDH mutants were shown to be associated with a CpG island methylator phenotype (CIMP) (11), and it was subsequently shown that mutant IDH1 was sufficient to establish the CIMP phenotype and generate gene expression patterns similar to CIMP gliomas (12).

Molecular Subclasses of Glioma

Genome wide expression profiling of large cohorts of gliomas has led to the discovery of distinct molecular subtypes of high grade gliomas. Phillips et al. (13) performed microarray expression profiling on a set of high grade gliomas (grades III and IV). Hierarchical clustering on genes correlated to survival identified three distinct groups of expression profiles. They termed these subgroups proneural, mesenchymal, and proliferative based on the character of the genes contained in the signature for each. They then showed that expression profiles for normal brain and fetal brain, as well as neural stem cells, were more proneural in character, while expression profiles for endothelial cells, dendritic cells, and hematopoetic stem cells had more mesenchymal character (Fig. 2A). Notably, the proneural subset contained most of the Grade III tumors, including almost all tumors with oligodendroglial histological features (Fig 2B).
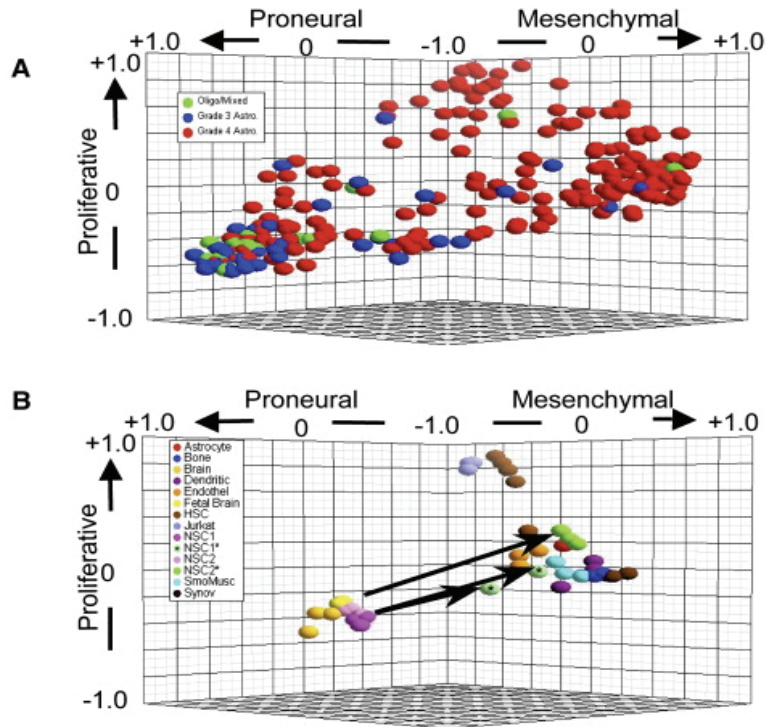
Figure 2. Most HGGs are characterized by strong similarity to one of three patterns of signature gene expression

Three-dimensional graphical representation in which the position occupied by each point represents the similarity (Spearman r) between an individual sample and each of three centroids defined by k-means clustering of the reference (MDA) sample set. (A) Nearly all grade III tumors of both astrocytic (blue) or oligodendroglial (green) morphology are most similar to the PN centroid, while the population of grade IV tumors (red) is more evenly divided by similarity to the centroids. (B) Different sets of normal cells or tissues resemble each of the three centroids. Samples are as follows: fetal brain, adult brain (brain), two neural stem cell lines derived from fetal tissue (NSC1, NSC2), Jurkat, hematopoietic stem cells (HSC), smooth muscle (SmoMusc), endothelial cells (endothel), synovium (synov), and bone. Neural stem cell lines treated by exposure to and withdrawal from the growth factor BDNF are designated NSC1∗ and NSC2∗. Reprinted from Cancer Cell, 9(3), Phillips HS, et al., Molecular subclasses of high-grade glioma predict prognosis, delineate a pattern of disease progression, and resemble stages in neurogenesis., 157-73, Copyright 2006, with permission from Elsevier.

Subsequently, Verhaak et al. used the expression profiling data from the the Cancer Genome Atlas (TCGA) to identify 4 subclasses of GBMs, proneural, mesenchymal, classical, and neural (14). The proneural and mesenchymal classes were largely congruous with the Phillips et al. classifications. Geneset enrichment analysis of the TCGA samples on signatures derived from various normal brain cell types from mice showed that proneural gliomas were enriched for oligodendrocyte signature genes. Neural and classical gliomas were enriched for astrocyte and to an extent neuron signature genes, while mesenchymal tumors most resembled cultured astroglia. Although secondary gliomas were rare in this study, they were concentrated in the proneural subtype, as in Phillips et al.

Comparison with genomic copy number and mutation data revealed that the GBM expression pattern subtypes were associated with specific genomic lesions (Fig 3). Almost all classical GBMs and most neural GBMs contain high level EGFR amplifications, and although some proneural and mesenchymal tumors also exhibit EGFR amplifications, elevated EGFR transcript levels are rare outside the classical and neural subgroups. PDGFRA amplifications and elevated PDGFRA transcript levels are highly enriched in the proneural subtype. NF1 mutation and copy number loss is almost exclusively confined to the mesenchymal subtype, and many mesenchymal tumors that have no genomic NF1 alterations nevertheless show lowered NF1 transcript levels. IDH1 mutations were almost exclusively found in proneural tumors. p53 mutations are enriched in proneural tumors and almost absent from classical tumors. Ink4a/Arf copy number loss is found in almost all classical GBMs, but is also common in neural, proneural, and mesenchymal GBMs.
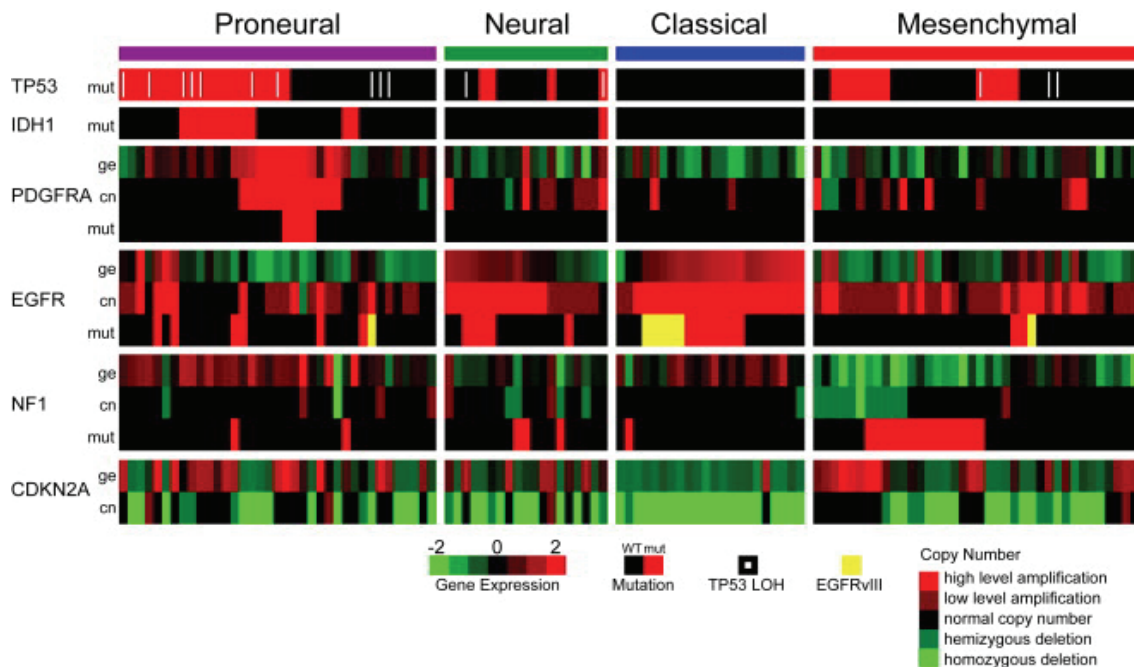
Figure 3. Summary of major genomic and expression alterations associated with GBM subtypes
Reprinted from Cancer Cell 17(1), R. Verhaak et al. Integrated Genomic Analysis Identifies Clinically Relevant Subtypes of Glioblastoma Characterized by Abnormalities in PDGFRA, IDH1, EGFR, and NF1. 98-110, Copyright 2010, with permission from Elsevier.

Brennan et al. performed Western Blotting for a panel of 55 cancer related antibodies on a set of glioma samples (15). Clustering of expression levels of these epitopes identified three groups, one associated with PDGF signaling, one with EGFR overexpression, and one with loss of NF1, confirming at the protein level the existence of distinct subgroups of gliomas delineated by PDGF, EGFR, and NF1 activity.

Taken together, these results indicate that high grade gliomas are comprised of 3-4 separate subtypes. Broadly speaking, the proneural set is characterized by PDGF signaling and is more oligodendroglial in character. The neural and classical subtypes are associated with EGFR activity and are more astrocytic in character. Finally, the mesenchymal subtype is associated with NF1 loss (and presumably Ras signaling), and is associated with mesenchymal or stromal cell types and/or serum cultured cell lines.

Glioma Microenvironment

The tumor microenvironment has been the subject of increasing interest in recent years as its importance for tumorigenesis and tumor progression has become clearer. Stromal cells can provide important pro-growth signaling cues via growth factors, cell-cell contacts, and extracellular matrix deposition. Stromal abnormalities appear to be capable of initiating tumors in otherwise healthy epithelial cells (16), even if the stromal cells themselves are not proliferative (17). Blood vessels are functionally required for tumor growth beyond a certain point, making the recruitment by tumor cells of the cell types needed for vessel formation a focus of intense study (18). Finally, invasiveness and migration, notable features of highly malignant tumors, are highly dependent on interactions with the tumor microenvironment (19). It seems increasingly likely that the

ability to interact with stroma may be a significant selective pressure on tumor cells, and that genomically abnormal tumor cells and stromal cells co-evolve during tumor evolution.

Gliomas have a large stromal component comprised of various cell types. High grade gliomas are one of the most highly vascularized tumors, containing abnormal vascular structures referred to as microvascular proliferation (MVP) and comprised of endothelial cells, vascular smooth muscle cells/pericytes (20), and astrocytes. The appearance of these highly proliferative, leaky, and disorganized vascular structures is associated with a more malignant phenotype and higher radial growth rates (1, 4). Other stromal cell types are also found closely associated with gliomas. Astrocytes are found throughout and surrounding gliomas. Microglia (brain-resident macrophages) have been found to contribute as much as 30% of the mass of a glioblastoma (21).

Endothelial cells

Endothelial cells comprise the lumen of blood vessels, and as such their recruitment, proliferation, and organization into functional vessels is critical for extensive tumor growth. Angiogenesis, a process in which new vessels are formed from locally existing blood vessels, is thought to be the main mechanism for new vessel formation in gliomas (22). A number of signaling molecules are involved in angiogenesis, with Vascular Endothelial Growth Factor (VEGF) thought to be particularly important.

VEGF is a potent modulator of endothelial cell behaviors, and is the major mediator of tumor angiogenesis (23-25). The majority of tumors, including gliomas, secrete high levels of VEGF (25, 26). Levels of VEGF production were shown to

directly correlate with glioma grade (24). Endothelial cells themselves secrete PDGF, which helps recruit pericytes and vascular smooth muscle cells (27). Nitric oxide and other factors are also secreted by endothelial cells (28). Finally, endothelial cells are also a critical component of the blood-brain barrier.

Vascular Smooth Muscle Cells and Pericytes

Pericytes and vascular smooth muscle cells (vSMCs) wrap around endothelial cells to form the basic unit of a blood vessel. In the developing normal brain, pericytes and vSMCs are recruited to nascent blood vessels, where they help the new vascular tube stabilize and mature (29, 30) . PDGF signaling is crucial in recruiting and regulating pericytes and vSMCs, which express PDGFRB (21). Pericytes are also involved in regulating the blood-brain barrier (BBB) in the normal brain, along with astrocytes (31). In brain tumors, pericytes and vSMCs are major components of the histologic structures referred to as microvascular proliferation (20). Pericyte and vSMC coverage and function are important for the survival of tumor blood vessels (32). Tumor associated pericytes are abnormal, expressing more smooth-muscle actin than their normal counterparts, and likely contribute to the leakiness of tumor vasculature (33). Pericytes regulate vascular behaviour through a number of signaling cues, including angiopoietin-Tie2 signaling (21).

Perivascular Niche

Recent studies have shown that endothelial cells and signals localized to the vasculature improve tumorigenicity in transplantation assays and genetically engineered mouse models (28, 34). Neural stem cells in the normal brain reside in niches associated with capillaries, and it has been suggested that a similar dynamic obtains in brain tumors, with the tumor vasculature forming a perivascular niche (PVN) that maintains stem-like brain tumor cells. The ability of the tumor vasculature to act as a niche might then explain some of the ability of the vasculature to enhance tumorigenesis and tumor progression. Notably, the pro-tumor effects of endothelial cell co-transplantation only occurred when the co-transplanted tumor cells expressed CD133, a putative glioblastoma stem cell marker. Also, Charles et al. saw an increase in side population, a functional assay which enriches for stem-like cells, upon treatment with NO, whose production in gliomas appears to be localized to the vasculature.

Microglia

Brain resident macrophages, referred to as microglia, are the predominant immune cell found in brain tumors and can make up a large percentage of brain tumor mass (35). In the normal brain, microglia have various roles, including in the injury response in which they proliferate, migrate to the site of injury, and release inflammatory cytokines that activate astrocytes and modulate BBB permeability (36). Various cytokines have been implicated in recruiting microglia to brain tumors, including monocyte chemoattraction protein-1 (MCP-1) and colony stimulating factor 1 (CSF-1). At the tumor site, microglia are thought to release cytokines that promote glioma

proliferation and migration (37). Microglia promote glioma cell migration and invasion by the expression of the membrane bound metalloprotease MT1-MMP (38). MT1-MMP activates the glioma-secreted metalloprotease 2, which then degrades the extracellular matrix and facilitates glioma cell migration. Microglia also appear to promote tumor angiogenesis (39).

Astrocytes

Astrocytes in the normal brain have roles as support cells and regulators of the blood brain barrier (21). In the event of injury, astrocytes take on a reactive morphology and migrate to the site of injury (40). Various signals can trigger this activation, including EGF and VEGF (36). Reactive astrocytes responding to injury secrete various factors, including Sonic Hedgehog (SHH), which induces proliferation of oligodendrocytes (41). In low grade tumors, astrocytes are primarily found on the periphery of the tumor and have a reactive morphology. In GBMs, which definitionally contain MVP, an additional second population of astrocytes is found in the perivascular niche. These perivascular astrocytes express CD44, in contrast with peritumoral astrocytes (40). Both populations of astrocytes express SHH (42).

Glioma Therapy

High grade gliomas remain incurable, and have several features that continue to frustrate attempts to improve therapy. The extremely high invasiveness of glioma ensures that complete resection is impossible. Glioma cells also appear to have substantial intrinsic radiation sensitivity. Finally, the blood-brain-barrier, which blocks

most molecules larger than 500Da, is a considerable obstacle to most pharmaceutical therapies (43).

Improvements to therapy have resulted in slow incremental improvements in survival. Early in the 20th century, the difficulty and dangers of intracranial operation meant that resection was of dubious benefit. Surgical techniques improved, and in the 1960s it became clear that extensive resection could extend median survival from 1 or 2 months to around 6 months (44). At this time, post-operative radiation was commonly used to supplement treatment, although treatment was not standardized and toxicity to the skin and ears was common (44, 45). In 1979 the dose-dependent benefits of post-operative radiation on overall survival were quantified, showing that higher doses improved median survival by approximately 6 months, and radiation became part of the standard of care (45, 46). Over the last 5 years, is has been shown that the inclusion of temozolomide along with resection and radiation therapy improves median survival from 12 months to 14.6 months (47).

Recent attempts to improve glioma treatment have turned to targeted treatments designed to inhibit frequently activated pathways in GBM. Several of these are in clinical trials. To date, success has been limited, although many of these early trials did not segregate patients by genomic or pathways alterations. EGFR is the most commonly altered RTK in GBM. EGFR inhibitors that have been tried in clinical trials include gefitinib, erlotinib, and nimotuzumab. Results have so far been disappointing, although one Phase II study with gefitinib suggested that patients who have poor reactions to gefitinib such as rash or diarrhea had improved overall survival (48). The PDGF signaling pathway is also commonly activated in glioma. Clinical trials with imatinib,

sunitinib, and dasatinib, all of which inhibit PDGFR along with other kinases, have failed to show a survival benefit (43).

One recent development in targeted therapy is the advent of anti-angiogenics that target the tumor vaculature. Bevacizumab, a monoclonal antibody against VEGF, has been the main agent tried so far in the clinic. In an initial, non-comparative phase II trial, bevacizumab improved 6-month progession free survival rates relative to historical rates (49). This result was controversial because progression is usually assessed by imaging, and anti-angiogenics can improve imaging results without a tumor response (43). However, further trials proceeded with the aim of assessing overall survival. A noncomparative trial found that standard of care plus bevacizumab resulted in median overall survival of 19.6 months. In a non-randomized comparative phase II trial, standard of care plus bevacizumab outperformed standard of care alone, with median overall survival of 24 months vs. 17.5 months (43). A large randomized double blind phase III trial is underway (50). It is worth noting that there is now strong evidence that bevacizumab increases the invasiveness of glioma cells (51).

Models of Glioma

Glioma Lines and Xenografts

Historically, cell lines derived by from human brain tumors and maintained under standard serum culture conditions have been extremely valuable tools for studying glioma biology. They are easily manipulated and simple to maintain and expand. These cell lines have become standardized and widely distributed, allowing easy reproduction and comparison of experiments.

However, serum cultured cell lines are maintained in an extracellular milieu that is very different from the *in vivo* microenvironment. Even before the full importance of the microenvironment for dictating tumor cell behavior was appreciated, it was understood that this was a critical shortcoming of cultured cell lines for preclinical testing. This led to the development of various xenograft brain tumor models. In xenograft models, cell lines are transplanted into immuno-compromised mice, either orthotopically (in this case intracranially) or subcutaneously. These models tend to generate tumors rapidly with high penetrance and reproducibility, and in the case of subcutaneous implantation, tumor progression is easily tracked visually. However, xenografted tumors typically do not resemble the human disease histologically; xenograft tumor are generally highly circumscribed, non-invasive, and have unusual vascularization. Additionally, effects of the immune system on tumor progression are absent, and in the case of subcutaneous xenografts, the anatomical location and stroma is inaccurate (52).

An additional problem with serum-cultured cell lines, and xenografts utilizing them, is that the standard lines have typically been passaged many times. The differences between the culture dish and the *in vivo* microenvironment represents a difference in selective pressure that results in divergence from the original tumor as the cell lines are passaged.(52). Early passage lines may ameliorate the issue of divergence from the parental tumor, but at the expense of the ability to widely distribute a standardized line.

Glioma Spheres and Xenografts

Over the last few years, so-called neurosphere culture techniques have become widely used in the study of glioma. Identification and culturing of neural stem cells from the adult brain was first achieved by growing dissociated brain cells in serum-free media in the presence of epidermal growth factor (EGF) and fibroblast growth factor (FGF) (53). The cells that grew out of these cultures formed into spheres that detached from the culture plate and have become known as neurospheres.

This culturing method has been applied to gliomas, and the resulting tumorspheres have been shown to retain more multipotency and generate tumors upon transplantation that more closely resemble *de novo* human disease (54). One study made a careful comparison between paired cell lines from the same parental tumor that were maintained separately in serum cultured and neurosphere conditions (55). They found that sphere cultures had expression profiles that were closer to human gliomas than the serum cultures. They also found that the sphere cultures maintained the karyotype of the parental tumor with high fidelity for many passages, while the serum cultures accumulated genomic alterations. When transplanted as a xenografts, sphere derived tumors were invasive and infiltrative like human gliomas, whereas serum cultured cells from the same tumors were well circumscribed, as were tumors derived from standard glioma cell lines. The sphere derived xenograft tumors were closer in expression profile to the parental and other human gliomas than the xenografts generated with serum cultured cells (55).

There are drawbacks to the use of sphere cultures and xenografts. Spheres are harder to culture, and much harder to manipulate via standard methods of transfection.

Sphere culture does not fully reproduce *in vivo* microenvironmental cues, which can result in wide divergence between *in vitro* and *in vivo* experiments; it has been shown that the radiation response of a tumorsphere line in culture is dramatically different than that of the same line when xenografted into a mouse (56). Xenografting of tumorspheres still requires immune compromised mice, resulting in a microenvironment that is lacking an immune component. The co-evolution that occurs between tumor and stroma in human disease is also absent. Despite the increased invasiveness of xenografted tumorspheres, they fail to reproduce all the histological features of de novo glioma, exhibiting a "peculiar" morphology (54).

Genetically Engineered Mouse Models

The ability to introduce genetic alterations into mice has allowed the development of genetically engineered mouse models (GEMMs) of glioma whereby tumors are generated *de novo* from mouse brain cells. These models are more faithful to the human disease in several ways. For one, the immune response is generally intact in these models. Also, GEMMs allow the co-evolution of tumor along with stroma as occurs in the human disease. Some GEMMs give rise to tumors with histological features that resemble those of human glioma, including pseudopalisades and microvascular proliferation (57). GEMMs are also singularly suited for studies of tumorigenesis.

One drawback of GEMMs is that the genomic lesions found in human disease may not generate tumors in mice. The need for high penetrance and low latency also informs the choice of oncogenic drivers. Because of this, some GEMMs use oncogenic drivers rarely or never thought to drive human glioma, such as oncogenic Ras or SV40 T-

antigen.   The need for low latency also precludes the use of models that may more faithfully represent the extended period over which the human disease acquires genetic alterations (57).   Finally, the complexity of the tumor microenvironment that these models strive to reproduce makes many *in vivo* studies difficult to perform and interpret. While cultured cells represent a relatively homogenous set of cells that can be studied in bulk, *in vivo* tumor models represent a collection of heterogenous cell types, and developing methods to understand the behavior of specific cell types can be challenging.

Transgenic Mouse Models

Many GEMMs utilize germline knockout of tumor suppressors or transgenic introduction of oncogenes.   The simplest knockout models involve constitutive tumor suppressor loss throughout the entire animal. $NF1^{+/-}/p53^{+/-}$ mice develop gliomas with astrocytic morphology with high penetrance and short latency (58).   However, these mice also develop non-brain tumors with high frequency.   More specific targeting of tumorigenesis to the brain can be achieved by utilizing recombinase systems such as Cre-Lox.   Expression of Cre recombinase in a cell bearing an allele flanked by loxP recombination sites (i.e. floxed) will result in the excision of the intervening allele.   By crossing mice bearing a floxed tumor suppressor allele with mice expressing Cre from a cell type specific promoter, tumor suppressor loss can be targeted to the tissue or cell type of choice.   p53+/- mice bearing floxed NF1 and expressing Cre from the GFAP promoter develop astrocytic gliomas almost exclusively, with high grade morphology including microvascular proliferation and pseudopalisading necrosis (59).

Overexpression of oncogenes can also be used to model gliomas, and because standard transgenic techniques usually afford the ability to choose a cell-type specific promoter, oncogene overexpression is usually done in a targeted manner. A constitutively active form of Ras, a downstream effector of RTK signaling and the target of NF1 inhibition, results in astroglial tumors with high penetrance when over expressed from the GFAP promoter (60). The SV40 T-antigen, which inhibits the Rb pathway, has also been used as an oncogenic driver from the GFAP promoter and results in astroglial gliomas (61). Oncogene overexpression and tumor suppressor loss can be combined in a single model. Each of the above models has been crossed into PTEN deleted mice, with an increase in penetrance and decreased latency in each case (57).

Somatic Gene Transfer Models

Strategies have also been developed to genetically alter the somatic cells of mice, bypassing the germline. Most of these systems utilize viral vectors for gene delivery. One of the earliest successful attempts to use somatic cell gene transfer to generate brain tumors utilized the Moloney Murine Leukemia Virus (MoMuLV) retrovirus. MoMuLV engineered to express PDGF-B was injected into newborn pups and generated a range of tumors (62). A subsequent development was the RCAS tv-a system, which uses an avian retrovirus as the gene delivery vehicle. RCAS was created from the Avian Sarcoma and Leukosis Virus by replacing the Src oncogene with a multiple cloning site (63). This virus is replication competent in avian cells, but is not replication competent in mammalian cells, nor can it infect normal mammalian cells. However, mammalian cells can be infected by ALV if they are made to express the avian receptor for ALV, tumor

virus-A (tv-a) (64, 65). By generating transgenic mice expressing tv-a in certain cell populations, specific and restricted cell populations can be transduced within a mouse brain (66, 67). This system has been used to generate astrocytic tumors using Ras and Akt, and oligodendroglial tumors using PDGF-B (68, 69). Mice expressing tv-a in a variety of cell types have been generated, including GFAP-tv-a (Gtv-a) and Nestin-tv-a (Ntv-a). RCAS can also be used to deliver Cre, and has been adapted to deliver shRNAs. Recently, some groups have begun using lentiviral gene transfer to generate gliomas. These vectors take advantage of the ability of lentiviruses to infect even non-dividing cells. Some have used Lox-Stop-Lox sequences upstream of an onocgene in combination with a cell-type specific Cre mouse to generate specificity (70). Others have been able to incorporate cell type specific promoters into the lentiviral construct to drive Cre in certain cell-types (71).

Somatic gene transfer models have several advantages over germline transgenics. Relative to standard transgenics, studies of tumorigenic drivers can be performed rapidly and in high-throughput fashion, as only cloning and construct validation is required to test potential oncogenes, and testing combinations of oncogenes can be done by mixing vectors. These systems also offer high degrees of regional control over tumorigenesis. It is somewhat more difficult to induce loss of gene expression in these systems. Prior to the advent of siRNA technology, only by the expression of Cre in a mouse carrying a floxed allele could these systems be used to reduce the expression of a target gene. Incorporating shRNA has greatly expanded the possibilities of these systems, but they are still limited by the efficiency of shRNA knockdown. Another downside of these systems

is that the viral vectors somewhat limit in the size of the transgene that can be delivered, although this is somewhat eased in lentiviral systems.

These somatic gene transfer systems can be also be combined with standard germline models to develop powerful tumor models. RCAS-PDGF injected into Ntv-a$^+$/Ink4a/Arf$^{-/-}$/PTEN$^{fl/fl}$ mice generates oligodendroglial gliomas with high grade histological hallmarks, complete penetrance, and low latency. Co-injection of RCAS-Cre results in PTEN deletion and even lower latency (72).

Translational Regulation of Gene Expression

Since most cellular processes are catalyzed or otherwise effected by proteins, the phenotype of a cell is ultimately determined by levels of protein expression and activity. Proteins are translated from messenger RNAs, which are themselves transcribed from genomic DNA. Regulation of the processes resulting in mRNA transcription and degradation, protein translation from mRNA, and post-translational modifications all affect protein activity.

Compared to transcription, translational regulation of existing mRNAs is able to more quickly alter cellular protein concentrations (73, 74). The process of translation occurs in three phases, initiation, elongation, and termination. Initiation is the rate limiting step. An mRNA is primed for initiation when various eukaryotic initiation factors (eIFs) bind to its 5' m^{7}G cap and its 3' poly-A tail via Poly-A Binding Protein (PABP). The resulting complex of eIFs is recognized by the preinitiation complex (PIC), which consists of other eIFs and the small ribosomal subunit loaded with the intiating methionine tRNA. The PIC then begins scanning along the 5' untranslated region (UTR)

of the mRNA until it reaches the AUG start codon, which is complementary to the methionine tRNA loaded in the PIC. At this point the large ribosomal subunit is recruited and translation is initiated. The phase during which the peptide chain is synthesized is known as elongation and occurs relatively processively until the stop codon is reached and translation terminates (74, 75).

Translational regulation can occur globally, and can also be transcript specific. Most regulation is thought to occur at the level of translation initiation. The recruitment of eIFs to the 5' mRNA cap structure is regulated by various mechanisms, including the 4EBP proteins that sequester key eIFs unless phosphorylated. Sequence specific RNA binding proteins or miRNA binding proteins can interfere with translation initiation by binding to the 3'UTR and recruiting eIF inhibitory factors. Secondary and tertiary structures in the 5' UTR of some mRNAs can impede scanning and may require specific factors with helicase activity to ensure efficient translation. Decoy start codons or internal ribosome entry sites (IRES) in the 5' UTR of some transcripts may further alter their translation patterns (73-75).

Translational regulation has been implicated in shaping the cellular response to various stimuli. Many of these take the form of rapid stresses or shocks, perhaps a reflection of the ability of translation to more rapidly adjust cellular protein levels than transcriptional control. Nutrient depletion or amino acid starvation, heat shock and cold shock, DNA damage, and hypoxia have all been reported to induce alterations in cellular translation profiles (73). One report on cultured glioma cells suggested that translational regulation in response to radiation contributes much more to gene expression alterations than transcriptional changes (76). mTOR, which acts as an integrator of cellular energy

and nutrient levels, is a well known regulator of translation and has been implicated in the response to several of the above stresses. The mTOR pathway is known to regulate protein translation through phosphorylation of 4EBP1 and the ribosomal subunit RPS6 (73). mTOR is regulated partially through PI3K/PTEN activity, which is frequently dysregulated in cancer.

MATERIAL AND METHODS

Mice and Gliomas

Ntv-a/Ink4a/Arf$^{-/-}$/PTEN$^{fl/fl}$ mice were described previously (77). For expression studies, Ntv-a/Ink4a/Arf-/-/PTENfl/fl mice were bred with Olig2 bacTRAP mice (78) (gift from Dr. Nathaniel Heintz). Resulting Olig2bacTRAP/Ntv-a/Ink4a/Arf$^{-/-}$/PTEN$^{fl/fl}$ mice were used for all expression profiling experiments, except where Ink4a/Arf heterozygous (Olig2bacTRAP/Ntv-a/Ink4a/Arf$^{+/-}$/PTEN$^{fl/fl}$) mice were used as noted. PDGF-driven gliomas were generated in neonatal mice by RCAS-mediated retroviral transduction as previously described (69, 72). Symptomatic (lethargy, weight loss, macrocephaly) tumor-bearing mice were treated with IR or temsirolimus. The table below summarizes all cohorts used for expression profiling. IR treatment was given as single 10Gy dose of total body irradiation using a Cs-137 source (Gammacell 40 Exactor, MDS Nordion). Temsirolimus (CCI-779) was administered for 3 days at 40mg/kg via IP injection as in (79) and samples collected 14-18 hours after the last dose.

26

Genotype	Treatment	# Samples	Total/Transl	Total/Transl Paired?
PDGF Ink4a/Arf-/-	Ctrl	4	Total	Y
PDGF Ink4a/Arf-/-	Ctrl	4	Transl.	Y
PDGF Ink4a/Arf-/-	6hrs IR	3	Total	Y
PDGF Ink4a/Arf-/-	6hrs IR	3	Transl.	Y
PDGF Ink4a/Arf-/- PTEN-/-	Ctrl	4	Total	Y
PDGF Ink4a/Arf-/- PTEN-/-	Ctrl	4	Transl.	Y
PDGF Ink4a/Arf-/- PTEN-/-	6hrs IR	4	Total	Y
PDGF Ink4a/Arf-/- PTEN-/-	6hrs IR	4	Transl.	Y
PDGF Ink4a/Arf-/- PTEN-/-	Temsirolimus	4	Total	Y
PDGF Ink4a/Arf-/- PTEN-/-	Temsirolimus	4	Transl.	Y
PDGF Ink4a/Arf-/- p53shRNA	Ctrl	7	Total	#N/A
PDGF Ink4a/Arf-/- p53shRNA	6hrs IR	7	Total	#N/A
PDGF Ink4a/Arf+/-	Ctrl	4	Total	N
PDGF Ink4a/Arf+/-	Ctrl	3	Transl.	N
PDGF Ink4a/Arf+/-	2hrs IR	4	Total	N
PDGF Ink4a/Arf+/-	2hrs IR	3	Transl.	N
PDGF Ink4a/Arf+/-	6hrs IR	4	Total	N
PDGF Ink4a/Arf+/-	6hrs IR	3	Transl.	N
Ink4a/Arf-/- Normal OPCs	Ctrl	4	Total	Y
Ink4a/Arf-/- Normal OPCs	Ctrl	4	Transl.	Y

For survival studies, cranial irradiation was delivered on postnatal day 18 by an X-RAD 320 (Precision X-Ray) as in (80). All animal studies were done in accordance with protocols approved by the Institutional Animal Care and Use Committee of Memorial Sloan-Kettering Cancer Center and followed National Institutes of Health guidelines for animal welfare. Genotyping primers will be provided on request.

Collection of ribosome-bound and total cellular RNA

For collection of total cellular RNA, normal brain or grossly-dissected tumor tissue was dissociated into a single cell suspension with papain by a method previously described (81) and fluorescent cells were collected by FACS. FACS sorted cells were collected with Trizol-LS reagent (Invitrogen), chloroform extracted, precipitated with sodium acetate in isopropanol overnight and purified according to manufacturer protocol

(Qiagen RNeasy MinElute Cleanup Kit). Ribosome-bound RNA was immunoprecipitated with anti-GFP conjugated magnetic beads from mechanically-homogenized tissue as previously described (82) and purified as above. Where applicable, tissue samples were divided equally for total and ribosome-bound RNA to generate paired datasets. RNA quantity was assessed by Nanodrop and/or Ribogreen RNA Assay Kit (Invitrogen).

For expression profiling experiments, RNA was amplified and biotin-labeled according to manufacturer protocol (Ambion AMIL1791) and hybridized to Illumina MouseRef-8 Expression BeadChips. RNA quality and labeling efficiency was assessed by microfluidics-based RNA electrophoresis (Agilent 2100 Bioanalyzer).

RCAS Generation and Constructs

DF1 cells overexpressing RCAS-PDGF, RCAS-Cre, RCAS-p53shRNA-RFP, and RCAS-PDGF-mRFP were maintained in media containing 10% FBS in a humidified atmosphere containing 5% carbon dioxide at 39 degrees.

TRAP Constructs

The VE-IE-EGFP plasmid containing the VECadherin promoter and first intron enhancer was a generous gift from Dr. Shin-Ichi Nishikawa. The pBS-SMA construct was a generous gift of Dr. Gary Owens. The CD44-eGFP construct was a generous gift from Dr. Vijay Sarthy. The CD11b promoter in pGEMf7 was purchased from Addgene. The Gtv-a construct was used to generate the GFAP-RPGFP lines. EGFPL10a was PCR amplified from the C2-EGFPL10a construct (a generous gift from Dr. Nathaniel Heintz) with oligonucleotide primers containing the appropriate restriction sites at the 5' termini

to allow cloning into the destination vectors by standard methods. Vectors were validated by sequencing. Transgenic mice were generated by the SKI Mouse Genetics Core Facility by pronuclear injection on a FVB/B6 background.

Histology and Immunohistochemistry

Tissues were fixed in 10% neutral buffered formalin and imbedded in paraffin according to standard procedures (83). Immunohistochemical staining of 5-μm tissue sections was performed using the Discovery XT automated staining system (Ventana Medical Systems). The following antibodies were diluted in PBS/2%BSA: PDGFRβ 1:300 (Cell Signaling 3169), PDGFRα 1:300 (Cell Signaling 3174), PTEN 1:100 (Cell Signaling 9559), Olig2 1:300 (Millipore AB9610), Nestin 1:100 (BD Biosciences 556309), phospho-histone H3 1:800 (Millipore 06-750), p53 1:500 (Novocastra NCL-p53-CM5p), phopspho-S6RP S235/236 1:300 (Cell Signaling 2211), SMA 1:100 (Dako M0851), GFAP 1:5000 (Dako M0761) and eNOS 1:100 (BD Biosciences 610296). Immunohistochemical TUNEL staining was performed with a terminal transferase recombinant kit (Roche 333-574-001) on the Discovery XT automated staining system. Olig2 staining was quantified as percent positive cells by dividing pixel area of DAB stain by pixel area of nuclear counterstain using MetaMorph imaging software (Molecular Devices)(84).

Immunoflourescent staining and immunofluorescent TUNEL reaction

Immunoflourescent staining on FFPE sections was performed according to methods previously described (85) using the following antibodies: Olig2 1:250 (Millipore AB9610), Nestin 1:100 (BD Biosciences 556309), HA 1:100 (Roche 10744700) and GFP

1:150 (Abcam ab13970). Immunoflourescent TUNEL staining was performed by following the protocol for standard immunofluorescent staining referenced above until the secondary antibody step, then applying 150 uL TUNEL reaction mix from the In Situ Cell Death Detection Kit (Roche 11684795910) in a dark humidified chamber at 37 C for 60 min prior to counterstaining tissue with 4',6‑diamidino‑2‑phenylindole (DAPI) nuclear dye.

Validation of all TRAP lines was performed on frozen sections. Adult mice were perfused intracardially with 40ml ice cold PBS followed by 20ml ice cold paraformaldehyde. Samples were left to fix overnight in formalin at 4C. The next day they were transferred to a 30% sucrose/PBS. Once tissues had sunk, they were embedded in OCT on dry ice and sectioned at 7-10μm thickness. Staining was performed overnight in 10% donkey serum with the following antibodies: GFP 1:750 (Invitrogen A11122), GFP 1:500 (Abcam ab13970), CD44 (1:1000, BD Pharmingen), GFAP 1:2000 (Dako M0761), SMA 1:200 (Dako M0851), VECadherin 1:100 (BD Pharmingen 550548) and eNOS 1:150 (BD Biosciences 610296).

RNase Assays

RNase activity of tissue lysates was measure using the RNaseAlert QC System (Invitrogen) according to manufacturer instructions.

Neurosphere studies

Mouse neurosphere cell lines were prepared as previously described (80). Briefly, RCAS-PDGF tumors generated in either Ntv-a/Ink4a/Arf-/- or Ntv-a/p53-/- mice were

grossly-dissected and mechanically dissociated by dicing and pipetting up and down in 1 × Earle's balanced salt solution (EBSS) (Gibco) containing 12% papain and 10 μg/ml DNase. Tumor tissue in papain solution was then incubated at 37°C for 15 min prior to inactivation of papain with ovomucoid (Worthington). Tumor cells were collected by centrifugation and subjected to three cycles of low speed spins and resuspension in ovomucoid solution to remove debris. For neurosphere culture, cells were grown in Neural Stem Cell Basal medium (Stem Cell Technologies) with the following supplements: mouse NSC Proliferation Supplements (Stem Cell Technologies), 10 ng/ml EGF (Invitrogen), 20 ng/ml basic- FGF (Sigma), and 1 mg/ml Heparin (Stem Cell Technologies). For IR studies, neurosphere cell lines were irradiated using a Cs-137 source (Shepherd Mark-1).

Western blotting

Western blotting was performed according to standard procedures. Briefly, cells or tissue were lysed in 1 × RIPA buffer (Thermo Scientific 89900) supplemented with protease and photphatase inhibitors (Complete Mini EDTA-Free; Roche 04693159001 and PhosSTOP; Roche 04906837001) by pipetting, vortexing and sonication. Precleared lysates were denatured in Laemmli Sample Buffer (BioRad 1610737) containing β-mercaptoethanol, separated electrophoretically in polyacrylamide gels and transferred to polyvinylidene fluoride (PVDF) membrane. Membranes were blotted with the following antibodies in TBST/4% BSA: phosphorylated RPS6 1:1000 (Cell Signaling 4856), phosphorylated Akt 1:150 (Cell Signaling 2965), Akt 1:2000 (Cell Signaling 4685) RPS6 1:1000 (Cell Signaling 2217), β-actin 1:1000 (Cell Signaling 4967).

QRT-PCR

RNA was extracted from mice as described above or cell pellets using the miRNeasy Mini Kit (Qiagen 217004) with an additional DNA digestion step according to manufacturer instructions. cDNA was synthesized from RNA using SuperScript III First-Strand Synthesis System (Invitrogen 18080-051) and quantitative real-time PCR was performed with the listed-below intron-spanning primers and SYBR Green PCR Master Mix (Applied Biosystems 4368706) on a 7900 HT Fast Real-Time PCR System (Applied Biosystems). mDdit4L QRT-PCR was performed with TaqMan Gene Expression Assay (Applied Biosystems Mm00513313_m1) and TaqMan Universal PCR Master Mix (Applied Biosystems 4304437).

Gene: Forward Reverse

mSestrin1: GTCCCAACGTTTCGTGTC TGGATAGAGACGATTCACCAGA

mSestrin2: ACATCCACTGCGTCTTTGG CGTCTTGATATAGATTTTGAGGTTCC

mDdit4: CCAGAGAAGAGGGCCTTGA CCATCCAGGTATGAGGAGTCTT

mP21: CTGGGAGGGGACAAGAG GCTTGGAGTGATAGAAATCTG

HPRT: GCTCGAGATGTCATGAAGGAGAT AAAGAACTTATAGCCCCCCTTG

VE-Cadherin: CACTGCTTTGGGAGCCTTC GGGGCAGCGATTCATTTTTCT

VEGFR2: TTTGGCAAATACAACCCTTCAGA GCAGAAGATACTGTCACCACC

CD31: CTGCCAGTCCGAAAATGGAAC CTTCATCCACCGGGGCTATC

eNOS: CGAAGCGTGTGAAGGCAAC TTGTACGGGCCTGACATTTCC

SMA: GTCCCAGACATCAGGGAGTAA TCGGATACTTCAGCGTCAGGA

SMCMHC: AAGCTGCGGCTAGAGGTCA CCCTCCCTTTGATGGCTGAG

Olig2: TCCCCAGAACCCGATGATCTT CGTGGACGAGGACACAGTC

NeuN: ATCGTAGAGGGACGGAAAATTGA GTTCCCAGGCTTCTTATTGGTC

GFAP: ACAGACTTTCTCCAACCTCCAG CCTTCTGACACGGATTTGGT

GAPDH: ATGTTCCAGTATGACTCCACTCAC

GAAGACACCAGTAGACTCCACGACA

PUMA: CCCCTGCCAGATTTGTGA GAGATTGTACAGGACCCTCCA

Statistical Tests

Partek Genomics Suite software was used to quantile normalize and log2 transform all data. For translational efficiency analysis, a detection p-value filter of 0.05 was applied to background subtracted expression values and data was exported to Partek

33

Genomics Suite software where it was quantile normalized and log2 transformed. Significance levels for individuals genes were assessed by 1-way ANOVA testing with FDR<0.05 using Partek software. Hierarchical clustering was performed in Partek. Gene set enrichment analysis was performed with the javaGSEA Desktop Application using 1000 gene set permutations, the provided gene ontology biological process and transcription factor motif genesets, and all other default settings (86). Genesets for glioma subtype signatures were obtained from (14).

Survival analysis performed using GraphPad Prism v6.0 software . Survival curves were analyzed using the Kaplan-Meier method, with groups compared by respective median survival of number of days taken to reach 50% morbidity; log rank p value was measured using the Mantel-Cox test. Other statistical test performed using GraphPad Prism v6.0 or Microsoft Excel.

For Gene Set Enrichment Analysis on relative expression changes after IR in PDGF-only and PDGF-p53shRNA tumors, a 3-way ANOVA was performed on all p53shRNA and PDGF-only glioma samples in the Partek Genomics Suite. Tumor type, treatment, and mRNA type (total or translated) were used as factors in the model, with interactions allowed between tumor type and treatment, and treatment and mRNA type. The p-value of the contrast (IR-PDGF and Ctrl-p53shRNA vs. Ctrl-PDGF and IR-p53shRNA) for each probe was used to construct a ranking metric for each probe consisting of the negative Log10 of the p-value multiplied by the sign of the expression change. This ranking metric was used for enrichment analysis via the GseaPreranked option in the javaGSEA Desktop Application. GOrilla (87) was used to analyze GO term over-representation amongst IR and temsirolimus regulated genes.

EXPERIMENT RESULTS I - IDENTIFICATION OF GLOBAL ALTERATION OF TRANSLATIONAL REGULATION IN GLIOMA IN VIVO (88)

The protein state of a cell is subject to multiple layers of regulation. Chromatin accessibility and transcription regulate mRNA concentration, along with factors affecting mRNA stability. Translational regulation controls both global and mRNA specific rates of protein synthesis, and post-translational mechanisms modulate protein half-life and activity. Integration of these multiple modes of regulation controls cell phenotype and dynamic regulation of these factors dictates how a cell responds to stress. Experimental techniques have been developed for measuring the mRNA content of cells, however, methods are less established for studying these other important modes of regulating gene output. This is especially true for the study of complex *in vivo* systems, where cell-type specific resolution is required to identify discrete biology of interacting cells in heterogeneous tissue.

Translation of mRNA into protein is regulated both globally and in a transcript-specific manner, and this process is frequently dysregulated in disease, especially in cancer (74, 89-92). Protein translation occurs in three discrete steps: initiation, elongation and termination. Translation initiation is the rate-limiting step and is where most regulation occurs (75). During canonical cap-dependent translation initiation, the small ribosomal subunit binds to the 7-methyl-GTP cap structure at the 5' end of an mRNA transcript and scans the 5' untranslated region (UTR) for the AUG start codon, at which point the large ribosomal subunit is recruited and translation elongation begins (75). The overall efficiency of this process is regulated by the activity of eukaryotic initiation factors (eIFs), and specific mRNA translation rates are modulated by transcript specific

features, such as 5'UTR secondary structure, decoy AUG codons and internal ribosome entry sites (IRESs) (74). The availability of individual mRNA transcripts to the translation machinery can also be regulated in a sequence-specific manner by microRNAs and RNA-binding proteins (93).

Translational regulation has traditionally been inferred from changes in ribosome-associated mRNAs isolated by sucrose-gradient profiling methods. This technology, however, has limited utility for studying translational regulation *in vivo* because of the cellular complexity of living tissue and the fragility of the polyribosome structure (82, 94). Here we adapt a method described by Heiman et al. of immunoprecipitating ribosome-bound RNA from genetically-determined cell populations *in vivo* to measure translational regulation in glioma (82). We demonstrate a broad range of relative ribosome occupancies amongst mRNA species in tumor *in vivo*. Comparison of the translation state of glioma tumor cells to their non-malignant counterpart cells in normal brain revealed widespread alteration of ribosome recruitment efficiencies amongst genes that are associated with malignant behavior. Furthermore, hyperactivity of phosphatidylinositol 3-kinase (PI3K) signaling due to phosphatase and tensin homolog (PTEN) deletion specifically altered ribosome association of mRNAs encoding proteins required for cellular respiration, biology classically associated with PI3K signaling but not previously described to be regulated at the translational level (95-97). The tight regulation of ribosome recruitment and the role of translational regulation in affecting discrete classes of genes in glioma demonstrate the importance of this mode of gene regulation. Applied to other disease models and normal tissue contexts, this method will allow for the first time global measurement of translational regulation *in vivo*.

Results

In vivo translation efficiency measurement in glioma

To study translational regulation in glioma *in vivo*, we generated high-grade tumors in mice using RCAS tv-a somatic gene transfer technology. (13-15, 69, 98, 99). An RCAS retroviral vector expressing the oncogene platelet derived growth factor B (RCAS-PDGF-B) was used to infect cells expressing the RCAS receptor tv-a driven by a Nestin promoter (Ntv-a) in the brains of newborn mice. Experimental mice also harbored somatic deletion of the Ink4a/Arf locus and floxed PTEN alleles (Ntv-a/Ink4a/Arf$^{-/-}$/PTEN$^{fl/fl}$). This GEM of glioma possesses genomic alterations typical of the Proneural subtype of human glioblastoma multiforme (GBM) and closely resembles the human Proneural tumor in gene expression and histology (14, 100). Like human GBM, PDGFB-driven mouse gliomas were cellularly heterogeneous, composed of transformed cells residing in a complex stromal microenvironment that contributes importantly to tumor progression, but also confounds gene expression study of individual cell populations *in vivo* (37). Immunohistochemical staining of PDGF-driven gliomas identified eNOS-positive blood vessels surrounded by perivascular regions staining positive for smooth muscle actin (SMA), nestin, and PDGF receptor beta (PDGFRβ), and tumor bulk (TB) regions that are nucleus-dense and stain positive for Olig2 and PDGF receptor alpha (PDGFRα) (Fig. 4A). Astrocytes (GFAP-positive) are numerous and located throughout the tumor (Fig. 4A). Immunofluorescent staining for the hemaglutinin (HA) epitope tag on the PDGF protein used to generate gliomas revealed that most, if not all, PDGF-HA expressing tumor cells colocalized with Olig2 expression in the TB regions (Fig. 4B). FACS analysis of gliomas generated with a bicistronic RCAS vector expressing both

PDGF and RFP in mice expressing GFP driven by the Olig2 promoter confirmed the identity of oncogene-expressing glioma cells as Olig2-positive (Fig. 4C).
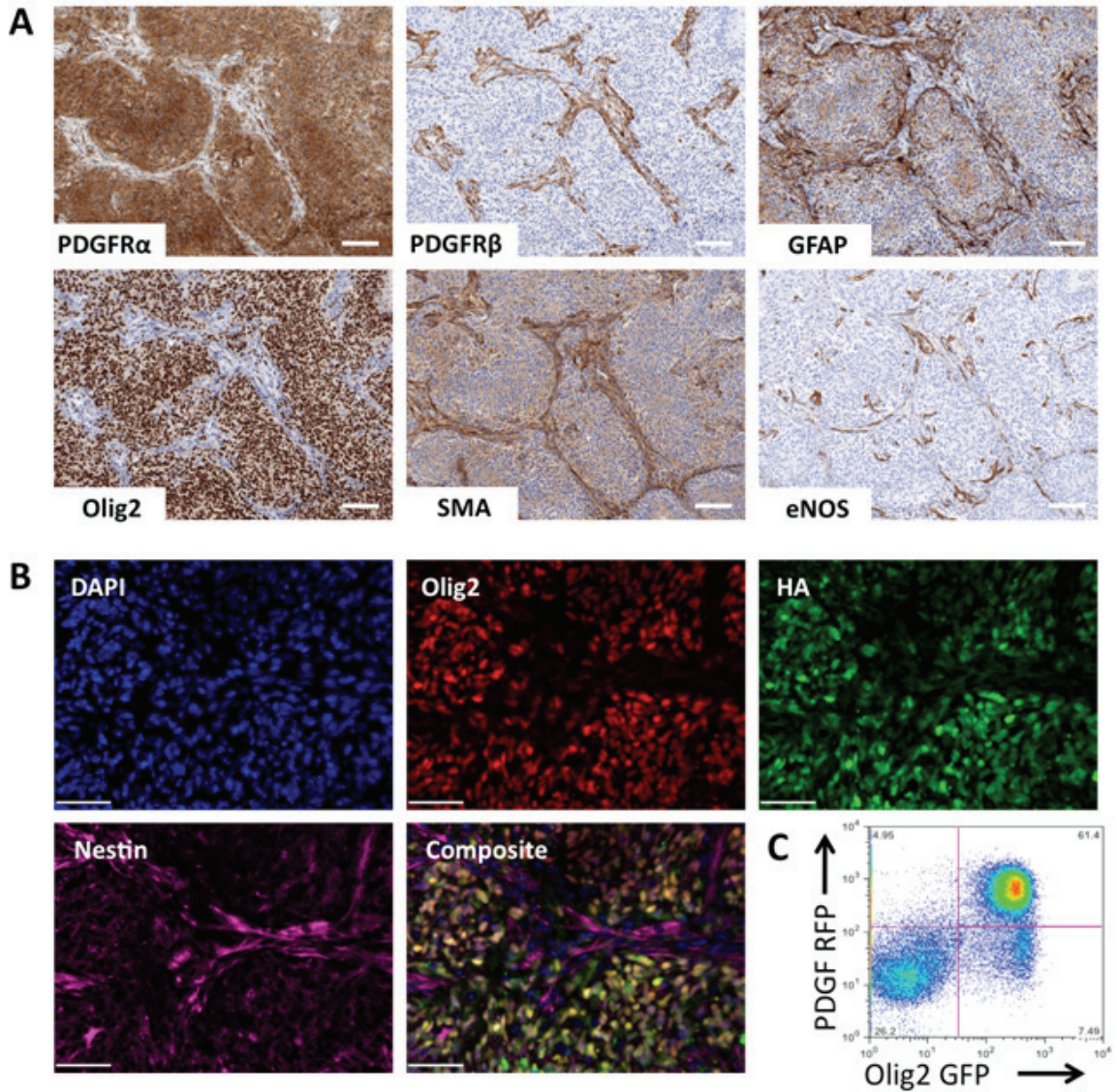
Figure 4. GBM is a heterogeneous tumor composed of multiple cell types, including both tumor and stromal cells.

(A) Immunohistochemical staining of mouse PDGF-driven glioma identified multiple tumor regions composed of different cell types. (B) PDGF-HA oncogene expressed from tumor cells colocalized with Olig2 staining by IHC. (C) FACS analysis of tumors generated in Olig2-eGFPL10a mice with PDGF-RFP bicistronic retrovirus identified tumor cells as Olig2+. Scale bar, 100μm. Reproduced from Helmy K, Halliday J, Fomchenko E, Setty M, Pitter K, Hafemeister C, Holland EC. Identification of global alteration of translational regulation in glioma in vivo. PLoS One 2012;7(10):e46965.

The ability to distinguish tumor cells from tumor stroma by Olig2 expression allowed us to develop a method for global quantification of translation efficiency for individual mRNAs in glioma cells residing in their native tumor microenvironment. PDGF-induced gliomas were generated in mice transgenic for the gene fusion of the large ribosome subunit protein L10a with eGFP (eGFP-L10a or RPGFP) under the transcriptional control of an Olig2 BAC promoter (72, 78). In these tumors, eGFP-L10a expression was restricted to Olig2+ cells in the tumor (Fig. 5A). This cell-type specific expression of eGFP-L10a enabled immunoprecipitation of ribosome-bound translating mRNA with anti-GFP-conjugated beads from only the Olig2+ tumor cells by a method previously described (78, 82). GFP expression also allowed flow cytometric sorting of Olig2+ tumor cells to isolate total cellular RNA from the same cell population. The translation efficiency (TE) for each mRNA transcript could then be expressed as a ratio of the expression values from translating ribosome-bound RNA and total cellular RNA (IP/Total). Since translation initiation has been shown to be the rate-limiting step of translation, the TE ratio should be a good proxy for the relative efficiency of protein production from individual transcripts. The TE measurement for each biological sample was then regarded as a discrete biological value because both pools of RNA were obtained as pairs from the same tumor.
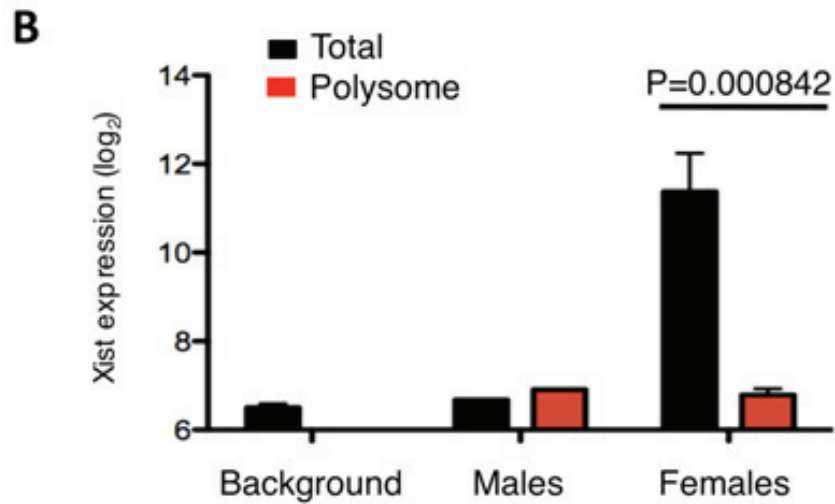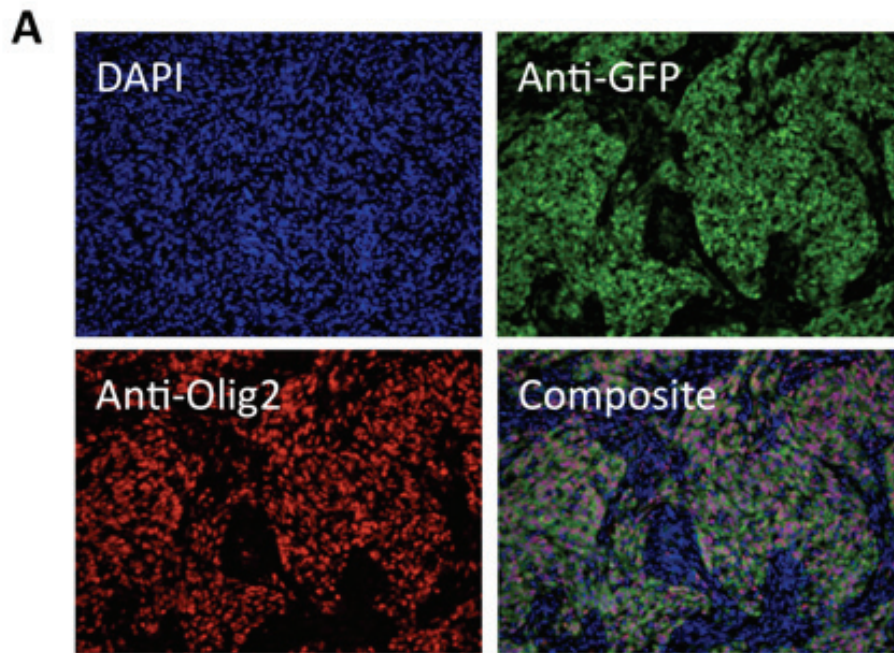
Figure 5. In vivo quantification of ribosome-bound and total RNA levels in PDGF-driven glioma.
(A) Olig2-eGFP-L10a expression faithfully reported endogenous Olig2 expression in tumor. (B) Xist mRNA was abundant in total RNA from tumors generated in female mice, but absent from the ribosome-bound fraction (SD bars shown). Reproduced from Helmy K, Halliday J, Fomchenko E, Setty M, Pitter K, Hafemeister C, Holland EC. Identification of global alteration of translational regulation in glioma in vivo. PLoS One 2012;7(10):e46965.

Ribosome-bound and total cellular RNA samples from Olig2+ mouse glioma cells were quantified by expression microarray (Fig. 6A). The specificity of the TE measurement could be demonstrated with the mRNA transcript Xist, which is highly transcribed from the silenced X-chromosome in females and mediates X-inactivation by coating the silenced chromosome without being translated (101). Xist mRNA transcript was abundant in the total RNA pool in tumors generated in female mice, but entirely absent from ribosome-bound RNA (Fig. 5B). Xist transcript was not present in either pool of RNA from tumors generated in male mice (Fig. 5B).
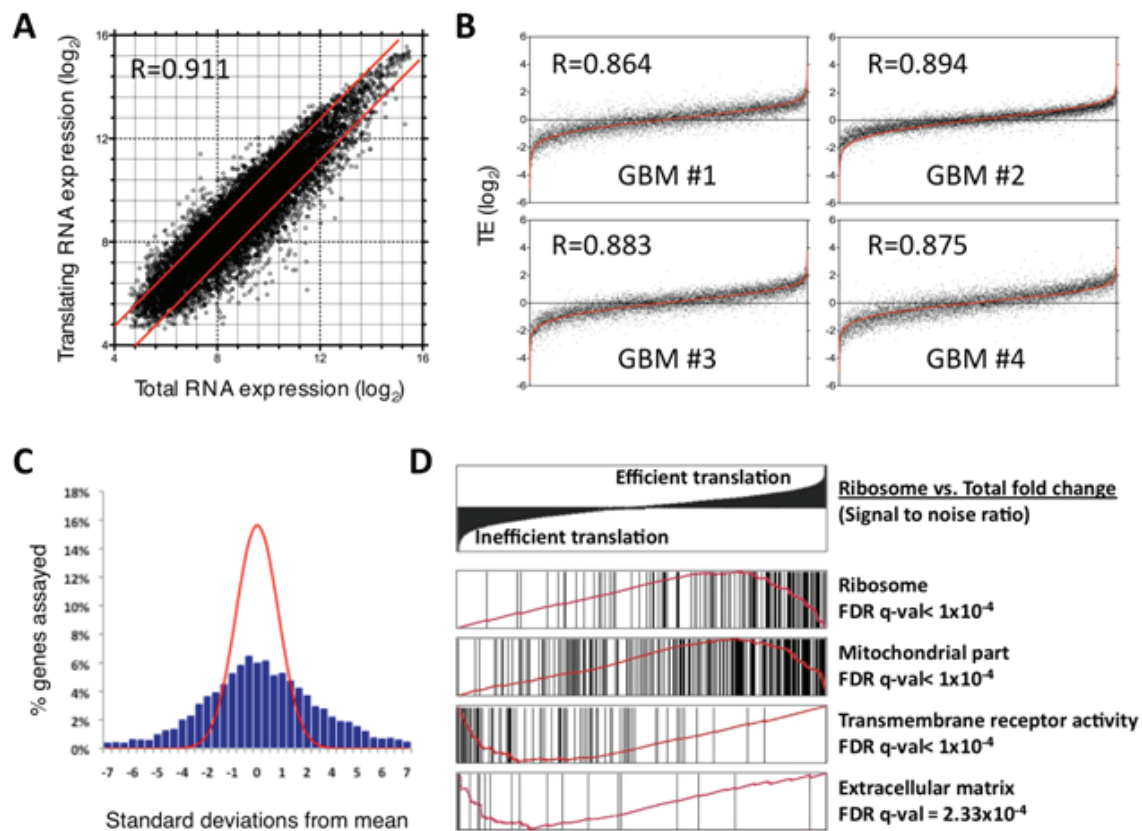
Figure 6. In vivo quantification of ribosome-bound and total RNA levels revealed a broad range of ribosome recruitment efficiencies amongst mRNA transcripts.
(A) Distribution of mRNA expression in ribosome-bound and total RNA pools from PDGF-driven glioma identified differential TE (N=4). (B) TE values for each biological replicate (black points) plotted with the average of the other three replicates (red line) demonstrated reproducibility of measurements. (C) Signal-to-noise ratios of TE measurements (blue bars) identified range of high confidence measurements relative to a normal distribution (red line). (D) GSEA identified statistical overrepresentation of defined gene ontologies amongst efficiently and inefficiently translated genes. Black bars represent distribution of mRNAs from indicated geneset amongst all genes ranked by signal to noise ratio (top panel). Red line represents GSEA output enrichment score. R= Pearson correlation coefficient. Reproduced from Helmy K, Halliday J, Fomchenko E, Setty M, Pitter K, Hafemeister C, Holland EC. Identification of global alteration of translational regulation in glioma in vivo. PLoS One 2012;7(10):e46965.

43

The translation efficiency for individual transcripts was highly reproducible across four independent tumor samples. Pearson correlation coefficients of relative TE for each biological replicate compared to the average of the other three tumor samples exceeded 0.86 for all four comparisons (Fig. 6B). Furthermore, distribution of signal to noise of TE values greatly exceeded normal error, with 1,177 probes (12.2%) measuring signal to noise ratios greater than five (Fig 6C). Reliability of TE measurements across the range of expression could be demonstrated by comparison of TE values for the 2,149 genes with multiple unique probes. Multiple probes to the same gene were found to measure very similar TE across the range of microarray probe values (Fig. 7).
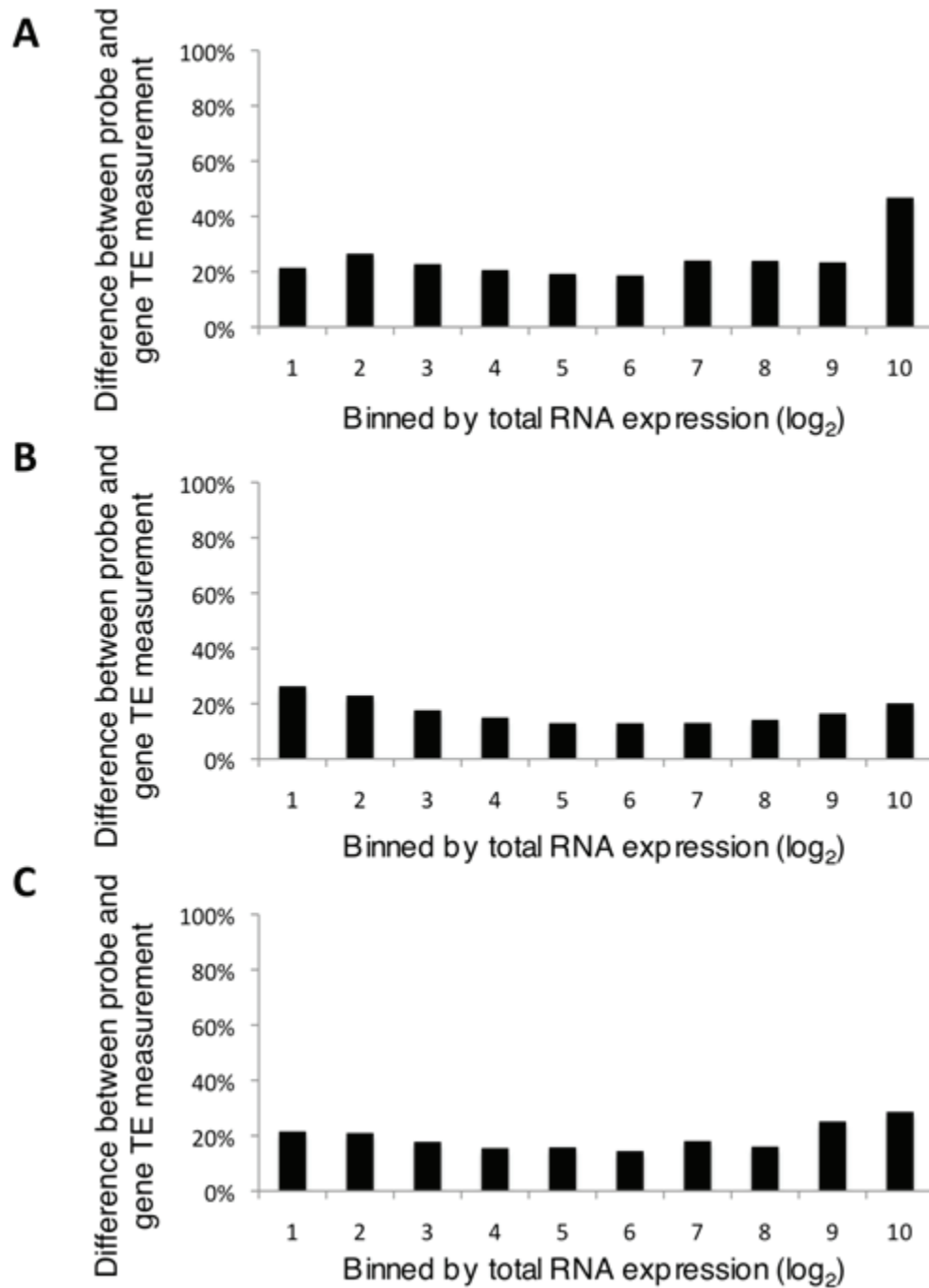
Figure 7. Multiple probes against the same gene identified similar TE measurements across the full range of expression values in total RNA.
Average percent difference in measures TE between probe and gene average were binned by expression value in total RNA for (A) PDGF-driven mouse glioma, (B) normal brain OPCs and (C) PDGF-driven mouse glioma with PTEN deleted. Reproduced from Helmy K, Halliday J, Fomchenko E, Setty M, Pitter K, Hafemeister C, Holland EC. Identification of global alteration of translational regulation in glioma in vivo. PLoS One 2012;7(10):e46965.

The TEs of mRNA transcripts in glioma tumor cells *in vivo* demonstrated more than a 600-fold range of translation efficiency amongst the 9,653 transcript probes with detectable expression by microarray, illustrating the substantial contribution of translational regulation to gene output. More than 60% (5,963) of all genes were identified as differentially represented in the total RNA and translating RNA pools using a conservative multiple testing correction filter of FDR<0.05. Of the probes measuring significant translational regulation, 1065 were at least 2-fold more prevalent in the translating pool (efficiently translated) and 1156 probes more than 2-fold less efficiently translated than average (Fig. 6A).

The high degree of similarity of TE measures between individual tumors suggests tight transcript-specific control of translation to modify gene output and regulate cell behavior. Gene set enrichment analysis (GSEA) identified overrepresentation of gene ontology (GO) categories amongst genes translated at different rates, implying that differential TE regulates specific cell behaviors (86, 102). RNAs encoding ribosomal and mitochondrial proteins were amongst the most efficiently translated messages in PDGF-driven mouse glioma (Fig. 6D), concordant with translation efficiency measures determined by ribosome footprint profiling for yeast cells collected during log-phase growth (103). GO categories encompassing transmembrane receptor activity and extracellular matrix components were amongst the least efficiently translated mRNAs (Fig. 6D).

While the data above describes the static translation state in PDGF-driven glioma, this method enables comparison of the translation state of genetically-defined cell types to characterize cell-type specific differences in translational regulation. We therefore

sought to compare the translation state of the transformed glioma cells with their untransformed normal cell counterparts.

Dysregulation of translation in neoplastic transformation

Dysregulation of protein synthesis is a common feature of cancer that modulates gene output and may contribute to malignant phenotype (89, 91). We had previously identified alterations of translation in cultured glial cells upon transformation with activated Ras and Akt (92). However, any *in vitro* culture system will naturally fail to recapitulate the complex set of extracellular signals and cues comprising the *in vivo* microenvironment. Hierarchical clustering of PDGF-driven mouse glioma gene expression profiles with various mouse neural cell types characterized these tumor cells as most similar to oligodendrocyte progenitor cells (OPCs) in the normal brain that also express Olig2 (104). This finding is consistent with the oligodendroglial phenotype of the Proneural subset of human gliomas that the PDGF-driven mouse model most closely resembles (14). Therefore, we were able to apply the *in vivo* TE profiling strategy to compare the translation state of transformed glioma cells *in vivo* with that of their non-transformed OPC counterparts, offering insight into the dysregulation of translation that occurs in glioma *in vivo*.

As in tumor, relative TE values in Olig2-positive OPCs in adult normal brain varied widely amongst mRNA species and were highly correlated across replicates (average R=0.959) (Fig. 9A, 9B). Comparison of relative ribosome occupancies of tumor and normal Olig2-positive cells revealed a positive correlation of 0.616, demonstrating substantial similarity in the measured translation states of the two cell populations (Fig.

8A). Many genes, however, were translated with altered efficiency in tumor compared to normal brain OPCs (3,902 probes FDR<0.05; 40.4%), with 799 probes detecting greater than 2-fold increases in TE in tumor, and 912 probes detecting more than 2-fold decreases in TE (Fig. 8B; Fig. 9D).
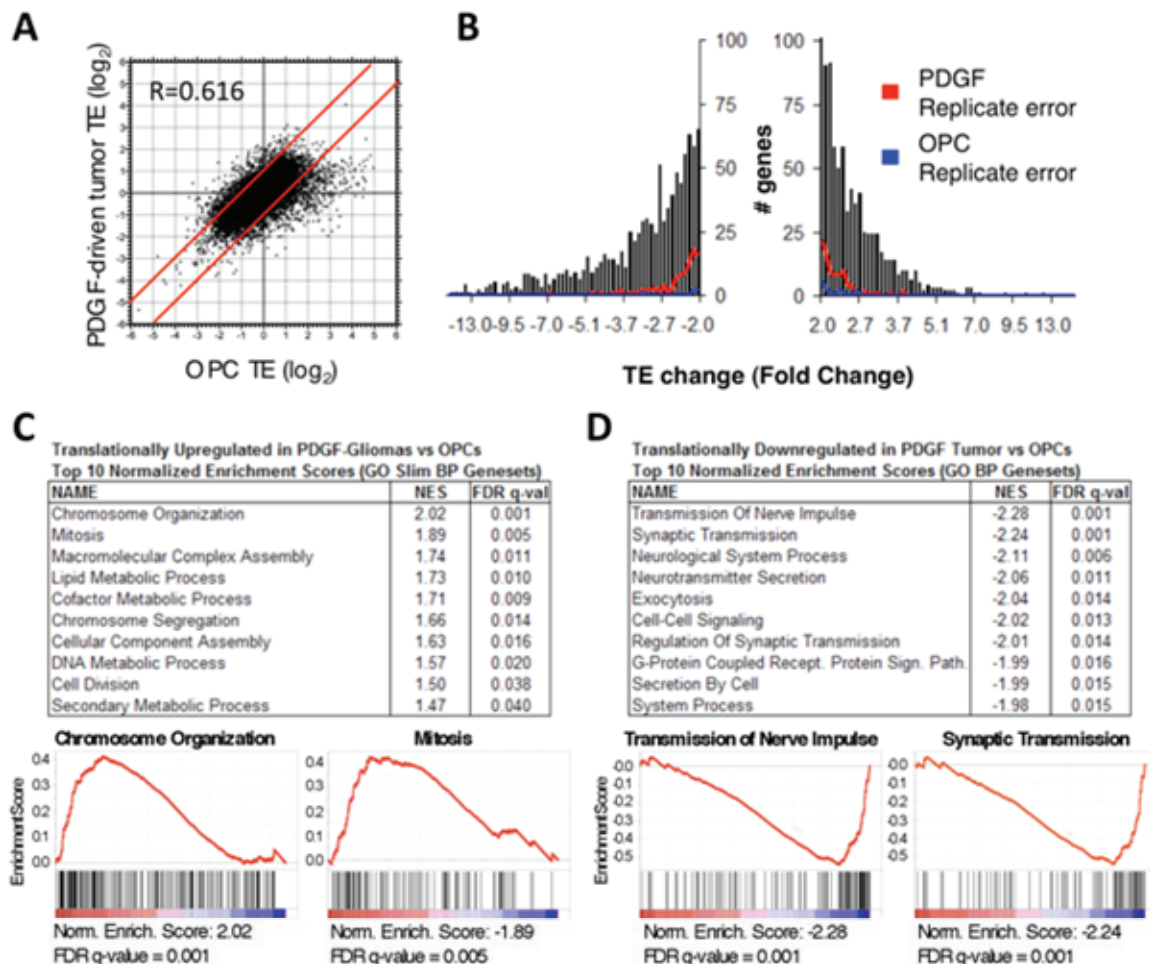
Figure 8. Translation efficiency was altered in glioma compared to normal brain OPCs.
(A) Changes in ribosome-bound mRNA correlated somewhat with changes in total cellular RNA between tumor and normal brain OPCs (N=4). (B) Alterations in TE between tumor and normal brain were reproducible, exceeding average replicate error. (C) Genesets associated with cell division and biosynthetic pathways predominated amongst GOSlim Biological Process genesets most enriched for transcripts translationally upregulated in Olig2+ tumor cells compared to normal brain OPCs. Enrichment plots for chromosome organization and mitosis genesets shown. (D) Genesets associated with synaptic signaling predominated amongst GO Biological Process genesets most enriched for transcripts translationally downregulated in Olig2+ tumor cells compared to normal brain OPCs. Enrichment plots for transmission of nerve impulse and synaptic transmission shown. NES = Normalized Enrichment Score. R = Pearson correlation coefficient. Reproduced from Helmy K, Halliday J, Fomchenko E, Setty M, Pitter K, Hafemeister C, Holland EC. Identification of global alteration of translational regulation in glioma in vivo. PLoS One 2012;7(10):e46965.
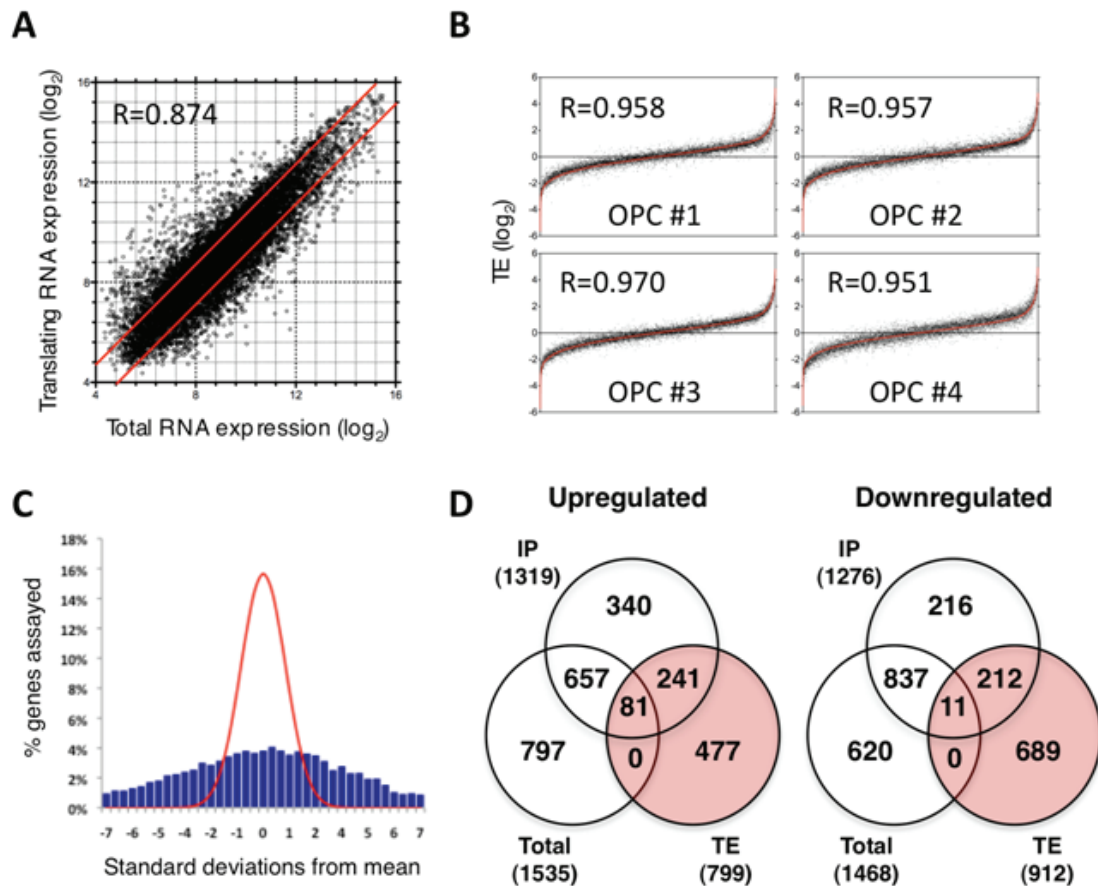
Figure 9. TE measurements in normal brain OPCs.
(A) Distribution of mRNA expression in ribosome-bound and total RNA pools from normal brain OPCs identified differential ribosome recruitment efficiencies. (B) TE values for each biological replicate (black points) plotted with the average of the other three replicates (red line) demonstrated reproducibility of measurements. (C) Signal to noise ratios of TE measurements (blue bars) identified range of high confidence measurements relative to normal distribution (red line). (D) Venn diagram of probes changed greater than 2-fold (and FDR<0.05) between tumor and normal Olig2+ cells in ribosome-bound RNA (IP), total cellular RNA (Total) and TE. Pearson correlation coefficients (R) are represented. Reproduced from Helmy K, Halliday J, Fomchenko E, Setty M, Pitter K, Hafemeister C, Holland EC. Identification of global alteration of translational regulation in glioma in vivo. PLoS One 2012;7(10):e46965.

Discrete biological functions were enriched amongst the translationally altered transcripts. GSEA identified significantly translationally upregulated GO genesets that fell into two broad categories: cell division and biosynthetic pathways. Genesets for chromosome organization and mitosis were the most upregulated genesets, and chromosome segregation and cell division were also among the genesets meeting a 0.05 FDR cutoff (Fig 8C). Accordingly, genes involved in chromatin packing and cytokinesis were among the most significantly translationally upregulated transcripts, with histones and tubulins together comprising 9 of the top 35 most upregulated transcripts (Hist1h3a 10.9-fold; Hist1h3e 5.9-fold; Hist1h3d 5.7-fold; Hist1h4m 5.6-fold; Hist1h4d 5.3-fold; Tuba3b 5.2-fold; Tubb4 4.9-fold; Tuba3a 4.9-fold; Hist1h4f 4.6-fold). Numerous major cell cycle regulators were also significantly translationally upregulated (CDCA7 9.0-fold; cyclin D2 4.1-fold; cyclin B1 2.7-fold; CDK2 2.0-fold), as well as multiple minichromosome maintenance proteins required for licensing DNA for synthesis (MCM6 3.0-fold; MCM10 2.8-fold; MCM2 2.7-fold). In addition, most major biosynthetic processes were translationally upregulated, including lipid metabolism, cofactor metabolism, DNA metabolism, and secondary metabolic processes (Fig. 8C). The upregulation of these synthetic pathways provides structural components needed for rapid cellular replication.

The genesets that were significantly downregulated translationally were associated with neural signaling, and specifically processes involved in pre-synaptic signaling (Fig. 8D, Fig. 9D). Some OPCs have been shown to give rise to neurons, and the translational downregulation of synaptic transmission related genes may be reflective of a lack of neuronal differentiation in the PDGF-driven tumor cell population (105, 106).

51

Lack of differentiation is a general feature of cancer and is indicative of higher grade and worse prognosis in gliomas (3, 19). The role of translational regulation in contributing to proliferative capacity and cell fate determination is of critical scientific and therapeutic interest and warrants further investigation into the mechanisms of this regulation.

PTEN loss reduces the ribosome occupancy of transcripts associated with cellular respiration in glioma

The PI3K pathway is an important transduction pathway downstream of receptor tyrosine kinase signaling that is frequently dysregulated in cancer (107). PI3K catalyzes the conversion of phosphatidylinositol (4,5) bisphosphate (PIP_2) to phosphatidylinositol (3,4,5) bisphosphate (PIP_3), which activates Akt and downstream mTORC1 signaling, a well-known regulator of protein translation (108). PTEN opposes PI3K function and is frequently altered in GBM, with 36% of tumors exhibiting homozygous deletion or mutation (5). In the Proneural subgroup of human GBMs, 69% of tumors had homozygous or hemizygous deletion of PTEN, and PTEN mutations were found in 16% of tumors (14). Deletion of PTEN in mouse PDGF-driven gliomas results in increased stem-like phenotype, reduced tumor latency, and histologically more aggressive tumors featuring increased pseudopallisading necrosis (81, 109). To determine if loss of PTEN altered the homeostatic translation state in glioma, we delivered RCAS-Cre virus along with RCAS-PDGFB into Ntv-a/Ink4a/Arf$^{-/-}$/PTEN$^{fl/fl}$ mice and collected ribosome-bound and total cellular RNA from Olig2+ cells. The resulting tumors exhibited an overall expression pattern similar to that of PTEN WT tumors (Fig. 11), but had undetectable levels of PTEN in the tumor bulk regions and elevated levels of phosphorylated Akt, a

marker of PI3K activity, and elevated phosphorylated ribosomal protein S6, a marker of

mTORC1 pathway activation (Fig. 10A and 10B).

A

	PDGF	PDGF+Cre
H&E		
PTEN		
PTEN		
pS6		

B

	PDGF			PDGF+Cre			
	1	2	3	1	2	3	
							pAkt
							Akt
							pS6
							S6
							Actin

C

$R=0.912$

Translating RNA expression ($\log_2$) vs Total RNA expression ($\log_2$)

D

TE ($\log_2$)

R=0.925 GBM #1
R=0.894 GBM #2
R=0.897 GBM #3
R=0.938 GBM #4

E

% genes assayed vs Standard deviations from mean

F

Upregulated

IP (384)

284

97   3

0

40   0   1

Total (137)   TE (4)

Downregulated

IP (530)

368

110   42

10

40   0   2

Total (160)   TE (54)

54
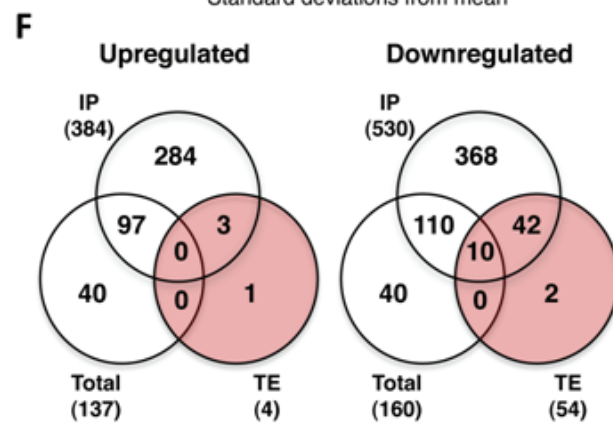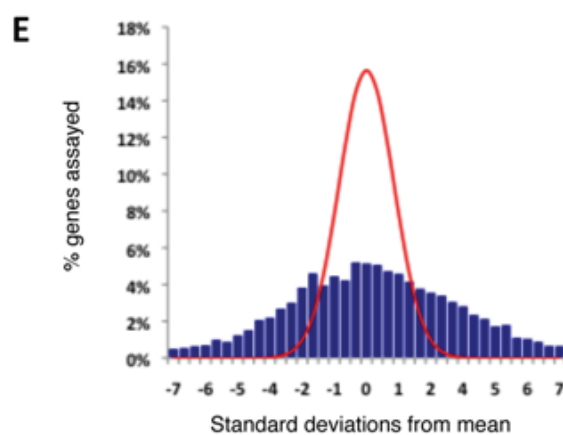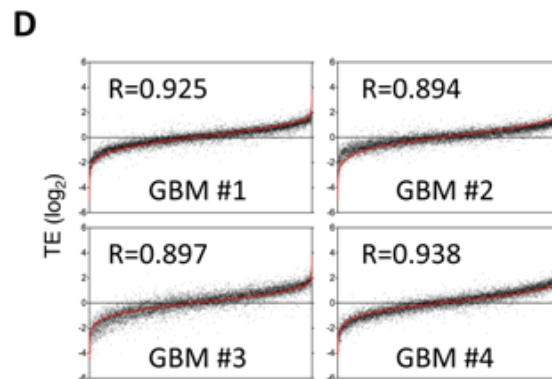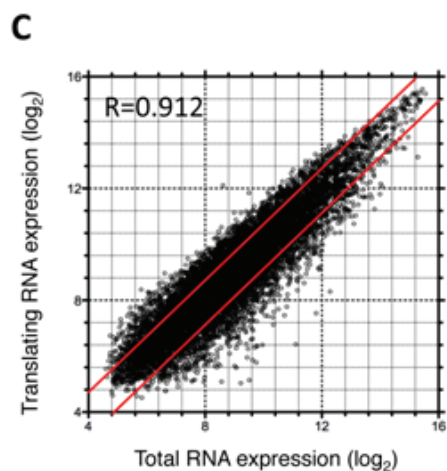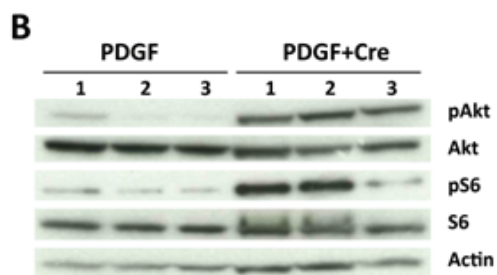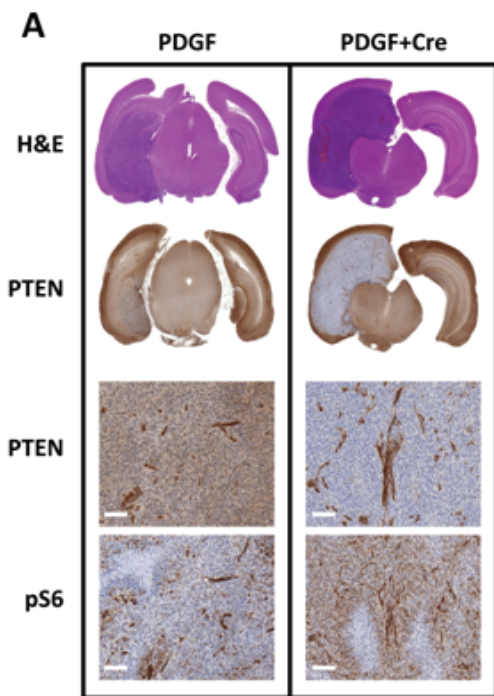
Figure 10. TE measurements in PDGF-driven glioma with PTEN deleted
(A) Immunohistochemical staining of tumor sections demonstrated the absence of PTEN protein and increased p-S6 positivity in mice receiving Cre virus in addition to PDGF. (B) Western blot of tumor lysates from mouse glioma demonstrates increased phosphorylation of Akt (T308) and S6 (S235/236) in tumors with PTEN deleted compared to tumors expressing PTEN. (C) Distribution of mRNA expression in ribosome-bound and total RNA pools from PDGF+Cre tumors identified differential translational efficiencies. (D) TE values for each biological replicate (black points) plotted with the average of the other three replicates (red line) demonstrated reproducibility of measurements. (E) Signal to noise ratios of TE measurements (blue bars) identified range of high confidence measurements relative to normal distribution (red line). (F) Venn diagram of probes changed greater than 2-fold (and FDR<0.05) between PTENfl/fl and PTEN-/- Olig2+ cells in ribosome-bound RNA (IP), total cellular RNA (Total) and TE. (G) mRNAs involved in cellular respiration and encoding components of the electron transport chain were translationally downregulated upon PTEN loss. Pearson correlation coefficients (R) are represented. Reproduced from Helmy K, Halliday J, Fomchenko E, Setty M, Pitter K, Hafemeister C, Holland EC. Identification of global alteration of translational regulation in glioma in vivo. PLoS One 2012;7(10):e46965.
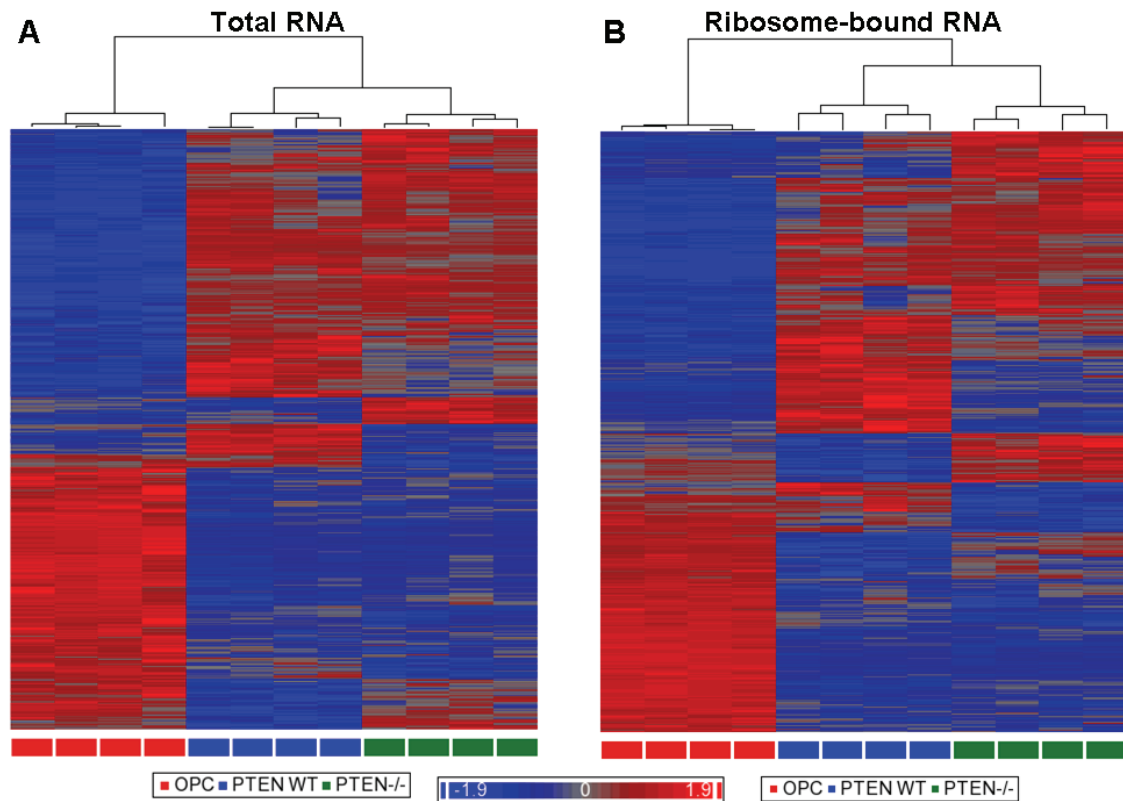
Figure 11. Hierachical clustering of normalized microarray expression data
Hierachical clustering of normalized microarray expression data from (A) total cellular RNA and (B) ribosome-bound RNA extracted from Olig2+ cells in normal brain and PDGF-driven glioma demonstrates the high degree of similarity of PTEN-expressing and PTEN-deleted tumors compared to normal brain OPCs. Hierachical clustering performed on transcripts significantly different by ANOVA at 0.05 FDR. Reproduced from Helmy K, Halliday J, Fomchenko E, Setty M, Pitter K, Hafemeister C, Holland EC. Identification of global alteration of translational regulation in glioma in vivo. PLoS One 2012;7(10):e46965.

Analysis of PTEN$^{-/-}$ gliomas relative to PTEN$^{fl/fl}$ gliomas demonstrated a high degree of similarity in TE between the two tumor types, in contrast to the widespread changes observed between tumor and normal OPCs (Fig. 12A). Reproducible changes in the transcriptome and translatome, however, were detected upon PTEN loss in glioma. 914 genes were more than 2-fold differentially expressed in the IP fraction and met an FDR cutoff of 0.05, resulting from alteration of both total mRNA content and translational regulation (Fig. 12B; Fig. 10E). Of these most changed genes (>2-fold in ribosome-bound mRNA), alteration of TE accounted for more than 40% of gene expression changes (Fig. 12B). Somewhat surprisingly, differential translation contributed most significantly to downregulated gene expression, with 54 probes measuring greater than 2-fold reduction in TE, and only 4 genes exhibiting greater than 2-fold increased TE upon PTEN loss (FDR<0.05) (Table 1; Table 2). These differences we observe in gene expression likely results directly from the increased PI3K/Akt/mTORC1 activity in the PTEN-deleted tumors in addition to differences in tumor initiation and evolution upon PTEN deletion.
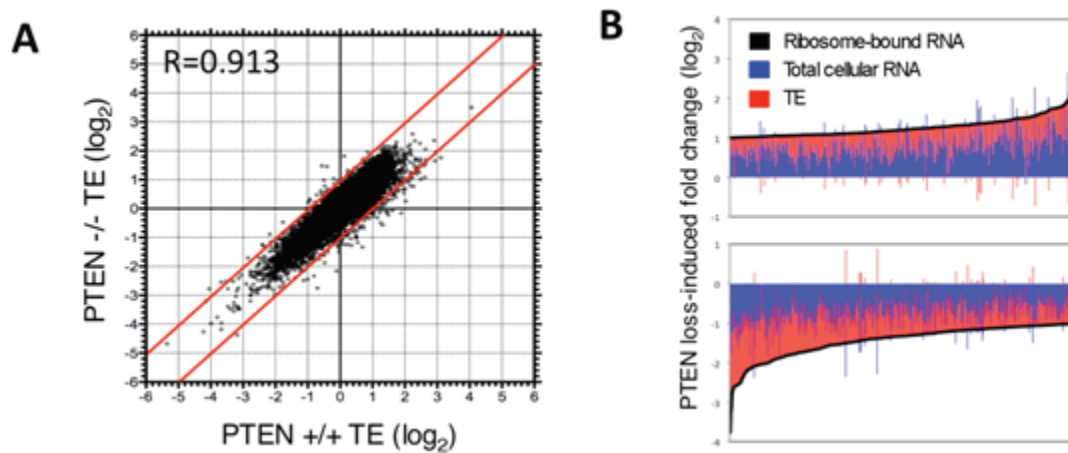
Figure 12. PTEN loss altered the translation state of glioma cells
(A) TE measurements of PTEN WT and PTEN deleted tumors were very similar (N=4). (B) Changes in both total RNA and TE contributed to alteration in ribosome-bound RNA caused by PTEN loss. Reproduced from Helmy K, Halliday J, Fomchenko E, Setty M, Pitter K, Hafemeister C, Holland EC. Identification of global alteration of translational regulation in glioma in vivo. PLoS One 2012;7(10):e46965.

Table 1. PDGF+Cre vs. PDGF only tumors; genes with >2-fold downregulated TE and FDR<0.05

Gene Symbol	Description	PDGF+Cre vs. PDGF Log2 Change		
		PC-P IP	PC-P Total	PC-P TE
UBE3A	ubiquitin protein ligase E3A	-2.71	-0.66	-2.05
CCT5	chaperonin containing Tcp1, subunit 5 (epsilon)	-3.26	-1.22	-2.03
SLC3A2	solute carrier family 3 (activators of dibasic and neutral amino acid transport), member 2	-2.04	-0.02	-2.02
EID1	EP300 interacting inhibitor of differentiation 1	-3.77	-2.00	-1.77
PCNA	proliferating cell nuclear antigen	-2.61	-0.86	-1.75
IDI1	isopentenyl-diphosphate delta isomerase	-1.91	-0.20	-1.71
RSPRY1	ring finger and SPRY domain containing 1	-2.37	-0.66	-1.71
LOC100048530	similar to coiled-coil domain containing 72	-2.25	-0.72	-1.53
FABP7	fatty acid binding protein 7, brain	-2.60	-1.10	-1.50
SOX2	SRY-box containing gene 2	-2.73	-1.27	-1.46
LOC668837	similar to ATP synthase, H+ transporting, mitochondrial F0 complex	-2.63	-1.16	-1.46
TAF9	TAF9 RNA polymerase II, TATA box binding protein (TBP)-associated factor	-1.86	-0.43	-1.43
ABCE1	ATP-binding cassette, sub-family E (OABP), member 1	-1.65	-0.24	-1.40
HUWE1	HECT, UBA and WWE domain containing 1	-2.21	-0.82	-1.40
GFRA1	glial cell line derived neurotrophic factor family receptor alpha 1	-0.94	0.43	-1.37
NDUFB4	NADH dehydrogenase (ubiquinone) 1 beta subcomplex 4	-2.03	-0.68	-1.35
PIK3CA	phosphatidylinositol 3-kinase, catalytic, alpha polypeptide	-1.77	-0.42	-1.34
UBE2N	ubiquitin-conjugating enzyme E2N	-2.04	-0.72	-1.33
STMN1	stathmin 1	-2.21	-0.89	-1.32
UBTD2	ubiquitin domain containing 2	-1.89	-0.61	-1.29
KLHL13	kelch-like 13	-1.65	-0.37	-1.28
ZFP647	zinc finger protein 647	-1.74	-0.46	-1.28
USMG5	upregulated during skeletal muscle growth 5	-2.03	-0.76	-1.28
2610528E23RIK	RIKEN cDNA 2610528E23 gene	-1.73	-0.45	-1.27
JAM3	junction adhesion molecule 3	-2.31	-1.06	-1.25
MXI1	Max interacting protein 1	-2.59	-1.34	-1.24
HNRNPA2B1	heterogeneous nuclear ribonucleoprotein A2/B1	-2.51	-1.30	-1.22
SNX1	sorting nexin 1	-2.12	-0.94	-1.19
SPCS2	signal peptidase complex subunit 2 homolog	-1.78	-0.60	-1.18
NDRG2	N-myc downstream regulated gene 2	-1.39	-0.21	-1.18
SNX3	sorting nexin 3	-2.04	-0.86	-1.17
OTTMUSG00000007855	predicted gene, OTTMUSG00000007855	-2.58	-1.41	-1.17
SDHD	succinate dehydrogenase complex, subunit D	-1.44	-0.28	-1.16
1500003O22RIK	RIKEN cDNA 1500003O22 gene	-1.61	-0.47	-1.14
TUG1	taurine upregulated gene 1	-2.05	-0.93	-1.13
PCMT1	protein-L-isoaspartate (D-aspartate) O-methyltransferase 1	-1.82	-0.69	-1.12
CHMP5	chromatin modifying protein 5	-2.08	-0.96	-1.12
SLAIN1	SLAIN motif family, member 1	-0.78	0.34	-1.12
CYCS	cytochrome c	-2.06	-0.94	-1.12
RP23-297J14.5	similar to oxidative stress responsive 1	-1.51	-0.40	-1.11
ZKSCAN3	zinc finger with KRAB and SCAN domains 3	-2.02	-0.92	-1.11
LOC100041703	similar to G protein gamma-5 subunit	-2.02	-0.93	-1.09
CRYZL1	crystallin, zeta (quinone reductase)-like 1	-1.68	-0.60	-1.08
RSU1	Ras suppressor protein 1	-2.06	-0.98	-1.08
LOC100046796	similar to polymerase (RNA) II (DNA directed) polypeptide K	-1.35	-0.28	-1.07
ST13	suppression of tumorigenicity 13	-1.27	-0.22	-1.05
LOC100044087	similar to brain protein 44	-2.16	-1.10	-1.05
GTF2E2	general transcription factor II E, polypeptide 2 (beta subunit)	-1.66	-0.61	-1.05
SPRR2A	small proline-rich protein 2A	-1.46	-0.41	-1.05
ZFP161	zinc finger protein 161	-1.85	-0.81	-1.04
PDCD5	programmed cell death 5	-1.74	-0.72	-1.02
CFL2	cofilin 2, muscle	-1.87	-0.85	-1.02
NIT2	nitrilase family, member 2	-1.76	-0.74	-1.02
COX7B	cytochrome c oxidase subunit VIIb	-1.60	-0.59	-1.01

Table 2 PDGF+Cre vs. PDGF only tumors; genes with >2-fold upregulated TE and FDR<0.05

		PDGF+Cre vs. PDGF Log2 Change		
Gene Symbol	**Description**	**PC-P IP**	**PC-P Total**	**PC-P RRO**
GALE	galactose-4-epimerase, UDP	1.38	0.28	1.10
D9ERTD402E	DNA segment, Chr 9, ERATO Doi 402, expressed	1.59	0.40	1.19
TTC14	tetratricopeptide repeat domain 14	0.66	-0.64	1.30
KLHDC9	kelch domain containing 9	1.51	-0.19	1.70

The genes translationally downregulated in PTEN null cells were significantly enriched for biological functions canonically associated with PI3K/Akt pathway activity. The catalytic subunit of PI3K, PIK3CA, was 2.5-fold downregulated translationally in PTEN null tumors. Deletion of PIK3CA results in reduced PI3K activity and Akt signaling, therefore it is possible that translational downregulation of PIK3CA represents a feedback mechanism to attenuate PI3K signaling in the absence of PTEN phosphatase (110).

Activation of the PI3K/Akt/mTOR signaling axis is well known to induce a shift in cellular metabolism from oxidative phosphorylation to glycolysis (Warburg effect) (97, 111). The GO geneset describing the electron transport chain was the most enriched geneset amongst translationally downregulated transcripts upon PTEN deletion (Fig 13). GO genesets for the respiratory chain, generation of precursor metabolites and energy, oxidoreductase activity acting on NADP or NADPH, and cellular respiration were similarly enriched. Amongst the most translationally downregulated individual transcripts in PTEN deleted tumors were critical components of the mitochondrial electron transport chain, including Complex I NADH dehydrogenase (NDUFB4), Complex II succinate dehydrogenase (SDHD) and Complex IV cytochrome c oxidase (COX7b) and cytochrome c (CYCS) (Table 1). Translational reduction of these important electron transport chain enzymes would be expected to reduce the cellular capacity for oxidative phosphorylation, consistent with the overall metabolic shift towards glycolysis observed in PTEN null cells. Interestingly, it was reported that dietary restriction in Drosophila results in a translationally mediated increase in oxidative phosphorylation (112). mTOR is known to function as a sensor of cellular nutrient and energy levels (113), and in this

case translational control over oxidative phosphorylation was regulated by the mTOR effector 4E-BP. Although this study was concerned with the effects of dietary restriction on lifespan, it likely represents a situation in which repression of mTOR activity translationally upregulates oxidative phosphorylation. This would be consistent with our findings that increased activity of the PI3K/Akt/mTOR pathway in tumors results in translational downregulation of genes required for oxidative phosphorylation.

Translationally Downregulated in PTEN -/- vs PTEN WT Tumors
Top 10 Normalized Enrichment Scores (GO Genesets)

NAME	NES	FDR q-val
Electron Transport Chain	-1.95	0.120
Microtubule-Based Process	-1.94	0.062
Proteasome Complex	-1.89	0.086
Respiratory Chain	-1.80	0.209
Microtubule-Based Movement	-1.74	0.296
Microtubule Cytoskeleton Organization	-1.74	0.258
Generation Of Precursor Metabolites And Energy	-1.72	0.263
Oxidoreductase Activity, Acting On Nadh Or Nadph	-1.71	0.263
Cellular Respiration	-1.70	0.244
Iron-Sulfur Cluster Binding	-1.70	0.226

Electron Transport Chain
Norm. Enrich. Score: -1.95
FDR q-value = 0.120

Cellular Respiration
Norm. Enrich. Score: -1.80
FDR q-value = 0.244
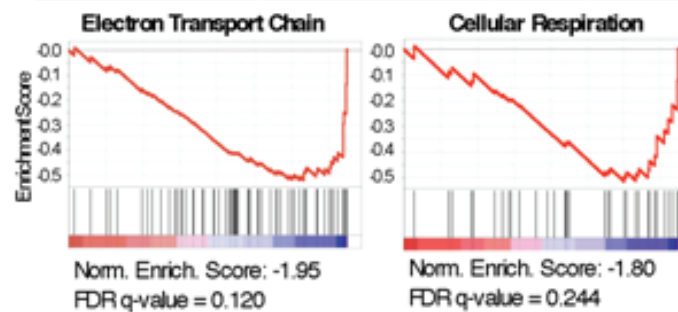
Figure 13. Most translationally downregulated genesets upon PTEN loss
GO genesets associated with oxidative phosphorylation were amongst those most enriched for transcripts translationally downregulated in PTEN-deleted vs PTEN WT tumors. Enrichment plots for electron transport chain and cellular respiration genesets shown. Reproduced from Helmy K, Halliday J, Fomchenko E, Setty M, Pitter K, Hafemeister C, Holland EC. Identification of global alteration of translational regulation in glioma in vivo. PLoS One 2012;7(10):e46965.

Despite the smaller fold changes in TE amongst the most translationally upregulated transcripts in PTEN deleted tumors, GSEA identified genesets enriched with similar significance amongst translationally upregulated transcripts. The GO genesets most enriched by PTEN deletion were associated with hydrolysis and transfer of glycosyl groups (Fig 4D). Secreted and extracellular proteins and lipids are the main substrates for glycosylation. Accordingly, translationally upregulated transcripts were also enriched for extracellular matrix and secretion genesets, as well as hexosyl modifications. Taken together, these data suggest that changes in translation efficiency contribute to an altered extracellular glycosylation profile in PTEN-deleted tumors. Proteoglycans comprise much of the extracellular matrix, and many of the proteins involved in sensing the extracellular environment, including growth factor receptors, integrins, and cadherins, are subject to glycosylation. Glycosylation can affect binding properties, half-life, and localization of these biomolecules. As such, alterations in glycosylation have widespread effects on cell behavior; there is evidence that alterations in glycosylation affect tumor growth, migration, invasion, and angiogenesis (114, 115). Indeed, aberrant glycosylation is known to be correlated with tumor aggressiveness, progression, and survival rates in various cancers (116, 117). Alterations of glycosylation via translational upregulation may be an underappreciated mechanism by which PTEN modulates tumor aggressiveness.

Translationally Upregulated in PTEN -/- vs PTEN WT Tumors
Top 10 Normalized Enrichment Scores (GO Genesets)

NAME	NES	FDR q-val
Hydrolase Activity, Acting On Glycosyl Bonds	2.02	0.034
Glycerolipid Biosynthetic Process	1.90	0.071
Hydrolase Activity, Hydrolyzing O-Glycosyl Compounds	1.86	0.074
Transferase Activity, Transferring Glycosyl Groups	1.84	0.066
Protein Amino Acid Autophosphorylation	1.73	0.165
Proteinaceous Extracellular Matrix	1.72	0.155
Extracellular Matrix	1.71	0.144
Transferase Activity, Transferring Hexosyl Groups	1.66	0.194
Extracellular Region Part	1.64	0.211
Secretion By Cell	1.62	0.231

Glycosyl Hydrolase Activity

Norm. Enrich. Score: 2.02
FDR q-value = 0.03

Glycosyl Transferase Activity

Norm. Enrich. Score: 1.84
FDR q-value = 0.07
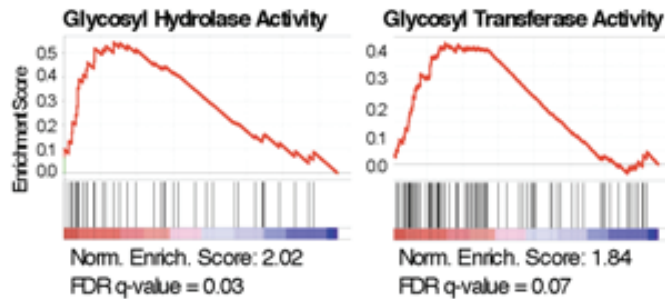
Figure 14. Most translationally upwnregulated genesets upon PTEN loss
Genesets associated with glycolysis predominated amongst GO genesets most enriched for transcripts translationally upregulated in PTEN-deleted vs PTEN WT tumors. Enrichment plots shown for genesets for hydrolase activity acting on glycosyl bonds and transferase activity transferring glycosyl bonds. NES = Normalized Enrichment Score. R = Pearson correlation coefficient. Reproduced from Helmy K, Halliday J, Fomchenko E, Setty M, Pitter K, Hafemeister C, Holland EC. Identification of global alteration of translational regulation in glioma in vivo. PLoS One 2012;7(10):e46965.

Discussion

Regulation of protein levels that dictate cell phenotype and behavior occurs by multiple mechanisms in the cell. Messenger RNA content is most commonly used to approximate gene expression because of the availability of genome-wide microarray and sequencing technologies. This approach, however, ignores important post-transcriptional regulatory mechanisms that have profound impact on gene expression. The technical challenges of interrogating post-transcriptional gene regulation are compounded in complex *in vivo* settings in which cells are often few and tissue is heterogeneous. Here we describe a sensitive method for measuring translational regulation in genetically-defined cell populations *in vivo*. We identified substantial differences in the abundance of mRNA transcripts in total cellular RNA and those bound to ribosomes in both glioma tumor cells and normal brain OPCs, demonstrating the important contribution of translational regulation to gene expression. Furthermore, differentially translated messages were functionally coherent, with transcripts encoding mitochondrial and ribosomal proteins enriched amongst the most efficiently translated mRNAs.

Comparison of TE measurements in glioma cells to their non-tumor cell equivalent OPCs in normal brain uniquely allowed insight into the dysregulation of translation that occurs in tumor cells in a relevant *in vivo* context. We identified broad alterations in TE in glioma that contribute significantly to gene expression changes. Many of the translationally upregulated mRNAs encode proteins that promote the proliferative capacity of the tumor cells by enhancing translation of proteins critical for DNA synthesis, chromosome packaging and segregation and lipid metabolism. The translationally downregulated mRNAs are enriched for processes of synaptic signaling,

reflecting the lack of differentiation of the tumor cells. We further identified alteration of translation of very specific transcripts upon PTEN deletion that are required for oxidative phosphorylation, a biological function classically associated with Akt pathway activity and a hallmark of cancer. We also identified enhanced translation of transcripts associated with glycosylation modification, whose dysregulation is associated with more aggressive cancers. The mechanisms of translational dysregulation in cancer and as a result of tumor suppressor loss are important areas of future investigation that may identify new therapeutic targets. Pharmacological modulation of transcriptional mechanisms have remained elusive, however, modulation of protein translation may be more amenable to therapeutic intervention and offer new approaches to targeting dysregulated gene expression in cancer.

In the present study, we characterized the homeostatic translation state of glioma cells and OPCs *in vivo*. Investigation of the variation in ribosome occupancy of specific transcripts between different cell types and at different stages of development would offer a broader view of the role of translational regulation in contributing to cellular diversity. This method can be further applied to study dynamic regulation of translation in response to stress or therapy. Translational changes may be more efficient than transcriptional regulation for rapidly altering the cellular concentration of proteins, and dynamic changes in translational efficiency have been identified in response to a variety of cellular stresses (74, 118). In fact, translational changes have been reported to be much more significant than transcriptional changes in glioma cell lines exposed to ionizing radiation, the first-line therapy for patients with glioma (76). A better understanding of the translational response to cellular stresses would enhance our understanding of dynamic gene

expression regulation and may have important clinical implications. The TE profiling method presented here provides a powerful tool for interrogating translational regulation in complex *in vivo* systems and may lead to a more complete understanding of homeostatic and dynamic gene expression control in different cell types and in changing conditions.

EXPERIMENTAL RESULTS II - THE *IN VIVO* RADIATION RESPONSE OF PRONEURAL GLIOMA IS CHARACTERIZED BY A PROTECTIVE P53 TRANSCRIPTIONAL PROGRAM AND A PRONEURAL-TO-MESENCHYMAL SHIFT

Glioblastoma multiforme is the most common and aggressive primary brain tumor in adults (2). Current standard of care for patients with GBM is surgical resection followed by local irradiation and temozolomide chemotherapy. Despite aggressive therapy, however, disease progression is universal and median patient survival is only 15 months (2). The vast majority of tumor recurrence occurs within the field of high-dose irradiation, suggesting that intrinsic radioresistance of glioma cells is currently the limiting factor in treatment effectiveness (119, 120). A more complete knowledge of the cellular response to radiation in glioma is critically important to understanding the radioresistant biology of this tumor and devising strategies for radiosensitization.

Features of the native GBM microenvironment such as hypoxia and tumor-stroma interactions are critical modulators of the radiation response (121-123). Additionally, interactions between GBM cells and the tumor microenvironment have been shown to affect the stem-like character of GBM cells (28), which has been linked to radio-resistance (85, 124). Much of the current understanding of the response to radiation of glioma cells comes from work done with glioma cells lines cultured *in vitro,* but glioma cells cultured *in vitro* can demonstrate markedly increased radiosensitivity compared to the same cells grown as intracerebral xenografts (56). For these reasons it is critical to develop an understanding of the response to radiation of glioblastoma cells after radiation *in vivo*.

In vivo studies of the radiation response are complicated by several factors. Glioblastomas are complex mixes of tumor cells and various stromal cell types, including astrocytes, immune cells, endothelial cells, and vascular smooth muscle cells (88). Meaningful analysis of *in vivo* gene expression changes after radiation therefore requires techniques for isolating the expression patterns of individual populations of cells. An important development in recent years has been the discovery that high-grade human gliomas actually encompass 3-4 distinct molecular subtypes of tumors (13, 14). These subtypes are associated with differential activation of oncogenic signaling pathways and correlate with specific genomic alterations. As many of these pathways have previously been implicated in the radiation response, in vivo studies of radiation must take care to use relevant models that resemble the subclasses observed human patients.

Furthermore, *in vivo* expression profiling has been restricted to total mRNA levels. Radiation-induced DNA damage has been reported to regulate translational efficiency both globally and in a transcript-specific manner (125, 126). In glioma cell lines cultured *in vitro*, irradiation was reported to cause a much larger change in the translating pool of RNA than in total cellular RNA, suggesting a more important role for translational regulation than transcriptional regulation in the GBM radiation response (76). Traditional polysome isolation methods, however, are not amenable to translational profiling *in vivo*.

In order to study the global radiation response in an *in vivo* model of a defined GBM subtype, we combined translating ribosome affinity purification (TRAP) methodology (82) with an RCAS/tv-a genetic model of the proneural GBM subtype (69). Irradiation of these tumors induced a rapid and transient cell cycle arrest and

asynchronous apoptosis. Interestingly, translational regulation was a relatively minor contributor to overall gene expression changes. Changes in total transcript levels dominated expression changes observed, with genesets for apoptosis and regulation of cell cycle upregulated. p53 and E2F targets were amongst the most frequently altered, with p53 appearing to regulate the most highly induced transcripts after radiation. We also observed a pronounced shift in glioma subtype from proneural to mesenchymal. This shift occurred rapidly - within 6 hours - and was highly significant regardless of genetic background. The proneural to mesenchymal shift occurred in tumor cells and was not a result of stromal enrichment after radiation.

Results

Response to IR is heterogeneous by cell type in GBM.

To study the glioma radiation response *in vivo*, we introduced platelet derived growth factor-B (PDGF-B) retrovirus into mice harboring somatic deletion of the Ink4a/Arf locus to generate highly penetrant high-grade gliomas that closely resemble the proneural subtype of GBM (13, 14, 69, 72, 127). We chose to use a single dose of radiation to enable time course studies after radiation, and had previously shown that a single dose of 10Gy radiation induces cell cycle arrest in these tumors (80). Tumor-bearing mice were subjected to a single dose of 10 Gy total body irradiation (TBI) and tumor tissue was collected at time points after treatment for immunohistochemical staining. Radiation caused a complete mitotic arrest, with nearly undetectable levels of phosphorylated-histone H3 (pH3) at 6 hrs after treatment (Fig. 15A). Proliferating cells reappeared by 24 hrs after IR and returned to pre-treatment levels by 72 hours and 6 days

71

after IR (Fig. 15A). By contrast, the apoptosis marker TUNEL was detected in only a small percentage of cells, but apoptosis was observed at all time points measured after IR, demonstrating an asynchronous mode of death (Fig. 15B). This limited, delayed apoptosis in response to IR contrasts sharply with the high levels of apoptosis we observe after irradiating the more radiosensitive medulloblastoma brain tumor (85). Previous experiments demonstrated that this radiation dose confers only a modest survival benefit of approximately 15 days, consistent with the radioresistant phenotype of human GBM and the relatively minimal apoptosis observed in these experiments (80).
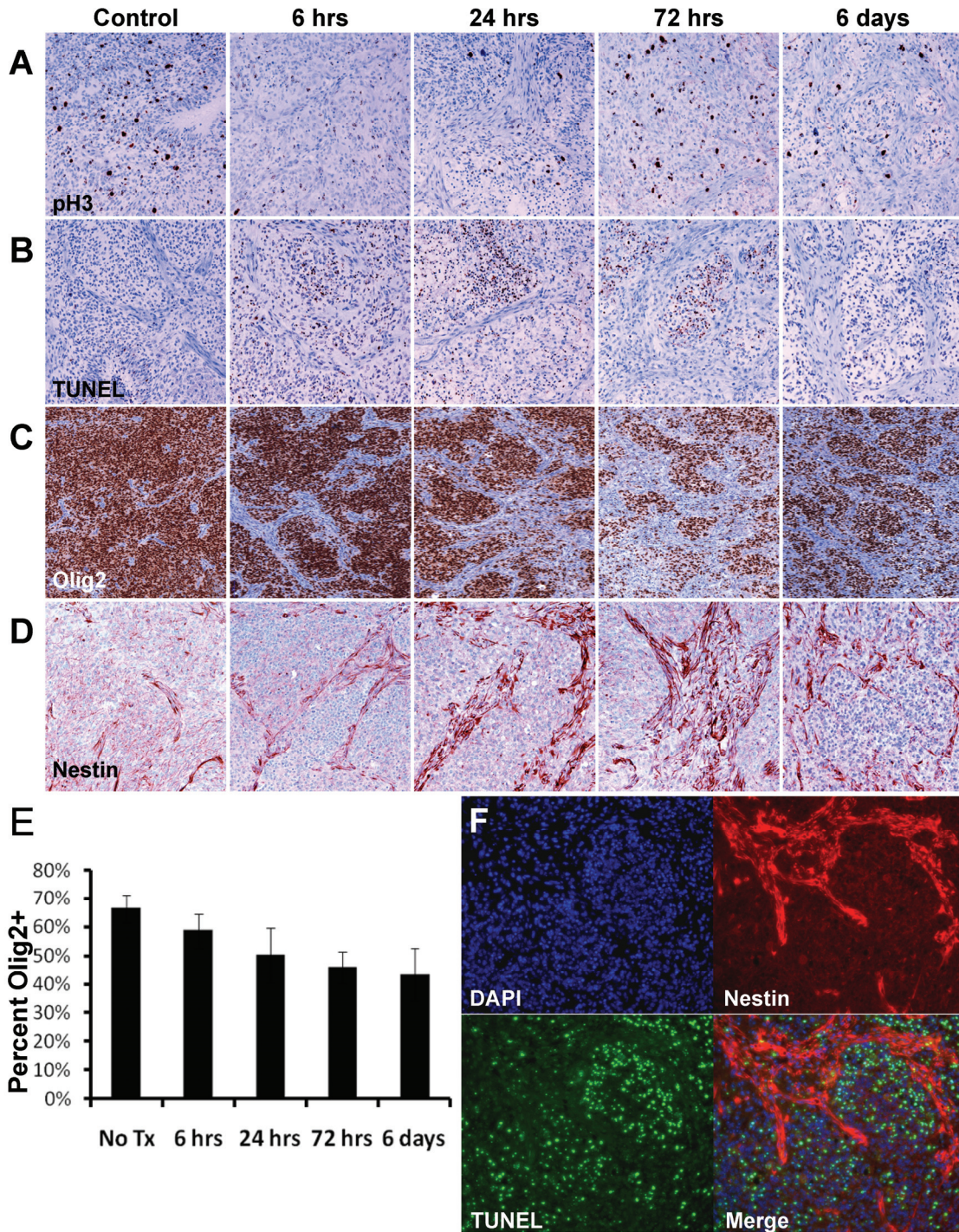
Figure 15. 10Gy IR of mouse glioma induces transient cell cycle arrest, asynchronous apoptosis, and depletion of Olig2+ cells
Staining for (A) phoshpo-histone H3, (B) TUNEL, (C) Olig2, and (D) Nestin. (E) Quantification of Olig2+ nuclei in glioma following IR. Error bars are standard deviation. (F) TUNEL+ cells predominantly in tumor bulk rather than Nestin+ perivascular region 24hrs post IR.

Human GBM is a heterogeneous tumor composed of several cell types and displaying multiple histological features. PDGF-driven mouse gliomas recapitulate this complexity, containing tumor bulk (TB) regions that are nucleus-dense and stain positive for olig2 and PDGF receptor alpha, and perivascular (PVN) regions that have a splindloid morphology and stain positive for nestin, smooth muscle actin, and PDGF receptor beta (88). Immunoflourescent co-staining for TUNEL and nestin revealed that IR-induced apoptosis occurs almost exclusively in the TB and minimally in the nestin-positive PVN (Fig. 15C). This accumulation of cell death in the TB causes a progressive reduction in the percentage of tumor cells staining positive for olig2, dropping from 66% prior to treatment to 43% after 6 days (p = 0.00037) (Fig. 15D-E). The regions of spindloid cells marked by nestin staining expand concurrently.

Tumors are composed of both transformed cells and recruited stroma. The PDGF oncogene used to generate gliomas in this mouse model contains a hemaglutinin (HA) tag, facilitating discrimination between oncogene-expressing tumor cells and non-tumor stromal cells. Immunohistochemical staining reveals that most, if not all, PDGF-HA expressing tumor cells reside in the Olig2+ TB both before and after IR (Fig. 16A,B). FACS analysis of gliomas generated with a bicistronic retroviral vector expressing PDGF and RFP in mice expressing GFP driven by the Olig2 promoter had previously confirmed the high degree of co-expression (88).
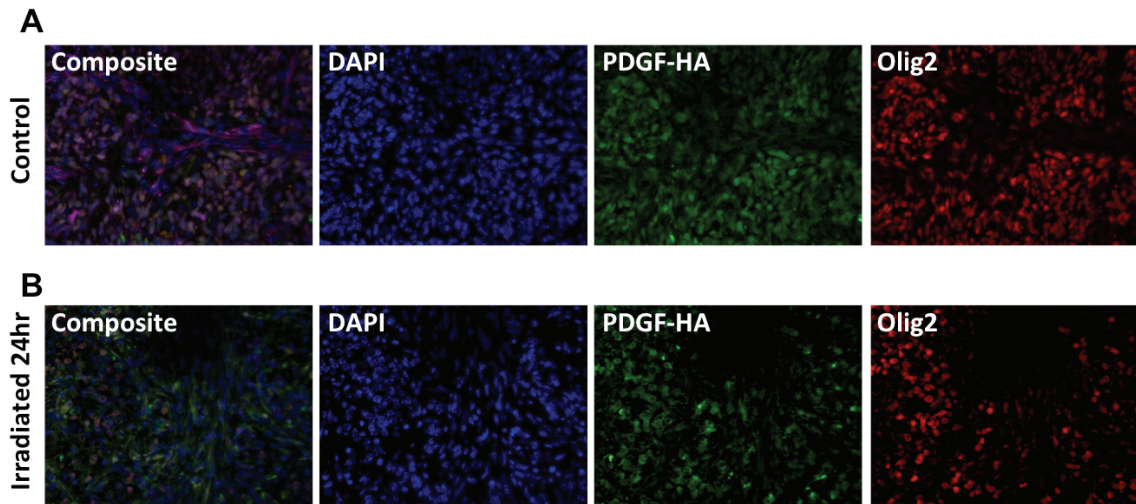
Figure 16. Olig2 is a Marker for RCAS-infected Cells Before and After IR
Immunofluorescence staining of unirradiated (A) and 10Gy irradiated (B) RCAS-PDGF gliomas shows high degree of overlap of Olig2 staining and the HA tag within the RCAS-PDGF construct both before and 24hrs after irradiation.

Taken together, this data suggests that PDGF-driven mouse glioma models the radioresistant phenotype of human GBM. Furthermore, we demonstrate that the cellular response to IR is heterogenous, with oncogene-expressing tumor cells responding differently than non-tumor stroma. It is therefore necessary to study the radiation biology of the different cell populations independently, as any differences in radiation response by cell type and changes in cellular composition after radiation would confound interpretation of the radiation biology of GBM studied as homogenous entity.

Regulation of Total Transcript Levels Dominates the Radiation Induced Changes in Ribosome-bound RNA

In order to study global gene expression changes, we adapted the TRAP methodology to the RCAS-PDGF glioma model, as previously described (88). Briefly, PDGF-induced gliomas were generated in Olig2 bacTRAP mice (78). Tumors were collected from untreated control mice and treated mice 6 hours after 10Gy irradiation. Tumor tissue was divided to collect both total RNA from sorted Olig2+/GFP+ cells and translating RNA by immunoprecipitation of GFP-tagged ribosomes from the same cell population. Paired ribosome-bound and total cellular RNA samples were analyzed by expression microarray.

Changes in the levels of individual transcripts present on polysomes can be divided into changes in the level of each transcript, and the efficiency with which each transcript is recruited to ribosomes for translation, i.e. translation efficiency. Previously, it had been reported that a much larger number of transcripts showed significant changes in translational efficiency than in overall transcript level after irradiation *in vitro* (76). In

our *in vivo* system, changes in translation efficiency contributed relatively little to overall changes in mRNAs present in polysomes after irradiation (Fig 17A-B). Changes in total mRNA and polysome-associated mRNAs were highly correlated (Pearson correlation of 0.82) (Fig 17A). 58 transcripts showed translational efficiency changes of more than 2-fold, compared to 429 transcripts showing 2 fold changes at the total mRNA level. Similarly low levels of translational efficiency changes were seen in irradiated tumors that additionally had PTEN deleted by co-injection of an RCAS-Cre virus (Fig 18A) (88). For reference, when comparing normal brain Olig2+ oligodendrocyte precursor cells to their PDGF-transformed tumor counterparts, 2239 transcripts exhibited greater than 2-fold changes in translational efficiency (88). Thus, the gene expression response to radiation of these gliomas does not appear to have a large translational regulation component *in vivo*.
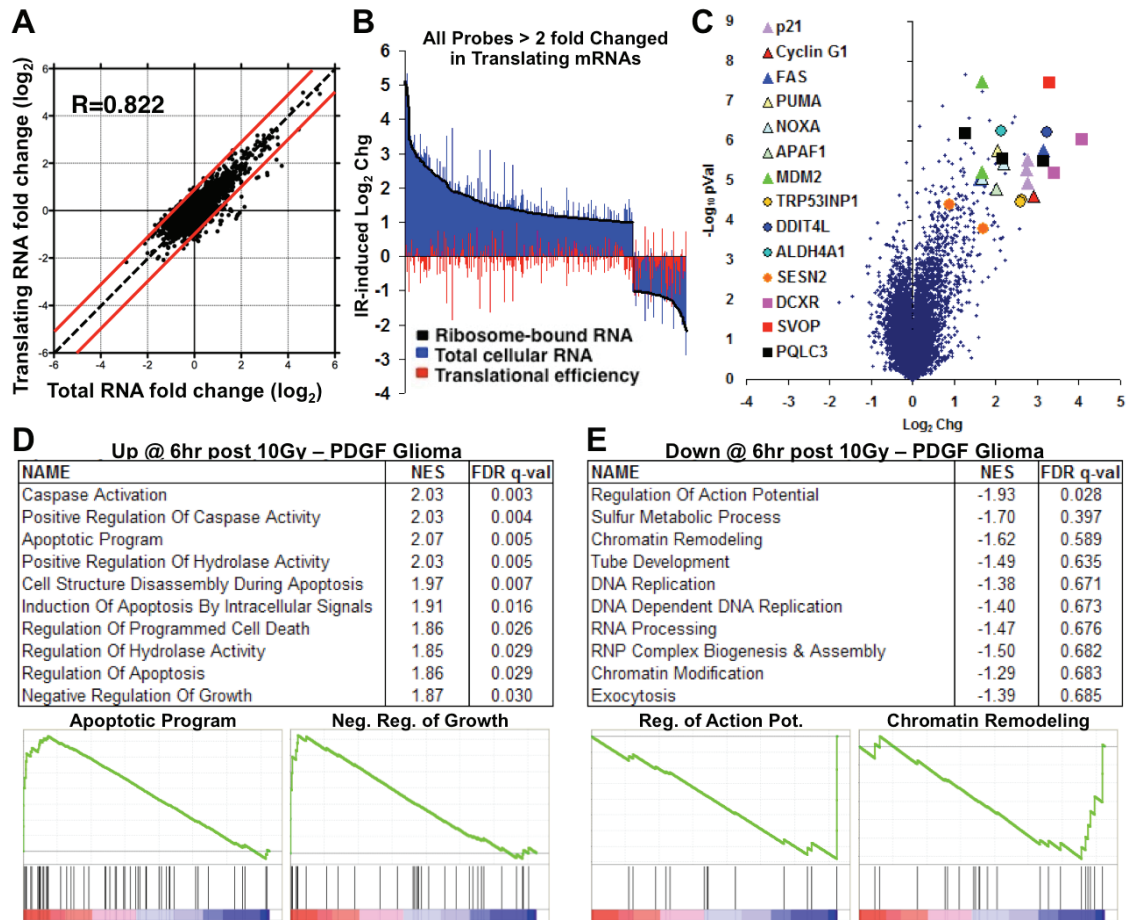
Figure 17. *In vivo* **Gene expression changes induced by IR in RCAS-PDGF Ink4a/Arf$^{-/-}$ gliomas**
Irradiated samples collected 6 hours after 10Gy IR. (A) Log change in total mRNA vs. log change in ribosome-bound translating mRNA 6hrs after 10Gy IR. R = Pearson correlation. (B) All probes altered more than 2-fold in translating mRNA, and corresponding changes in total mRNA and translational efficiency. (C) Volcano plot of expression changes 6hrs after 10Gy IR. Genesets most significantly enriched (D) and depleted (E) amongst translating mRNAs after IR, with selected enrichment plots. NES is Normalized Enrichment Score, FDR q-val is calculated false discovery rate.

78
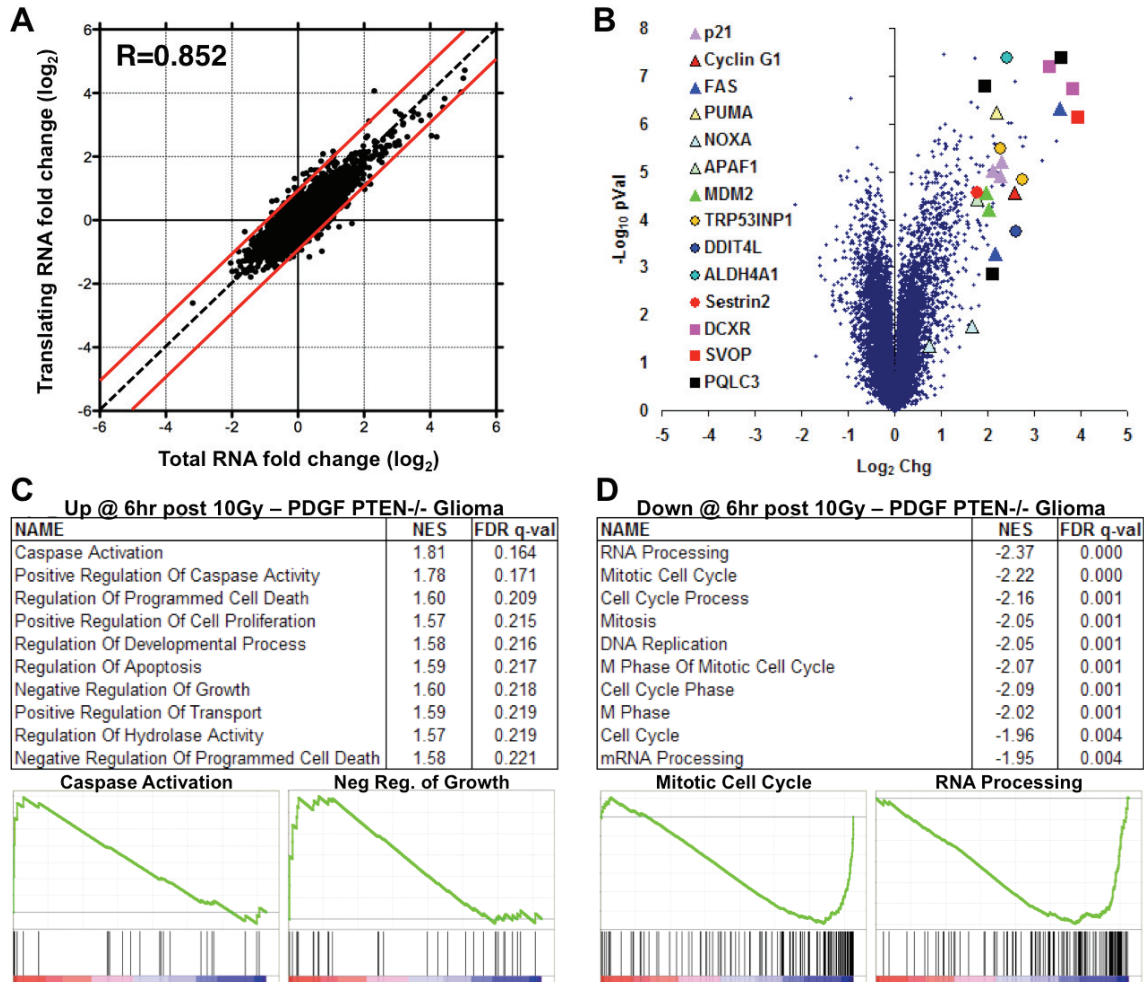
Figure 18. *In vivo* **Gene expression changes induced by IR in RCAS-PDGF Ink4a/Arf^{-/-} PTEN^{-/-} gliomas**

Irradiated samples collected 6 hours after 10Gy IR. (A) Log change in total mRNA vs. log change in ribosome-bound translating mRNA 6hrs after 10Gy IR. R = Pearson correlation. (B) All probes altered more than 2-fold in translating mRNA, and corresponsing changes in total mRNA and translational efficiency. (C) Volcano plot of expression changes in translating mRNA 6hrs after 10Gy IR. Genesets most significantly enriched (D) and depleted (E) amongst translating mRNAs after IR, with selected enrichment plots.

Gene Expression Changes are Primarily Apoptotic Programs and Cell Cycle Arrest

We next sought to characterize the gene expression changes induced by radiation *in vivo*. Few genes were highly downregulated 6hrs post 10Gy IR in the Olig2+ TB, but a number of genes were highly upregulated (Fig 17C, Fig 18B). The most upregulated genes by fold change included several genes known to be involved in cell cycle arrest and apopotosis. Fas, Puma, Noxa, and Apaf1 are all associated with induction of apoptosis, while cyclin G and p21 are cell cycle inhibitors, and MDM2 and TRP53INP1 have roles in both functions. Additionally, several genes such as Ddit4L, Aldh4A1, and Sestrin2 were upregulated, which like TRP53INP1, are involved in the response to various stresses including DNA damage and redox imbalances Some genes of unknown relevance were highly upregulated as well; carbonyl reductase 2 (DCXR) and synaptic vesicle 2-related protein (SVOP) were the most upregulated genes and have no known function in the radiation response, while PQ loop repeat containing 3 (PQLC3) is largely uncharacterized. To validate the reliability of the array results, we selected some of the most highly upregulated genes and related genes, and perfomed qPCR on RNA extracted from treated and control neurospheres derived from PDGF driven Ink4a/Arf-/- gliomas. The fold induction in neurospheres at 6 hours closely matched the fold change seen on the array for each transcript examined (Fig. 19A,B).
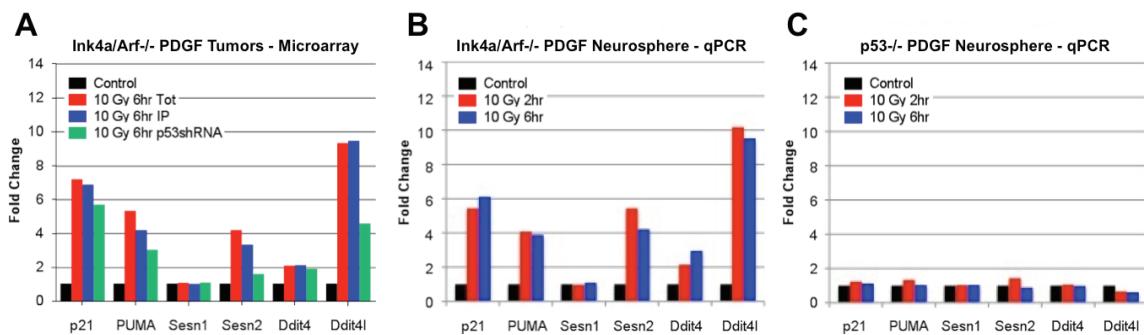
Figure 19. Highly IR sensitive *in vivo* transcripts and family members show similar in vitro radiation sensitivity

(A) Fold change of selected highly IR sensitive transcripts (p21, PUMA, Sesn2, and DDit4L) and family members (Sesn1, DDit4) after 10Gy irradiation of Ink4a/Arf-/- PDGF driven tumors. Tumors compromised for p53 response (p53shRNA) showed muted upregulation after IR. RT-qPCR for same transcripts from control and irradiated neurospheres cultured from Ink4a/Arf-/- PDGF driven tumors showed the same pattern of radiation sensitivities with similar fold changes (B). (C) RT-qPCR for same transcripts from PDGF-driven p53-/- neurospheres showed complete ablation of IR sensitivity.

To understand what classes of genes are altered by radiation, we performed geneset enrichment analysis (GSEA) (86). In PDGF driven gliomas with both PTEN intact or deleted, genesets associated with caspase activation and induction of apoptosis were the highest scoring genesets, while the geneset for negative regulation of growth also was significantly upregulated (Fig. 17D, 18C). Curiously, the geneset for positive regulation of cellular proliferation was also the 13th most upregulated geneset. However, an inspection of the leading edge of this geneset revealed that its significance is driven largely by the upregulation of signaling molecules rather than bona-fide cell-cycle genes (p21 is also included in this geneset). Irradiated Olig2+ tumor cells increased the expression of a range of growth factors and cytokines, including PDGF-A, CSF1, PGF, LIF, and EGFR were highly upregulated.

With relatively few individual transcripts significantly downregulated, the only geneset highly significantly enriched for downregulation in PDGF gliomas was "Regulation of Action Potential". The significance of this geneset was driven by downregulation of genes associated with oligodendrocyte development and myelination, including MBP, MOG, S100b, and SHH, raising the possibility of a loss of differentiation in response in these cells to irradiation (Fig. 17E). PTEN-/- tumors had more significantly downregulated transcripts and genesets, and genesets associated with mitosis were highly downregulated (Fig. 18D). Both PTEN WT and PTEN-/- tumors showed downregulation of RNA Processing and DNA replication genesets. Additionally, during initial experiments we also generated expression profiles from the less aggressive PDGF Ink4a/Arf+/- model (72), which showed similar regulation of both individual transcripts and broader genesets after radiation (Fig. 20A, B).

A

B

Up @ 6hrs post 10Gy - PDGF Ink4a/Arf+/- Glioma

NAME	NES	FDR q-val
Caspase Activation	2.16	0.002
Positive Regulation Of Caspase Activity	2.14	0.002
Regulation Of Growth	2.17	0.002
Regulation Of Cell Growth	2.18	0.005
Negative Regulation Of Growth	2.04	0.009
Positive Regulation Of Hydrolase Activity	2.02	0.009
Anti Apoptosis	2.00	0.010
Growth	1.98	0.015
Regulation Of Programmed Cell Death	1.94	0.016
Negative Regulation Of Programmed Cell Death	1.96	0.016

Down @ 6hrs post 10Gy - PDGF Ink4a/Arf+/- Glioma

| NAME	NES	FDR q-val
Mitosis	-2.52	0.000
DNA Replication	-2.47	0.000
M Phase Of Mitotic Cell Cycle	-2.46	0.000
Mitotic Cell Cycle	-2.44	0.000
Cell Cycle Process	-2.44	0.000
Cell Cycle Phase	-2.42	0.000
M Phase	-2.41	0.000
Cell Cycle GO	-2.32	0.000
DNA Dependent DNA Replication	-2.27	0.000
DNA Metabolic Process	-2.16	0.000

Figure 20. *In vivo* **Gene expression changes induced by IR in RCAS-PDGF Ink4a/Arf**^{+/-} **gliomas.** Irradiated samples collected 6 hours after 10Gy IR. (A) Volcano plot of expression changes in translating mRNA. (B) Genesets most significantly enriched and depleted amongst translating mRNAs after IR.

To further determine which gene changes are specific for irradiation, and which are general features of cells undergoing arrest, we used an alternative method for generating cell cycle arrest. We used mTOR inhibition with temsirolimus for this comparison. Temsirolimus is non-genotoxic and induces cell-cycle arrest in PDGF-driven gliomas (79). Olig2+ cells from PDGF induced PTEN -/- gliomas that were either irradiated or temsirolimus-treated shared many of their respective downregulated genes (Fig. 21). These shared downregulated genes were enriched for genesets associated with cell cycle, nuclear division, and mitosis. While much of the downregulated genes were overlapping, the upregulated genes in each case were largely unique to the given treatment. The genes upregulated after temsirolimus treatment were not significantly enriched for any genesets. By contrast, the genes that were relatively upregulated in the irradiated tumors were enriched for apoptosis, DNA-damage, and checkpoint related genesets.

A

CCI vs Ctrl (-Log₁₀ pval) → $CCI\ vs\ Ctrl\ (-Log_{10}\ pval)$

IR vs Ctrl (-Log₁₀ pval) → $IR\ vs\ Ctrl\ (-Log_{10}\ pval)$

- ▲ Up in IR
- • Up in CCI
- ■ Down in IR vs Ctrl and CCI vs Ctrl

C GO Enrichment: Up in CCI vs Ctrl (p-value $< 10^{-10}$) in PTEN-/-Gliomas

GO Description	P-value	FDR q-value
Cellular Metabolic Process	1.6E-05	0.18
Regulation Of Cellular Metabolic Process	3.9E-05	0.22
Cellular Macromolecule Metabolic Process	4.4E-04	0.27
Organic Substance Biosynthetic Process	5.8E-04	0.27
Aromatic Compound Biosynthetic Process	4.2E-04	0.27
Heterocycle Biosynthetic Process	4.0E-04	0.27
Regulation Of Metabolic Process	2.4E-04	0.27
MAPK Cascade	2.6E-04	0.27
Primary Metabolic Process	5.7E-04	0.27
Glycosyl Compound Metabolic Process	3.7E-04	0.28

D GO Enrichment: Up in IR vs Ctrl (p-value $< 10^{-10}$) in PTEN-/-Gliomas

GO Description	P-value	FDR q-value
Sign. Trans. By P53 Class Mediator	1.5E-10	1.7E-06
Sign. Trans. Involved In Mitotic Cell Cycle Checkpoint	4.1E-09	9.2E-06
Sign. Trans. Involved In DNA Integrity Checkpoint	8.0E-09	1.1E-05
Intrinsic Apoptotic Sign. Pthwy In Respon. to DNA Damg.	2.0E-09	1.2E-05
Sign. Trans. Involved In Mitot. G1 DNA Damg. Chkpnt.	4.1E-09	1.2E-05
Sign. Trans. Involved In DNA Damage Checkpoint	8.0E-09	1.3E-05
Sign. Trans. Involved In Cell Cycle Checkpoint	8.0E-09	1.5E-05
DNA Damage Response, Sign. Trans. By P53 Class Mediator Resulting In Cell Cycle Arrest	4.1E-09	1.5E-05
Positive Regulation Of Biological Process	1.9E-08	2.5E-05
Response To DNA Damage Stimulus	4.1E-08	4.2E-05
Apoptotic Signaling Pathway	3.7E-08	4.3E-05

B GO Enrichment: Down in IR vs Ctrl and CCI vs Ctrl (p-values $< 10^{-5}$) in PTEN-/- Gliomas

GO Description	P-value	FDR q-value
Cell Cycle	2.9E-12	1.6E-08
Dna Metabolic Process	2.1E-12	2.3E-08
Cell Cycle Process	1.8E-09	6.8E-06
Regulation Of Cell Cycle Process	9.5E-09	1.5E-05
Mitosis	6.9E-09	1.6E-05
Cell Division	8.8E-09	1.7E-05
Organelle Organization	1.4E-08	1.7E-05
Nucleic Acid Metabolic Process	1.4E-08	1.9E-05
Nuclear Division	6.9E-09	2.0E-05
Organelle Fission	2.0E-08	2.2E-05
Nucleobase-Containing Compound Metabolic Process	6.0E-08	5.6E-05

Figure 21. IR and Temsirolimus treatment share downregulated genes, but upregulated genes are unique to each treatment and not a general feature of cell cycle arrest

(A) Scatterplot of expression changes in PDGF-driven PTEN-/- gliomas after treatment with temsirolimus (CCI-779) vs expression changes after treatment with IR. Values are negative Log_{10} p-values multiplied by the sign of the expression change. (B) Genes downregulated after both treatments (p-value $< 10^{-5}$ for both, green in scatterplot) were enriched for cell cycle and mitosis related genesets. (C) Genes upregulated after CCI treatment (p-value $< 10^{-10}$, blue in scatterplot) were not significantly enriched for any genesets, with weak enrichment for genesets related to regulation of metabolism and biosynthesis. (D) Genes upregulated after radiation treatment (p-value $< 10^{-10}$, red in scatterplot) were significantly enriched for genesets related to DNA damage, cell cycle checkpoints, and apoptosis. Categorical overrepresentation analysis performed using GOrilla (87).

p53 and E2F activity are Major Transcriptional Drivers of the Radiation Response

Having established that the *in vivo* radiation response is largely determined by changes in total mRNA levels rather than translational modulation, we sought to understand which transcription factors might be responsible for the changes in transcript levels observed. GSEA was performed to identify transcription factors whose binding motifs were most commonly found in the promoters of genes regulated by radiation. Genes containing a p53 binding site in their promoter were among the most significantly upregulated in both PTEN WT and deleted tumors, consistent with our previous observation of several p53 targets amongst the most significantly upregulated transcripts (Fig 22A, B, Fig 23A). Immunohistochemistry of irradiated tumors showed that p53 becomes nuclear localized after irradiation, and is restricted to the tumor bulk rather than the perivascular regions (Fig 23C). To confirm p53 regulation of specific transcripts, we used irradiated and unirradiated p53-/- tumorspheres as in (80), and performed qPCR for the same panel of genes as in Fig. 19A-B. Each gene that was upregulated after IR in p53 intact neurospheres was unaltered in p53-/- neurospheres (Fig 19B, C).

A

Transcription Factor Targets
Up in Ribosome mRNA 6hrs 10Gy

NAME	NES	FDR q-val
IRF_Q6	1.78	0.054
p53_Q2	1.78	0.076
MEF2_04	1.67	0.076
ICSBP_Q6	1.69	0.080
CEBP_Q3	1.67	0.084
p53_02	1.65	0.090
ISRE_01	1.80	0.112
IRF_Q6	1.69	0.112
STAT3_01	1.56	0.163
NF1_Q6	1.58	0.166
CEBPB_02	1.57	0.167

Transcription Factor Targets
Down in Ribosome mRNA 6hrs 10Gy

NAME	NES	FDR q-val
E2F1_Q4	-1.70	0.112
TFIII_Q6	-1.57	0.119
E2F_Q4	-1.38	0.146
KLF8_Q6	-1.38	0.150
E2F_Q3	-1.58	0.150
E2F_Q6	-1.39	0.153
E2F_02	-1.37	0.154

B

p53   E2F

C

Ctr ■ IR ■ PDGF ■ p53shRNA ■ Ribo ■ Total

D

PDGF + p53shRNA
Survival post IR (day 18)

— IR
— no IR

**p=0.0066

E

50 Most Induced Transcripts in Total RNA from PDGF Gliomas

■ PDGF
■ PDGF-p53sh

87
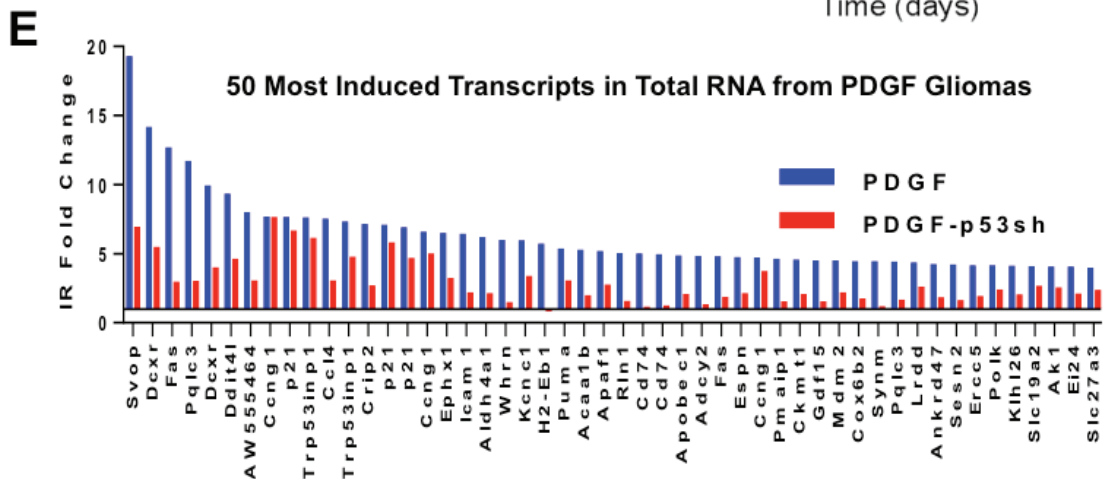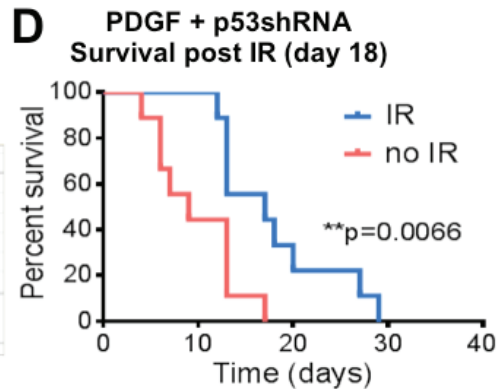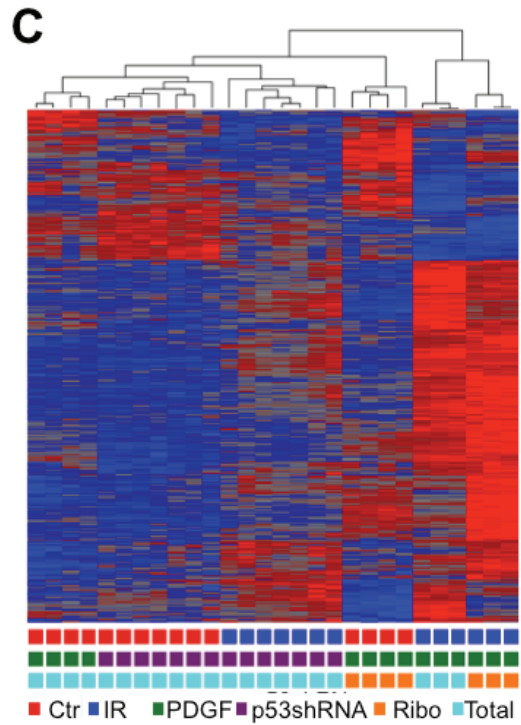
Figure 22. p53 and E2F are major drivers of *in vivo* radiation response
(A) Transcription factors whose targets are most significantly enriched and depleted amongst translating mRNAs after IR. (B) Enrichment plots for targets of p53 and E2F.   (C) Unsupervised hierarchical clustering on genes significantly altered by IR. (D) Kaplan-Meier survival curves of unirradiated and irradiated PDGF/p53shRNA gliomas in Ink4a/Arf-/- mice after randomization and treatment on day 18 post-injection/birth. (E) Comparison of the fold changes of the 50 most induced transcripts 6hrs after 10Gy IR in PDGF driven gliomas, and the corresponding fold change in PDGF/p53shRNA tumors.

A Transcription Factor Targets
Up in Ribosome mRNA 6hrs 10Gy

PTEN -/-

NAME	NES	FDR q-val
CEBP_Q3	1.58	0.127
NF1_Q6	1.58	0.129
BACH2_01	1.59	0.132
MYOD_Q6	1.54	0.143
ATF3_Q6	1.59	0.144
p53_Q2	1.67	0.147
CREBP1_01	1.54	0.152
p53_02	1.54	0.161
CEBPB_02	1.61	0.167
AP1_Q6	1.63	0.177

Transcription Factor Targets
Down in Ribosome mRNA 6hrs 10Gy

PTEN -/-

NAME	NES	FDR q-val
E2F_Q6	-2.37	0.000
E2F1DP1RB_01	-2.37	0.000
E2F_Q4	-2.34	0.000
E2F_03	-2.28	0.000
E2F_Q4_01	-2.25	0.000
E2F1_Q4	-2.24	0.000
E2F_02	-2.24	0.000
E2F1_Q6	-2.23	0.000
E2F1DP2_01	-2.23	0.000
E2F1_Q4_01	-2.23	0.000

Figure 23. Transcriptional drivers of the radiation response
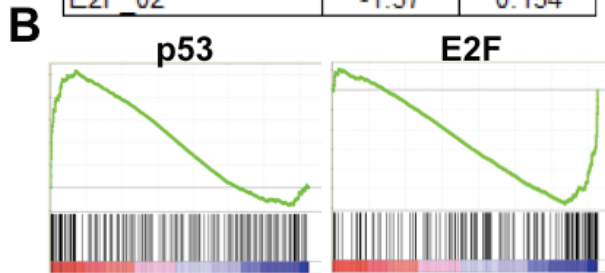(A) Transcription factors whose targets are most significantly enriched and depleted amongst translating mRNAs after 10Gy IR of PTEN-/- mice, and enrichment plots for targets of p53, CEBP, and E2F. (B) Time course of p53, IRF, and E2F targets, in PDGF Ink4a/Arf$^{+/-}$ gliomas. Average of total and translating mRNA pools, dotted lines represent standard error. (C) Immunohistochemistry for p53 shows nuclear localization 6hrs post 10Gy IR.

Several other transcription factor binding motif genesets were significantly upregulated after 6 hours, including genesets for CEBP, myocyte enhancer factor 2, interferon regulatory factor (IRF), and STAT3. IRF is a tumor suppressor that has been shown to enhance the transcriptional activity of p53 (128). Genesets for downreglated genesets were dominated by those associated with E2F-binding motifs.

In our experiments with Ink4a/Arf$^{+/-}$ mice, we collected RNA at both 2 hours and 6 hours after 10Gy IR. The Ink4a/Arf$^{+/-}$ dataset was consistent with the Ink4a/Arf$^{/-}$ dataset; for transcription factors with targets upregulated in Ink4a/Arf$^{/-}$ tumors, their targets were already upregulated by 2 hours in Ink4a/Arf$^{+/-}$ tumors, and further upregulated at 6 hrs as the radiation response progressed (Fig 23B). Likewise, E2F targets were down by 2 hours and further decreased at 6hrs.

p53 Drives Most of the Highly Induced Genes in the In Vivo Radiation Response

The gene encoding p53 is altered in 35%-50% of proneural tumors, including tumors that exhibit downregulation of p53 expression without genomic changes (14, 129). These alterations in p53 expression may co-occur with Ink4a/Arf loss and are independent of Ink4a/Arf status. As p53 is such a large component of the radiation response in our PDGF-Ink4a/Arf-/- glioma model, we compared the radiation response of tumors with compromised p53 to p53 wild type tumors. We generated gliomas using a p53shRNA-RFP RCAS retroviral vector in combination with RCAS-PDGF in Ink4a/Arf-/- Olig2-TRAP reporter mice. Consistent with previous work, p53shRNA-containing tumors exhibited shorter latency compared to PDGF-only tumors, and a course of fractionated radiotherapy conveyed a survival benefit of only 8 days, as compared with

90

15 days for PDGF-only tumors (Fig 22D, (80)). Immunohistochemistry of p53shRNA-PDGF tumors revealed lower levels of nuclear p53 after IR (Fig 24B). To perform expression profiling, we collected RFP/GFP double positive cells via FACS to isolate tumor cells definitively infected with the p53shRNA virus. p53 transcript levels were significantly lower in p53shRNA-PDGF tumors compared to PDGF-only tumors (Fig 24A). Interestingly, unsupervised clustering placed p53shRNA tumors closer to unirradiated tumors than irradiated tumors with p53 intact, underlining the importance of p53 in shaping the overall radiation response (Fig 22C).

A

B

PDGF | PDGF + p53shRNA

2 hrs

6 hrs

C

Up 6hrs post 10Gy - PDGF + p53shRNA - GO BP Genesets

NAME	NES	FDR q-val
Negative Regulation Of Growth	2.00	0.024
Regulation Of Growth	2.04	0.024
Positive Regulation Of Developmental Process	1.95	0.037
Positive Regulation Of Hydrolase Activity	1.92	0.038
Positive Regulation Of Caspase Activity	1.93	0.038
Caspase Activation	1.88	0.050
Apoptotic Program	1.86	0.052
Growth	1.88	0.053
Apoptosis_GO	1.84	0.055
Programmed Cell Death	1.86	0.055

Up 6hrs post 10Gy - PDGF + p53shRNA - GO BP Genesets

NAME	NES	FDR q-val
RNA Processing	-2.09	0.002
Mitosis	-2.09	0.002
M Phase Of Mitotic Cell Cycle	-2.11	0.003
Mitotic Cell Cycle	-1.96	0.011
RNA Splicing	-1.95	0.011
M Phase	-1.90	0.015
Microtubule Cytoskeleton Org. And Biogenesis	-1.91	0.016
Cell Cycle Process	-1.90	0.017
mRNA Processing GO	-1.87	0.017
Nucleobase/side/tide & Nucleic Acid Transport	-1.77	0.036

D

Enriched after IR in PDGF only vs p53shrNA

NAME	NES	p-val	FDR q-val
P53	1.97	0.000	0.009
TTAYRTAA_E4BP4	1.84	0.000	0.015
E2A	1.78	0.000	0.016
YY1	1.82	0.000	0.016
LHX3	1.87	0.000	0.016
CIZ	1.85	0.000	0.016
NKX61	1.81	0.000	0.016
TEF	1.78	0.000	0.016
NKX25	1.79	0.000	0.016
CEBPA	1.79	0.000	0.017
NFMUE1	1.75	0.000	0.017
PAX4	1.76	0.000	0.017
CEBP	1.89	0.000	0.017
CREBP1	1.75	0.000	0.018
CDC5	1.82	0.000	0.018

Figure 24. PDGF driven p53shRNA Tumors have Reduced p53 Activity
(A) p53 probe intensities significantly reduced in PDGF p53shRNA tumors compared with PDGF only and PDGF PTEN-/- tumors. ** = P < 0.01, **** = p <0.0001 by Tukey's multiple comparisons test. (B) Immnunohistochemistry for p53 shows reduced p53 induction in response to IR at 2 and 6 hours. (C) Genesets enriched and depleted by IR in PDGF p53shRNA tumors at 6hrs. (D) Transcription factors whose targets are most differentially induced in PDGF only gliomas vs PDGF p53shRNA tumors.

The most upregulated transcripts after IR in the p53shRNA-PDGF gliomas were similar to those of the PDGF-only tumors, but the p53 short hairpin markedly inhibited the upregulation of virtually all of the most highly upregulated transcripts in p53 intact tumors (Fig 22E), suggesting that p53 is required for the vast majority of the largest gene expression changes in p53 intact tumors. The induction of each previously ex-vivo validated p53 target was also lower in the p53shRNA/PDGF tumors (Fig 19A).

Radiation Triggers a Shift from the Proneural Subtype towards the Mesenchymal Subtype

When Phillips et al. first described the major high-grade glioma subtypes, they noted that some proneural tumors tended upon recurrence to shift towards a mesenchymal gene signature (13). Because that report and subsequent works have relied on gene expression profiling of whole tumor lysates, and because the mesenchymal subgroup tends to express high levels of markers typical of perivascular stromal cells types in glioma (13, 88), it is unclear whether any shifts in subtype, and indeed whether significant differences between the groups in general, are due in part to varying amounts of stroma which expresses mesenchymal markers. Recently it was reported that Stat3 and CEBPB acted as master regulators of mesenchymal transformation, whose expression could drive neural stem cells along a mesenchymal lineage, and whose inhibition in tumor cells caused both a loss of mesenchymal signature and tumor aggressiveness (130). As such, we noted with interest the presence of both CEBPB and Stat3 targets high on out list of most upregulated transcription factor motifs in the Olig2-expressing cells specifically after radiation (Fig 25A-B, 22A). Immunohistochemistry for

nuclear phospho-Stat3 was increased at 6hrs, and significantly increased at 24hrs (Fig

25E, F).
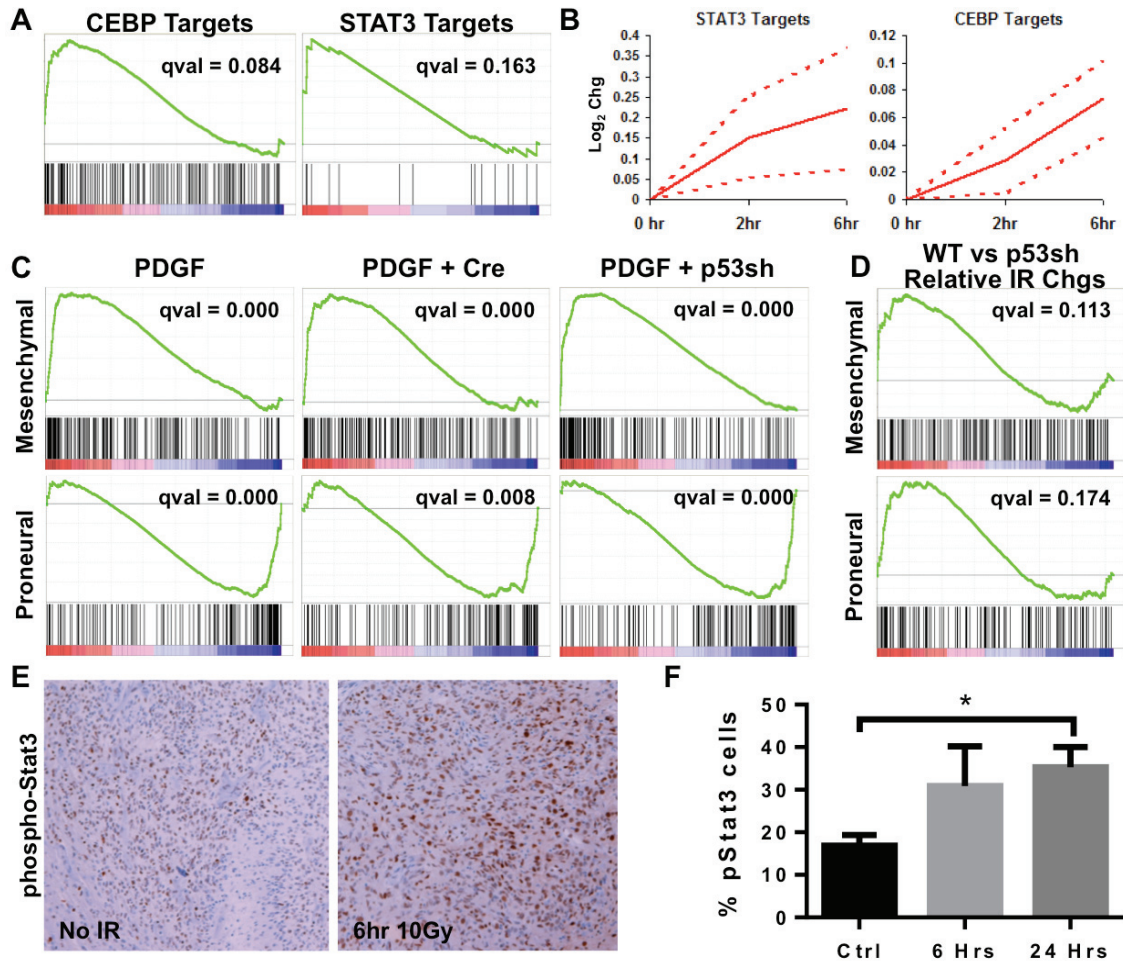
Figure 25. IR induces Proneural to Mesenchymal Shift in PDGF gliomas
(A) Enrichment plots of CEBP and STAT3 targets in translating mRNA after 10Gy IR in PDGF Ink4a/Arf$^{-/-}$ gliomas. (B) Time-course of CEBP and STAT3 target upregulation in PDGF Ink4a/Arf$^{+/-}$ gliomas. Average of total and translating mRNA pools, dotted lines are standard error. (C) Enrichment plots of mesenchymal and proneural signature genes in translating mRNA after 10Gy IR in PDGF-driven Ink4a/Arf$^{-/-}$, Ink4a/Arf$^{-/-}$/PTEN$^{-/-}$, and Ink4a/Arf$^{-/-}$/p53shRNA gliomas. (D) Enrichment plots of mesenchymal and proneural signature genes in the relative changes of translating mRNA after IR of PDGF Ink4a/Arf$^{-/-}$ tumors vs PDGF Ink4a/Arf$^{-/-}$/p53shRNA tumors. (E) Immunohistochemistry for p-Stat3 in PDGF Ink4a/Arf$^{-/-}$. (F) Quantification of p-Stat3 after IR. * = p<0.05.

To determine whether radiation did in fact induce a shift from proneural to mesenchymal lineages in these tumor cells in vivo, we performed GSEA on proneural and mesenchymal gene signatures from Verhaak et al. Olig2+ cells in irradiated tumors did in fact exhibit highly significant enrichment of genes in the mesenchymal gene signature, and equally significant loss of proneural signature genes (FDR q-value of 0.000 for both genesets) (Fig 25C). The shift is detected in RNA isolated from Olig2+ tumor bulk cells via either cell sorting or cell-type specific TRAP, and also occurred in tumors with PTEN deleted (Fig 25C). Thus, the proneural to mesenchymal shift induced by irradiation occurs in the tumor cells themselves, and is not an artifact of changing stromal content.

Unlike many of the changes observed after irradiation, the shift from the proneural to mesenchymal group does not appear to be highly sensitive to p53 activity. p53shRNA tumors also showed highly significant loss of proneural markers and gain of mesenchymal markers (Fig 25C). GSEA on the relative expression changes after irradiation for PDGF-only vs PDGF+p53shRNA tumors showed weak enrichment in the PDGF-only tumors for both proneural and mesenchymal genesets, with proneural signature transcripts actually being more highly enriched in the p53 intact tumors (Fig 25D). Thus, it does not appear that the decrease in p53 activity in the p53shRNA tumors significantly inhibits the proneural to mesenchymal shift in those tumors.

Previously we had shown that treatment of a Ras/Akt glioma model with temsirolimus shifted surviving tumor cells towards a more oligodendroglial phenotype, including induction of the proneural marker Olig2 (77). Since mTOR activity as measured by pS6 activity is higher in PTEN-/- PDGF driven tumors (88), we wondered

whether our PTEN deleted tumors were more mesenchymal. Indeed, PTEN-/- tumor cells are shifted from proneural towards mesenchymal in our expression dataset (Fig 26A). However, temsirolimus treatment of PTEN-/- tumors did not trigger a reversal of the proneural to mesenchymal shift (Fig 26B), and IHC of irradiated tumors does not suggest an increase in mTOR activity (Fig 26C). Taken together, this suggests that the irradiation-induced proneural to mesenchymal shift is not driven by mTOR signaling.
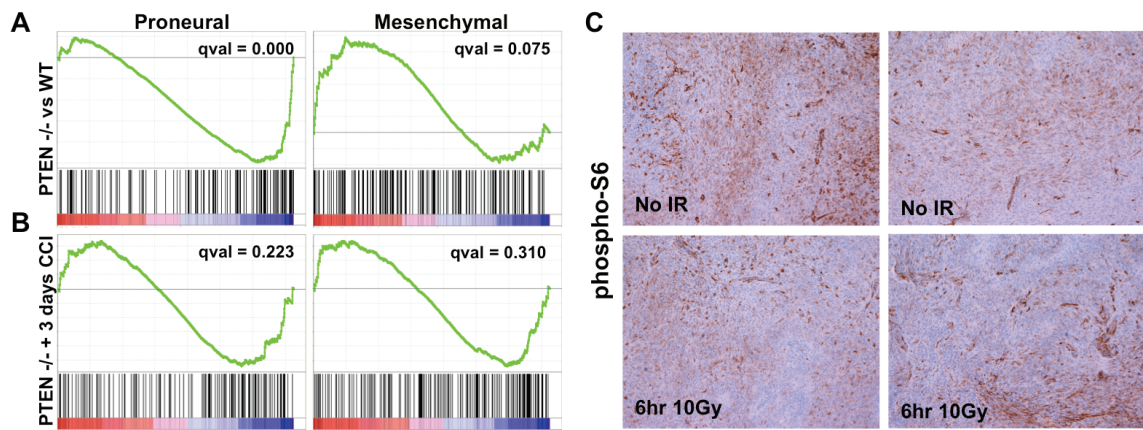
Figure 26. mTOR unlikely to be driver of IR induced Proneural-to-Mesenchymal Shift
(A) PTEN null PDGF gliomas show enrichment of mesenchymal markers and loss of proneural markers relative to PTEN WT PDGF giomas. (B) Treatment with mTOR inhibitor temsirolimus (CCI-779) did not result in significant reversal of proneural to mesenchymal shift of PTEN-/- gliomas. (C) Immunohistochemistry for phosphorylation of mTOR target S6. Control and 10Gy irradiated gliomas shows lack of induction of mTOR activity by IR.

Overall, these results show that radiation rapidly induces a shift in expression profile from proneural to mesenchymal over the course of a few hours. This shift occurs specifically in proneural tumor cells and is not a function of stromal enrichment. Furthermore, unlike much of the response to radiation, the proneural to mesenchymal transformation does not appear to be highly sensitive to p53 activity.

Discussion

GBM is a devastating disease for which there is no cure. Radiation is standard therapy for patients with glioma, however, therapeutic response is limited and disease progression occurs universally. A better understanding of the radiation biology of glioma is critical to making progress in treating this destructive disease. Much of our current understanding of the radiation response of glioma is based on data from cultured glioma cells. The *in situ* tumor microenvironment differs greatly from that provided by cell culture, and work has shown that cells grown in vivo may have a markedly different radiation response than those grown in culture(56). However, interpretation of in vivo glioma radiation studies are complicated by the highly heterogenous cellular composition of glioma.

In this study we used a PDGF-driven mouse model of glioma to study the in vivo radiation response in a defined population of proneural tumor cells. Radiation of PDGF driven gliomas with a single 10Gy dose of resulted in transient cell cycle arrest and asynchronous apoptosis. The effects of radiation vary by cell type, as apoptosis is largely restricted to the Olig2+ tumor cells and is accompanied by a decrease in the proportion Olig2+ cells over time. We utilized the TRAP system targeted to the Olig2+ proneural

tumor bulk to study both translating and total RNA populations specifically in the Olig2+ cells before and after radiation. Somewhat surprisingly, and in contrast with previous work done in cell culture, the translational contribution we measure to overall gene expression changes is minimal in this *in vivo* system.

Consistent with our histological data, we find that apoptotic gene expression programs are highly induced within 6 hours by IR and are accompanied by a loss of expression of genes associated with cell cycle progression. Several transcripts are also highly induced that are involved in stress responses, including redox imbalances which may be important in modulating the genotoxic effect of radiation (122). A range of transcripts for secreted growth factors and cytokines are also upregulated after radiation.

The transcription factors contributing most to these effects appear to be p53 and E2F. p53 activity drives the largest expression differences observed and modulates tumor resistance to IR. The targets of both were amongst the most significantly altered sets of transcription factor targets in each of the tumor types we studied. The targets of IRF, a transcription factor known to cooperate with p53, were also amongst the most heavily induced by radiation. The largest expression differences observed are p53 dependent, and suppression of p53 activity by shRNA modulates tumor resistance to IR. p53 controls the overall expression changes after radiation to such a large extent that irradiated p53 knockdown tumors cluster more closely with unirradiated tumors than with irradiated p53 intact tumors.

A shift towards mesenchymal subtype at recurrence in previously proneural gliomas has been noted (13). In this work, we have identified a clear shift in expression pattern from proneural to mesenchymal within 6 hours in response to radiation. This

shift was observed after radiation in each of the tumor types we examined. The proneural to mesenchymal shift we see is tumor cell specific and is not the result of stromal enrichment via higher rates of cell death in the tumor bulk. While changes in the stromal compartment may also affect tumor subtype as measured by profiling of whole tumor lysate, we show here that the tumor bulk cells themselves undergo a subtype shift after radiation treatment. CEBPB and Stat3 have previously been suggested to act as master regulators of a proneural to mesenchymal shift in glioma cells, but the signaling network in that case was inferred from expression data from whole tumor lysates. In RNA isolated from Olig2+ tumor cells, both CEBPB and Stat3 were amongst the transcription factors whose targets were highly induced by radiation. Our data is evidence that a proneural-to-mesenchmal shift occurs in the same subset of cells in which CEBPB and Stat3 activity is elevated, supporting the reported link between CEBPB and Stat3 and the proneural to mesenchmal shift.

The subtype shift we observe is not clearly affected by p53 activity, and is also not likely to be driven my mTOR signaling. Stat3 can be phosphorylated through a variety of pathways, including Src, Abl, mTOR, and JAKs. IL-15, LIF, and IL-7 are all amongst the most upregulated transcripts after IR in Olig2+ cells themselves, and all are known activators of Stat3 via gp130/JAK (131, 132), suggesting that in irradiated proneural gliomas, cytokine activation of JAKs may drive the proneural to mesenchymal shift. Further studies are necessary to fully elucidate the mechanism by which radiation induces a proneural to mesenchymal shift.

The recent discernment of distinct subtypes of high-grade glioma and the identification of distinct growth factor pathways active in each subtype suggested that

targeted pharmacological inhibition of these pathways on a subtype specific basis might lead to better clinical outcomes. Subtyping of patient gliomas has already begun in an effort to develop more targeted individually tailored courses of therapy. However, the shift in subtype from proneural to mesenchymal that we observe here within 6 hours after irradiation has important implications for this paradigm. The speed of the shift is evidence that the subtypes may not be as hardwired as previously believed. The apparent plasticity of gliomas with regard to subtype may indicate a need to target not only the oncogenic pathways typically associated with a given subtype, but also to identify and target other pro-growth pathways that may become activated by treatment. Radiation-induced shifts are of particular importance, since radiation is a nearly universally component of glioma therapy. As various targeted therapies are being tested in combination with radiation, understanding the shifting signaling patterns in response to radiation will be crucial to interpreting the results of these trials.

EXPERIMENTAL RESULTS III - EXTENDING TRAP TO THE GLIOMA STROMA

The TRAP system has proven very useful for cell-type specific *in vivo* studies. It is currently the only method available for studies of *in vivo* translational regulation. It is also very flexible and has benefits for standard expression profiling. Translating mRNAs should more closely represent protein output than total mRNA levels. Rapid tissue homogenization into cycloheximide allows quicker stabilization of RNA profiles than dissociation methods. Furthemore, TRAP does not require scheduling time on or purchasing of an expensive cell sorter; ribosome-associated RNA can be isolated with minimal equipment at the bench on short notice. This is invaluable when dealing with highly aggressive mouse tumor models, where onset of symptoms can be unpredictable and progression to morbidity rapid.

Significant data from our lab and others indicates the importance of other cell types in modulating glioma growth and response to treatment. These cells, including endothelial cells, vascular smooth muscle cells, astrocytes, and microglia, all have complex interactions with tumor cells and other stromal cells that can only be studied in an *in vivo* system and require tools such as the TRAP system. Having used TRAP to study the tumor bulk cells, we wished to extend the system to the other cell types in gliomas to enable future studies on those cell types as well. We also wished to make the system as broadly useful as possible, as many of these cell types are found in other organ systems. For example, an endothelial TRAP mouse would be useful to study endothelia in a variety of organs. Furthermore, for tissues or structures that are difficult to dissociate

into single cells, TRAP may represent the only way of retrieving RNA from specific cells for study.

Endothelial cells appear to be critically important in the progression of glioma and its response to treatment. Endothelial cells form the lumen of blood vessels, and their recruitment or proliferation is a required and crucial step in the generation of new vasculature. The blood supply provided by a functioning vasculature is required for tumors to progress beyond a certain size. The acquisition of the ability to recruit new vasculature is a potentially rate-limiting step in the progression of tumors to malignancy (18). Endothelial cells may also have an instructive signaling role in gliomagenesis, rather than a strictly supportive physiological role. Recent studies have shown that endothelial and associated cells may form a perivascular niche (PVN), which promotes tumorigenesis and may support stem-like character in glioma cells. Endothelial cells were shown to promote tumor cell stem-like characteristics, such as sphere-formation, that have been associated with tumorigenecity, and dissociated endothelial cells promoted tumorigenesis when co-transplanted with brain tumor cells (34). In PDGF-driven gliomas, nitric oxide (NO) synthesized by eNOS in endothelial cells was shown to induce Notch signaling in surrounding perivascular cells expressing the receptor for NO, soluble guanalyl cyclase (sGC). This in turn resulted in enhanced stemness characteristics and tumor formation (28). Endothelial cells are also the target of the new wave of anti-angiogenics in glioma clinical trials. The biology of the glioma response to these therapies is poorly understood (133) and well suited to study in a mouse model.

Vascular smooth muscle cells (vSMCs) and pericytes are ubiquitous features of microvascular proliferation in both humans (20) and the RCAS-PDGF model of glioma

(88). vSMCs and pericytes are also a feature of microvascular proliferation in other tumors (melanoma, breast, prostate, endometrial, neuroblastoma), where it is also a poor prognostic indicator (134, 135). The recruitment of these cells is crucial for angiogenesis (32) and likely modulates the response to anti-angiogenics. Given the cross-talk between vSMC/perictyes and endothelial cells, they likely also modulate the function of the perivascular niche. vSMC/pericytes are located in the regions where sGC is expressed (28, 88) and known to be regulated by NO via that same pathway in other contexts (136). Due to their importance in angiogenesis, vSMCs and pericytes are also potential targets of anti-angiogenic therapies. Being reliant on different signaling pathways than endothelial cells (PDGFRB and possibly mTOR (29, 69)), they may present alternative pathways to target therapeutically.

Work from our lab has shown that peritumoral and perivascular astrocytes secrete sonic hedgehog (SHH) in PDGF-driven gliomas (42). Based on staining, these astrocytes appear to be the major source of SHH in tumors. Previous work from our lab has shown that SHH secreted by astrocytes can induce normal Olig2+ OPC cells to proliferate and migrate (41). Given that the RCAS-PDGF gliomas are largely comprised of Olig2+ OPC like cells, this may have a functional role in promoting the aggressiveness of high grade tumors. Indeed, a luciferase readout of pathway activity downstream of SHH was correlated with glioma grade in RCAS-PDGF tumors (42). Work from other labs has indicated that SHH is required for glioma growth and stem cell character (137). The population of astrocytes localized to the perivascular niche is unique to high grade gliomas. We have shown that CD44 is a marker of this population of SHH producing astrocytes associated with the PVN (40).

Macrophages/microglia are found throughout gliomas, including the RCAS-PDGF driven model of glioma, and can make up a substantial portion of tumor mass (35). Microglia are implicated in promoting glioma proliferation and invasiveness by cytokine release (37). They also promote glioma invasiveness via activation of matrix metalloproteases, which degrade the extracellular matrix and facilitate migration. Microglia also promote angiogenesis in some contexts (39).

Results

We sought to generate TRAP mice targeting each of these cell types of interest to facilitate *in vivo* study. We first selected promoter constructs to be used to drive eGFP-L10a expression in transgenic mice. We performed a literature search for promoters that showed high but restricted expression in the cell type of interest. For some cell types, expression in the brain was rarely validated or even absent, so we chose promoters with demonstrated expression in the brain where possible. Where appropriate, we sought constructs that were shown to drive expression throughout as many organ systems, to allow the tools to be as broadly useful as possible.

To target endothelial cells, we chose a vascular endothelial cadherin (VE-Cadherin) promoter construct. The Tie2 promoter had been the promoter of choice for broad endothelial expression, but is problematic in cancer models given the identification of large Tie2 expressing monocyte populations in tumors (138). VE-Cadherin has also been shown to drive highly specific and restricted expression, but the most commonly used promoter, the 2.5kb 5' flanking promoter characterized by Gory et al (139), lacks expression in brain endothelial cells (140). The addition of an enhancer element from the

first intron of VE-Cadherin to the 2.5kb promoter results in higher yet still specific expression in a wider range of brain endothelial cells (140). The eGFP-L10a fusion was cloned into this construct to generate the VECad-RPGFP construct used for transgenesis.

Alpha-smooth muscle actin (SMA) is expressed by tumor associated pericytes and vSMCs in gliomas, and in similar cells throughout the body. The 5.2kb 5' flanking and first intron promoter/enhancer from the rat characterized by Mack and Owens (141) drives widespread expression, and significantly was demonstrated to express in the brain (142). The eGFP-L10a fusion was cloned into this construct to generate the SMA-RPGFP construct used for transgenesis.

Glial Fibrillary Acidic Protein (GFAP) has commonly been used to identify astrocytes. The 2.2kb human 5' flanking GFAP promoter/enhancer (143) has been used to create a large number of transgenic mice expressing in astrocytes (144), including the Gtv-a mouse that we use with the RCAS system (145). This construct was used to generate the GFAP-RPGFP construct used for transgenesis. Our lab has also identified CD44 as a specific marker of perivascular astrocytes (40). There is one reported transgenic CD44 mouse in the literature, a CD44-GFP mouse reported by Sarthy et al (146). Characterization of GFP expression in this mouse was limited to the retina, and the brain was not characterized. Nevertheless, we used this promoter construct to generate a CD44-RPGFP construct in the hopes of targeting CD44 astrocytes in the PVN.

CD11b is expressed at high levels in mature macrophages. The 1.7kb upstream promoter is the most commonly used macrophage specific promoter, and has been used to make a range of macrophage specific mice, including mice targeting brain microglia

(147-150). We cloned eGFP-L10a into this construct to generate the CD11b-RPGFP

construct used for transgenesis.

Endothelial Targeted Lines

Transgenesis with the VECAD-RPGFP construct resulted in 6 transgene positive

founders, which gave rise to 6 single integrant breeding lines. Expression was observed

by anti-GFP staining in 4 of these lines. 2 lines, VECad10a and VEcad6, expressed

particularly well and were chosen for further characterization.

VECad10a had high transgene expression in a range of organs (Fig 27).

Expression in the liver was low, as it was in the original lines using this promoter (140),

however expression in the heart was low as well, unlike the lines in (140). To confirm

expression in tumors, these mice were crossed with Ntv-a/Ink4a/Arf-/- lines so that

PDGF-driven brain tumors could be generated. GFP staining in brain tumor vessels was

observed (Fig 28). Despite intracardial perfusion with PBS to wash away blood, vessels

can result in non-specific false positive staining due to the prevalence of antibody binding

epitopes such as Fc receptors in the blood, particularly in brain tumor regions that may

perfuse poorly due to abberant vasculature. Staining of adjacent sections with secondary

antibody did not show vessel staining, suggesting that staining is specific (Fig 29). To

further confirm the specificity of staining, we showed that incubation with primary and

recombinant GFP also abolished staining, confirming that staining was due to GFP

expression (Fig 29). Double staining with endothelial markers eNOS and VE-Cadherin

confirmed correct expression and broad coverage of endothelial cells (Fig 30). Flow

cytometry confirmed the presence of a clear population of endogenously fluorescence

GFP+ cells (Fig 31). We also confirmed widespread expression in the VECad-6 line (Fig

32). Expression patterns were similar to the VECad10a line, and expression was also

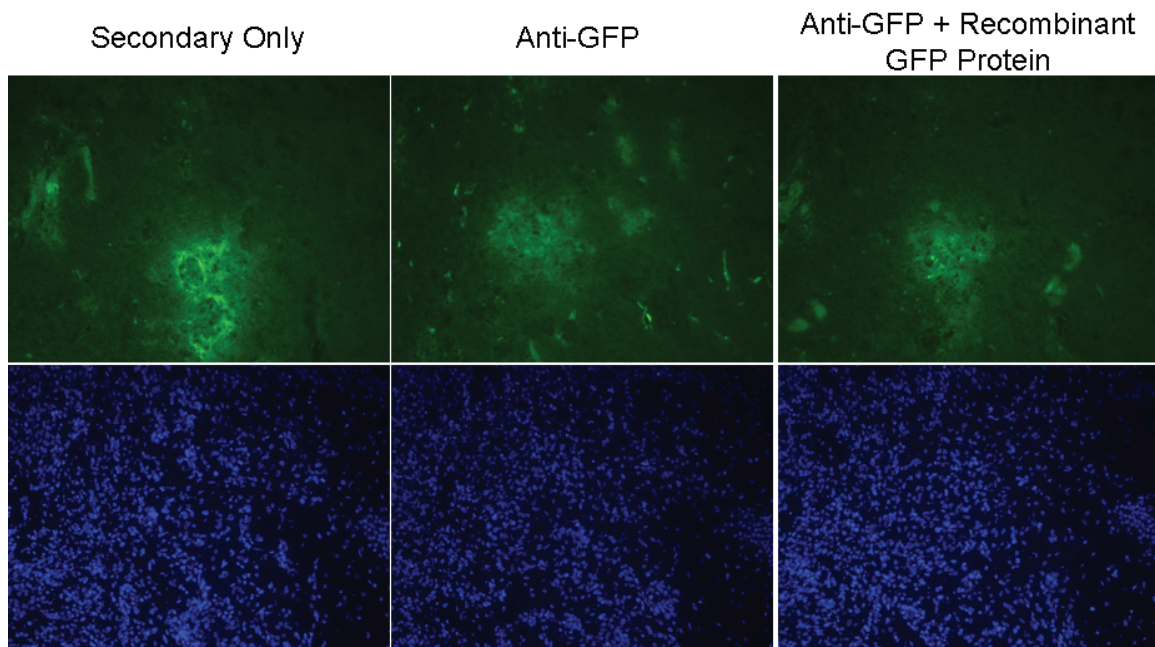seen in the pancreas and spleen (not tested in VECad10a).
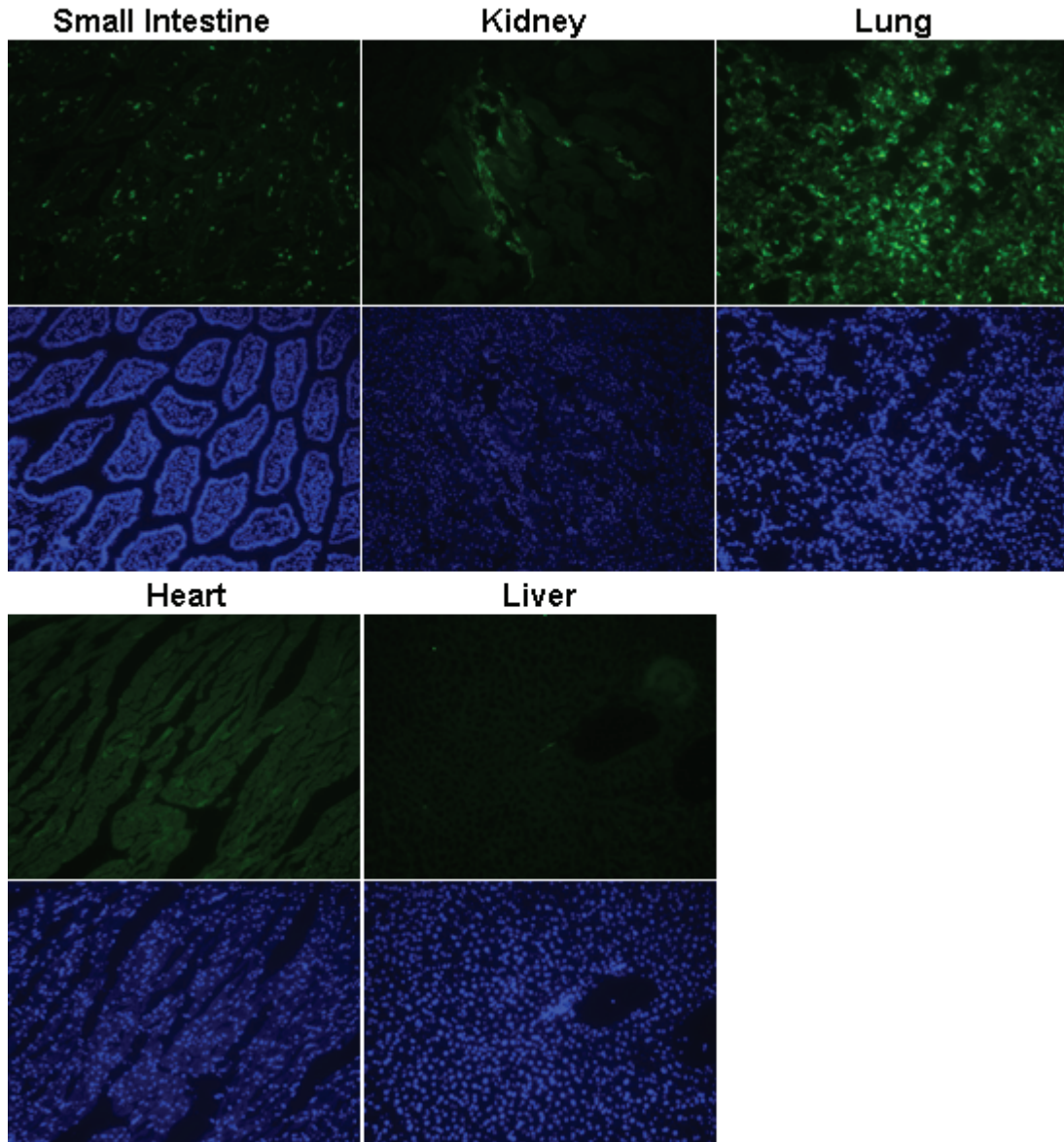
Figure 27. VECad10a mouse transgene expression in a variety of tissues.
VECad10a line expressed well in small intestine, kidney, and very highly in lung. Expression in liver and heart was low.
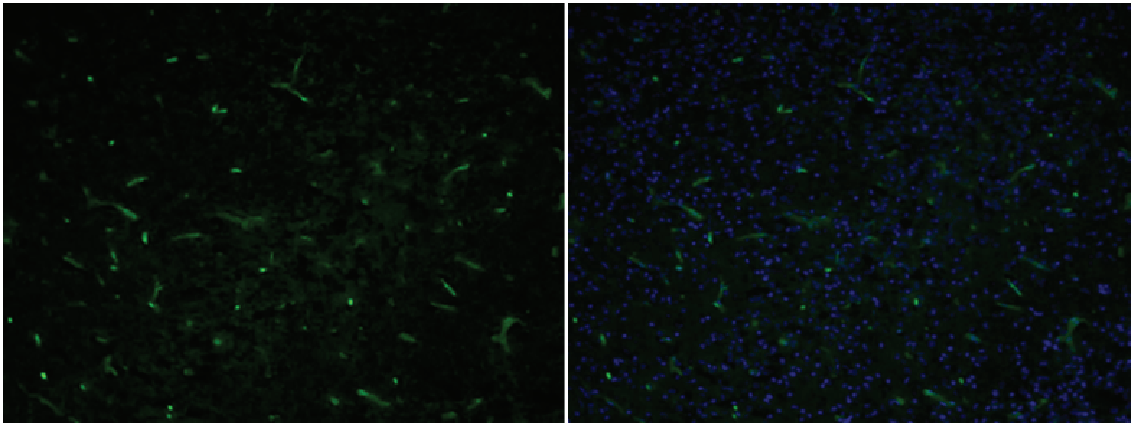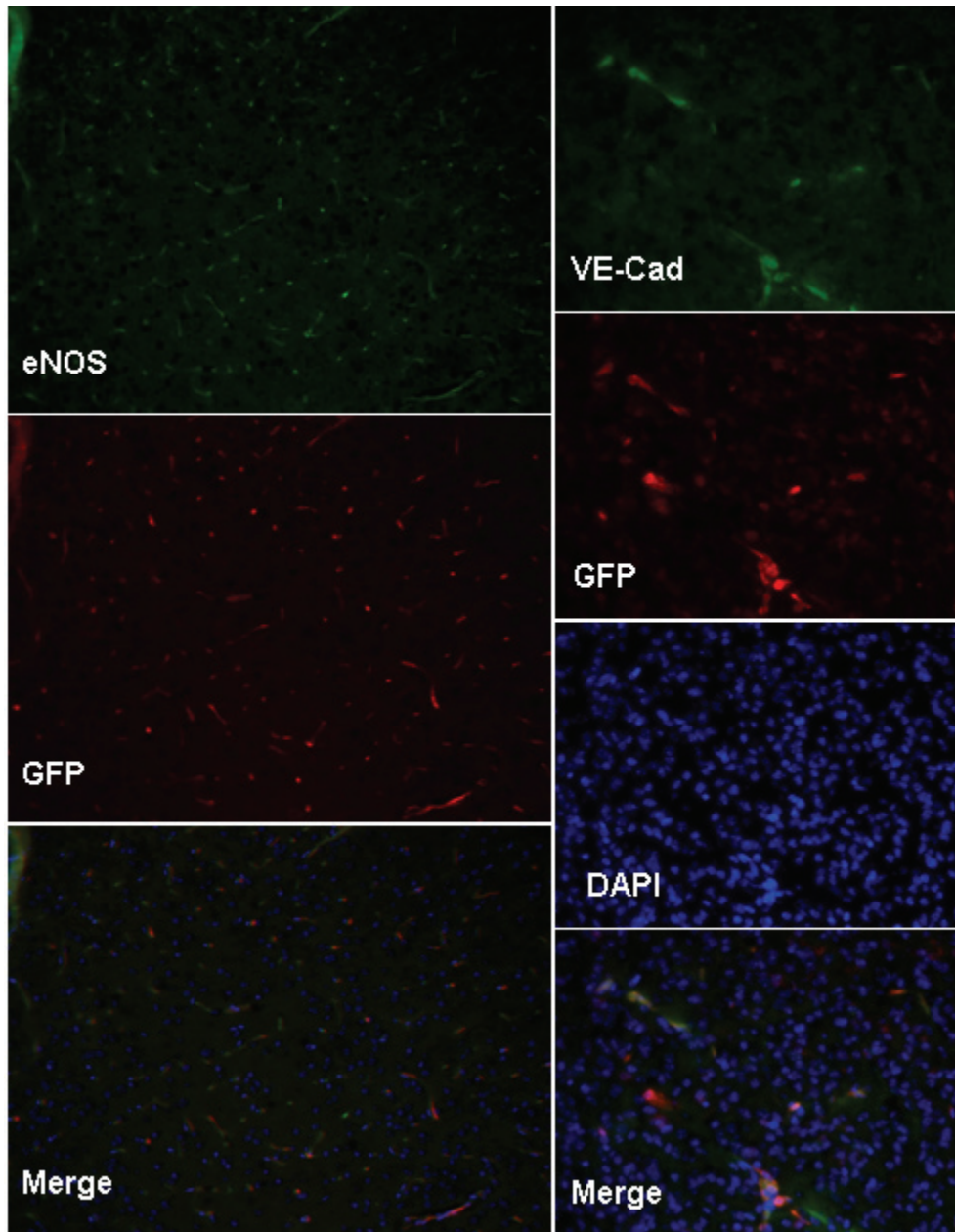
Figure 28. VECad10a GFP Expression in Brain Tumor Associated Endothelia

Figure 29. Confirmation of GFP specificity of staining.
Immunofluorescence on adjacent sections. Secondary only staining shows no vessels, suggesting lack of background vessel staining. Anti-GFP staining clearly reveals tumor associated blood vessels. Recombinant GFP is able to abolish vessel staining, confirming that vessel staining is specific for GFP and represents expression.

Figure 30. VECad10a GFP Co-expression with Endothelial Markers
Co-immunofluorescence for GFP and the endothelial markers eNOS and VE-Cadherin demonstrate that GFP expression in VECad10a mouse is specific and overlaps with most if not all brain tumor vessels.
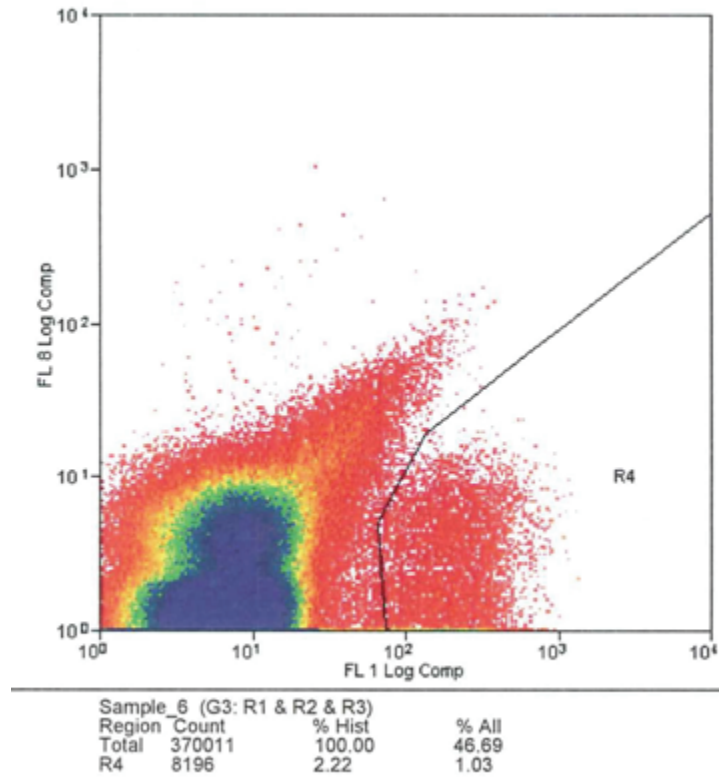
**Figure 31. GFP+ fluoresecent population in VECad10a brain**
Flow cytometry of dissociated VECad10a brain demonstrates clearly defined population of endogenously fluorescent GFP+ cells.
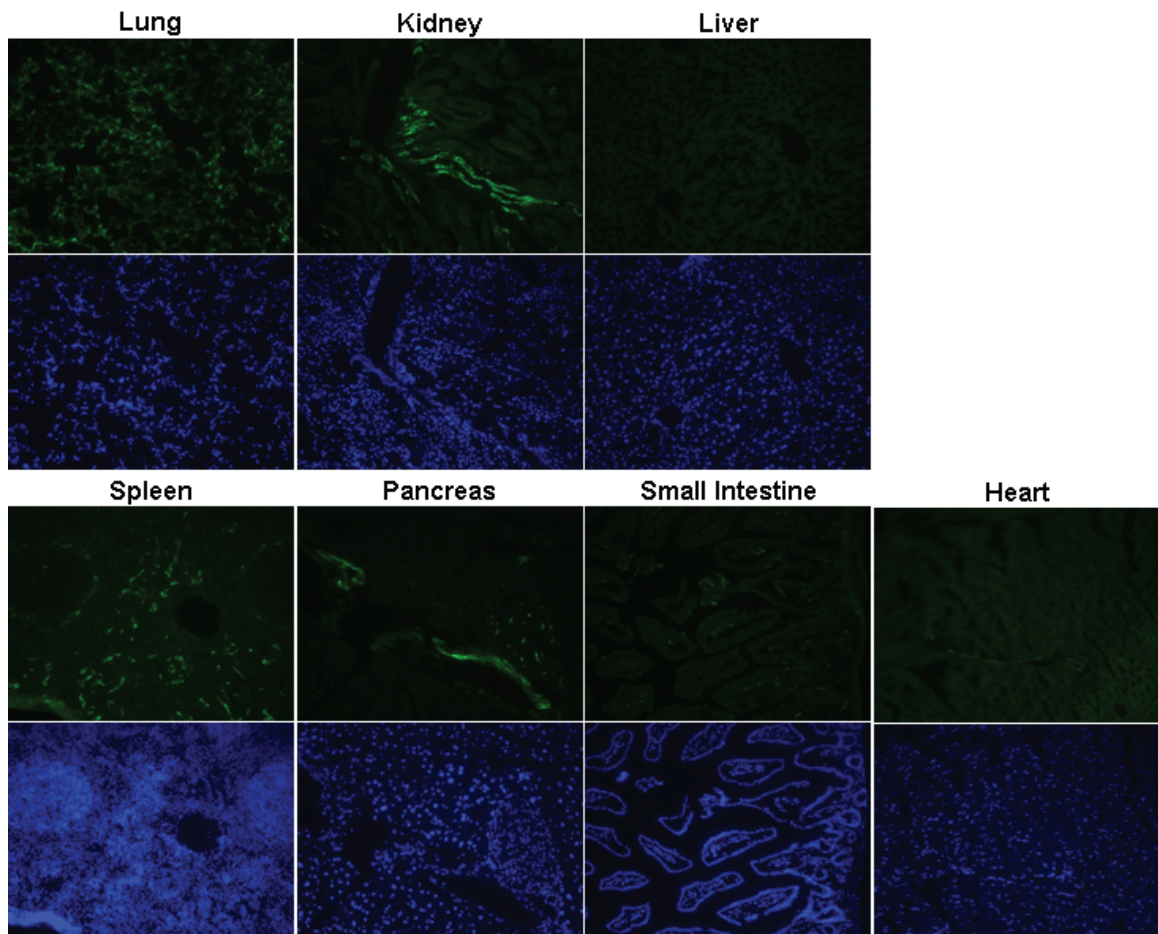
Figure 32. VECad6 mouse transgene expression in a variety of tissues
VECad10a line expressed well in small intestine, kidney, spleen, pancress, and very highly in lung. Expression in liver and heart was low, as in VECad10a.

The VECad10a line was chosen for initial attempts to immunoprecipitate RNA. A range of tissues was selected for IP. As yields were uncertain, organs from 5 mice were pooled initially. Varying amounts of RNA were recovered from brain, kidney, lung, liver, spleen, and small intestine, with brain yielding the least (~300ng) and spleen the most (~2.2ug) (Fig 33). RT-qPCR was performed for markers of endothelial cells (CD31, eNOS, VECadherin, VEGFR2), smooth muscle cells (SMA, smooth muscle myosin heavy chain - SMMHC), and where applicable Olig2 and the neuron marker NeuN. We saw strong enrichment in the IP fraction relative to the unbound fraction for endothelial markers in brain, kidney, and lung (Fig 34). Olig2 and NeuN were depleted in the brain sample, and smooth muscle markers were highly depleted in the lungs. Enrichment was not seen in the liver, which does not express the transgene. Data from from the spleen and small intestine was inconsistent.
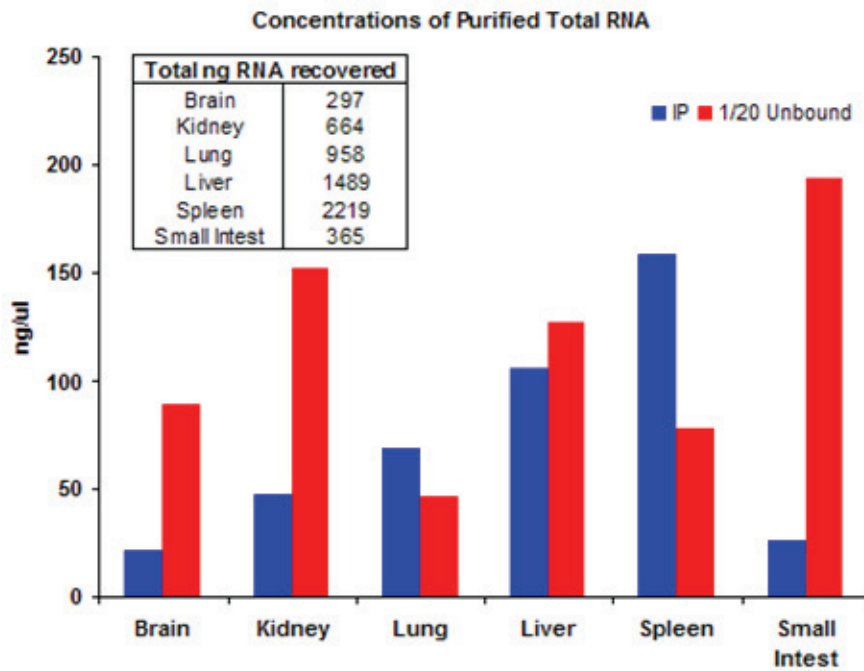
Figure 33. RNA Recovered by TRAP of 5 animals from VECad10a line.
Each sample recovered by TRAP from homogenate of given organs from 5 animals.
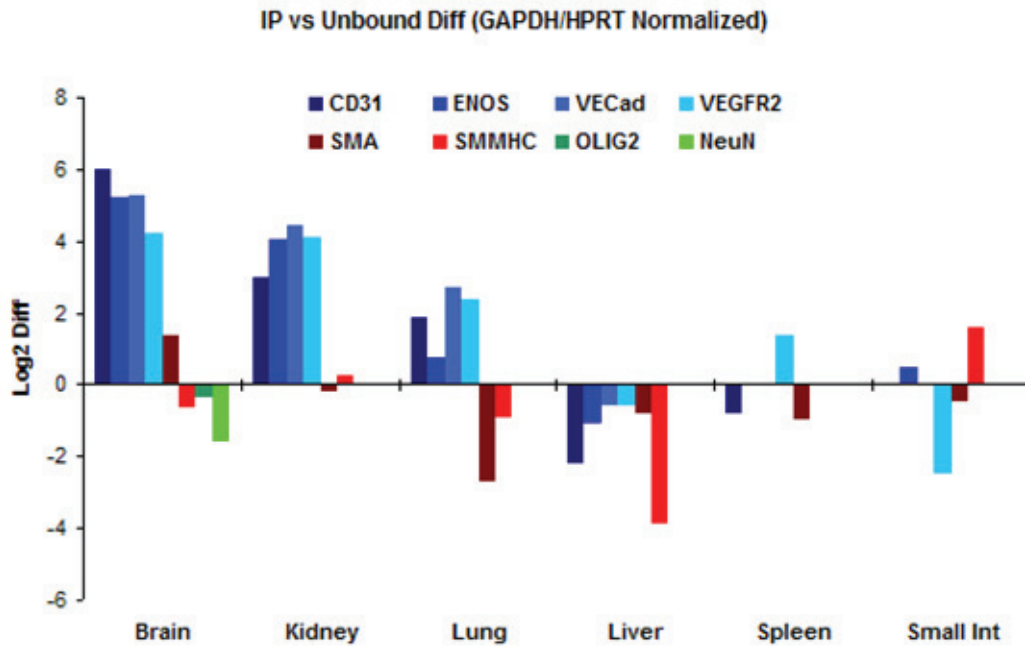
Figure 34. Enrichment of endothelial markers in VECad10a TRAP samples
qPCR was performed for markers of endothelial cells (CD31, eNOS, VECadherin, VEGFR2), smooth muscle cells (SMA, SMMHC), oligodendrocyte precursor cells (Olig2) and neurons (NeuN). Each sample recovered by TRAP from homogenate of given organs from 5 animals. Enrichment in the IP fraction versus the unbound fractions was seen for endothelial transcripts was seen in brain, kidney, and lung. Depletion of brain cells markers was seen in the brain, and depletion of smooth muscle cell markers was seen in the lungs. CT values from spleen and small intestine were very high.

We noticed that despite having used equivalent amounts of input RNA, there were huge discrepancies between the CT values for housekeeping genes for both IP and unbound fractions, with spleen and small intestine having particularly high CT values (Fig 35). This raised the possibility that degradation is a problem in some tissues. An Invitrogen study reported that the brain has the lowest level of RNase activity of any tissue they tested. They reported that the kidney has 8 fold more RNase activity than brain, the liver 64-fold more, the lung 5,300 fold more, the spleen 10,600 fold more, while the pancreas has 181,000 fold more RNase activity than the brain. These results matched roughly with the relative decreases seen in measured household gene expression in our samples. Small intestine, which was not tested by Invitrogen, had the lowest levels of housekeeping genes and has various enzymes secreted directly into it by the pancreas, including RNase.
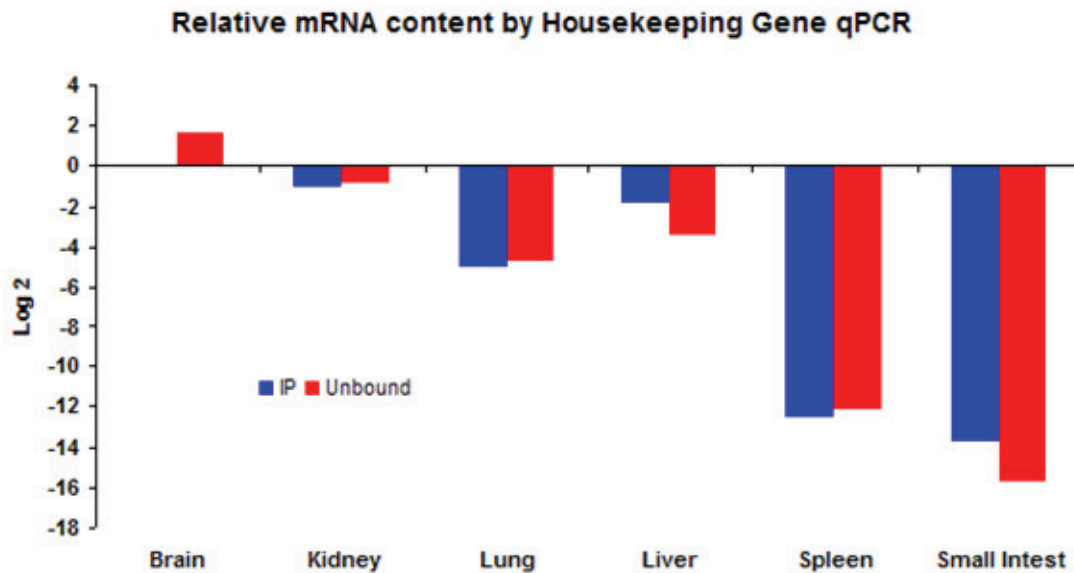
Figure 35. Widely differing CT values for housekeeping genes from different tissues after TRAP
qRTPCR was performed on RNA recovered by TRAP from 5 mice. Equal amounts of RNA were used for RT for each tissue. CT values for housekeeping genes (GAPDH and HPRT) varied by as much as 15 cycles (>30,000 fold). CT values were normalized to brain tissue.

Based on the qPCR results, housekeeping gene levels, and expected levels of RNase activity, we decided to focus on brain, kidney, and lung as representing a workable combination of IP yield and tolerable RNase activity. To more clearly define expected yields and background from these tissues, we performed IPs on organs from single VECad10a, VECad6, and transgene null mice. The VECad10a mouse yielded on the order of 50ng by IP from the brain, 450ng from kidney, and 860 from the lungs (Fig 36). Relative to a transgene null mouse, this represented a 4-fold enrichment over background in the brain, 11-fold for the kidney, and >200 fold enrichment for the lungs. The VECad6 mouse yielded similar levels of RNA, but was lower in all cases.

Single Mouse Extractions

Total ng

		VECad (-/-)			VECad10a			VECad6		
		Brain	Kidney	Lung	Brain	Kidney	Lung	Brain	Kidney	Lung
IP	No Dnase	13.1	48.9	6.9	47.3	447	860	42.6	184	644
IP	Dnase	9.5	32.4	4.9	41.2	358	1134	34.4	179	613
Input	No Dnase	5,763	9,866	2,724	4,044	10,807	2,629	6,002	13,208	2,544
Input	Dnase	5,996	8,944	2,976	3,692	10,673	2,626	5,820	11,819	2,218

Figure 36. RNA amounts recovered by TRAP from single mice
Organs equivalent to 1 mouse (i.e. 1 brain, 2 kidneys, 2 lungs) were homogenized and RNA recovered by TRAP. Concentrations measure with and without DNase step (some RNA is lost during DNase step).

Analysis of RNA quality via BioAnalyzer revealed signs of degradation in kidney and lung samples, but RIN numbers were generally good enough for microarray experiments (Figure 37). qRT-PCR showe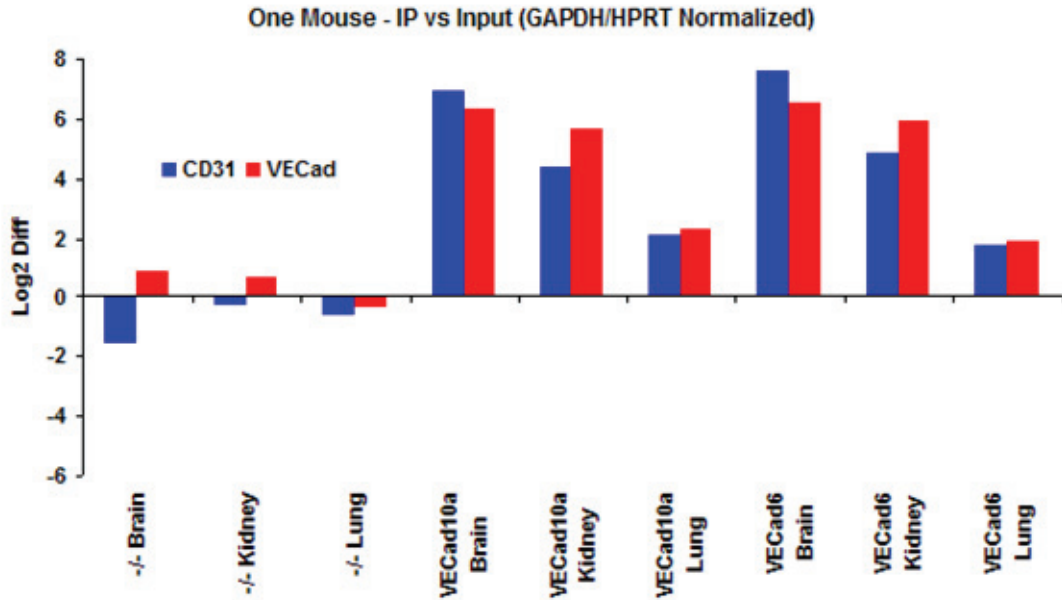d enrichment for endothelial markers in the IP fraction relative to input for each organ, demonstrating the endothelial specificity of eGFP-L10a expression (Fig 38). Lung showed the lowest enrichment. However, lung shows by far the highest level of endothelial markers relative to housekeeping genes of these three tissues, and also had widespread bright GFP staining throughout the entire organ (Fig 39). It is likely that endothelial cells are simply highly abundant in lung tissue, precluding the large fold enrichments relative to the input fraction seen in organs with sparser endothelial cells.
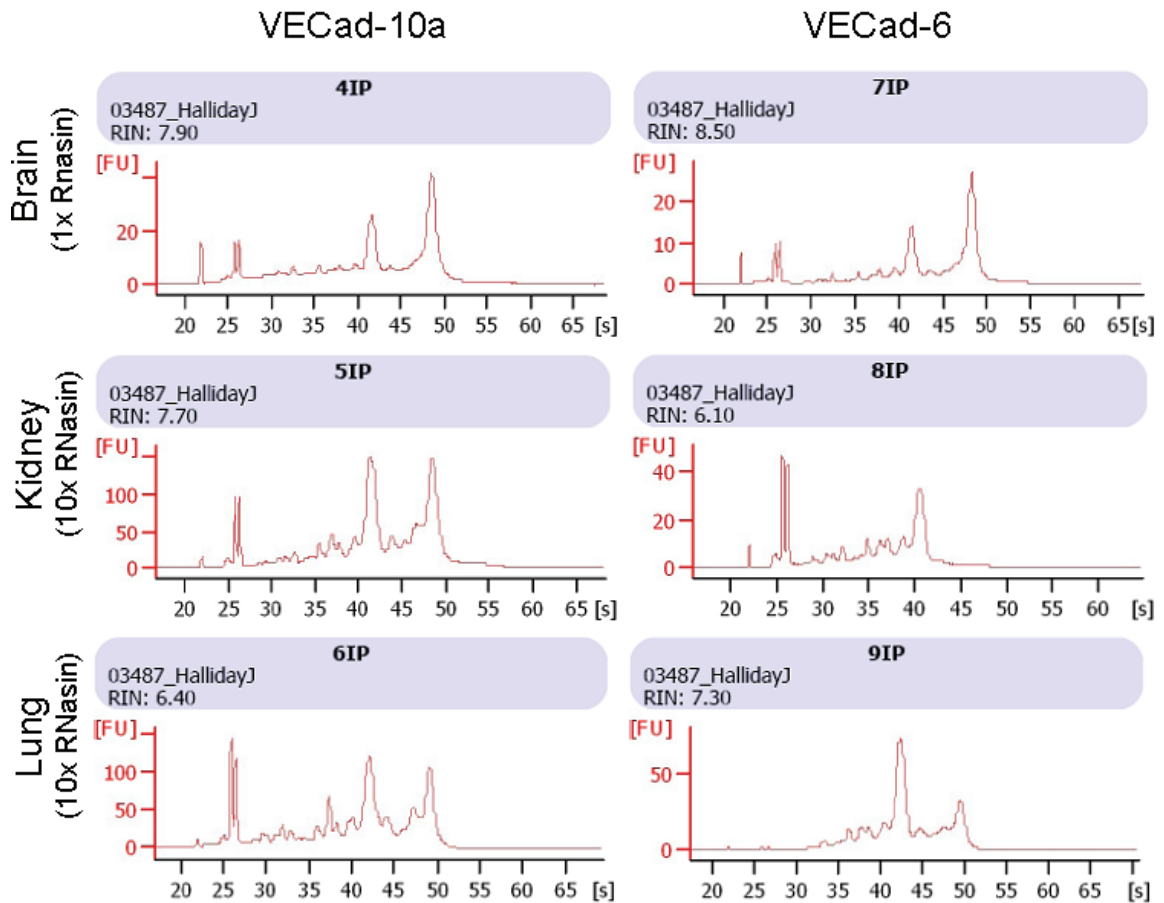
Figure 37. Quality of RNA obtained by TRAP from different tissues
RNA quality was assessed by BioAnalyzer. Highest quality RNA was obtained from brain, with higher levels of degradation in kidney and lung. TRAP for kidney and lung was performed with 10ul/ml RNasin Plus in homogenization buffer, brain with 1ul/ml. Each sample is equivalent to one mouse.

Figure 38. Relative enrichment for endothelial markers in single mouse TRAP
qPCR of single mouse TRAP samples. IP fraction was compared to the input fraction after normalization to GAPDH/HPRT. Transgene negative mice showed no enrichment of endothelial markers in the IP fraction. Transgene positive mice showed enrichment in each tissue studied for both mouse lines.

Single Mouse Extractions

Legend:
- Input -/- Ctrl CD31
- Input -/- Ctrl VECad
- Input 10A CD31
- Input 10A VECad
- Input 6 CD31
- Input 6 VECad
- IP -/- Ctrl CD31
- IP -/- Ctrl VECad
- IP 10A CD31
- IP 10A VECad
- IP 6 CD31
- IP 6 VECad

Y-axis: Log 2 Diff

X-axis categories: Brain, Kidney, Lung
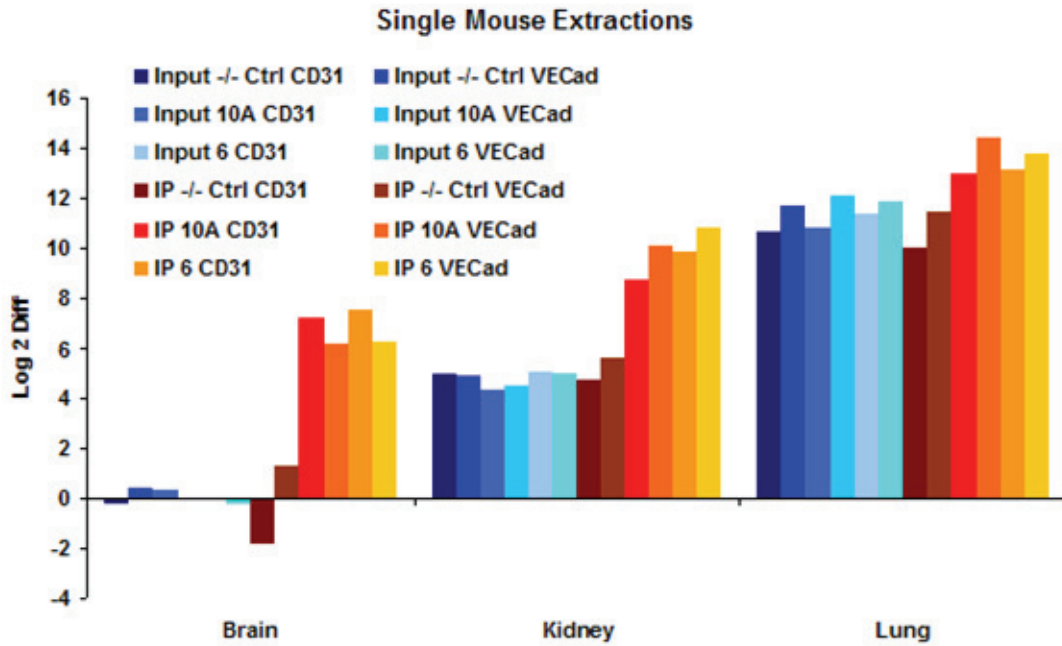
Figure 39. Endothelial marker expression relative to housekeeping genes normalized to brain
High levels of endothelial marker expression relative to GAPDH/HPRT in lung likely reflect high proportion of endothelial cells in the lung. Conversely brain has lower endothelial content, resulting in lower levels of endothelial marker expression relative to GAPDH, and lower levels of RNA recovery per unit of input RNA and unit background (as in Fig 36). From single mouse TRAP.

We next examined the yield of TRAP from brain tumors generated in VECad10a mice. Immunoprecipitation of translating RNA from a PDGF-driven brain tumors VECad10a mouse yielded approximately 50-60ng of RNA, while background levels from a transgene negative mouse tumor were similar to that from whole brain, ~10-15ng. qRT-PCR showed enrichment of endothelial markers and depletion of smooth muscle, glial, and neural markers (Fig 40).
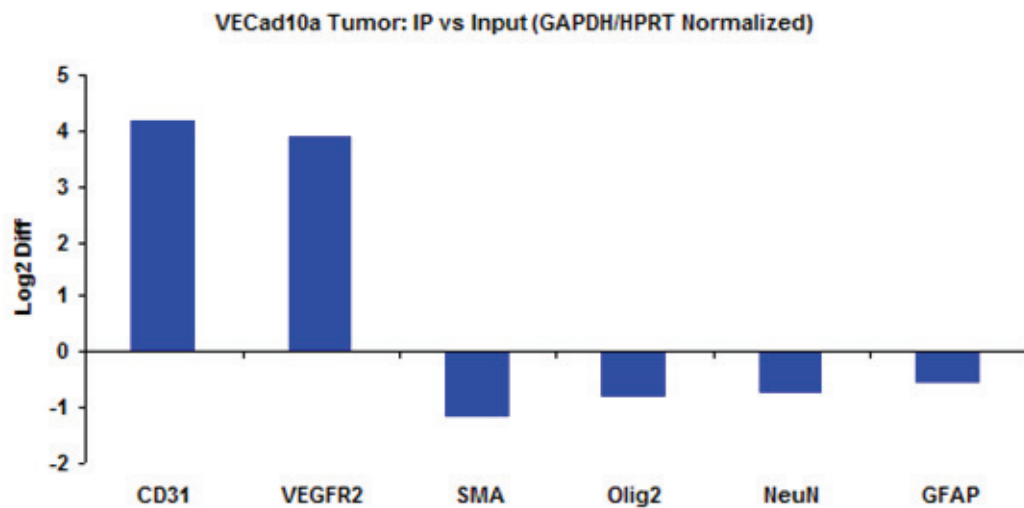
Figure 40. TRAP from PDGF-glioma in VECad10a line enriches for endothelial markers
qPCR on RCAS-PDGF tumor in VECad10a line. Endothelial markers CD31 and VEGFR2 were enriched. Markers of smooth muscle cells (SMA), OPCs/tumor cells (Olig2), neurons (NeuN), and astrocytes (GFAP) were all depleted.

vSMCs/Pericyte Targeted Lines

Transgenesis with the SMA-RPGFP construct resulted in 6 transgene positive founders, which gave rise to 7 single integrant breeding lines. Expression was observed by anti-GFP staining in 5 of these lines, but one bred poorly and was eventually lost. Expression was broadly similar across lines, but varying in intensity. Extensive overlap with SMA expression seen in a number of tissues and across lines (Fig 41). We did notice a correlation between the overall strength of expression in a given line and its tendency to express in non-SMA expressing cells. SMA-9 was the easily the strongest expressing line, and stained for GFP in non-vessel associated, non-SMA expressing cells in some tissues including (Fig 42). In the brain, GFP+ non-vessel associated SMA- cells were seen in clusters in the cortex (Fig 42).
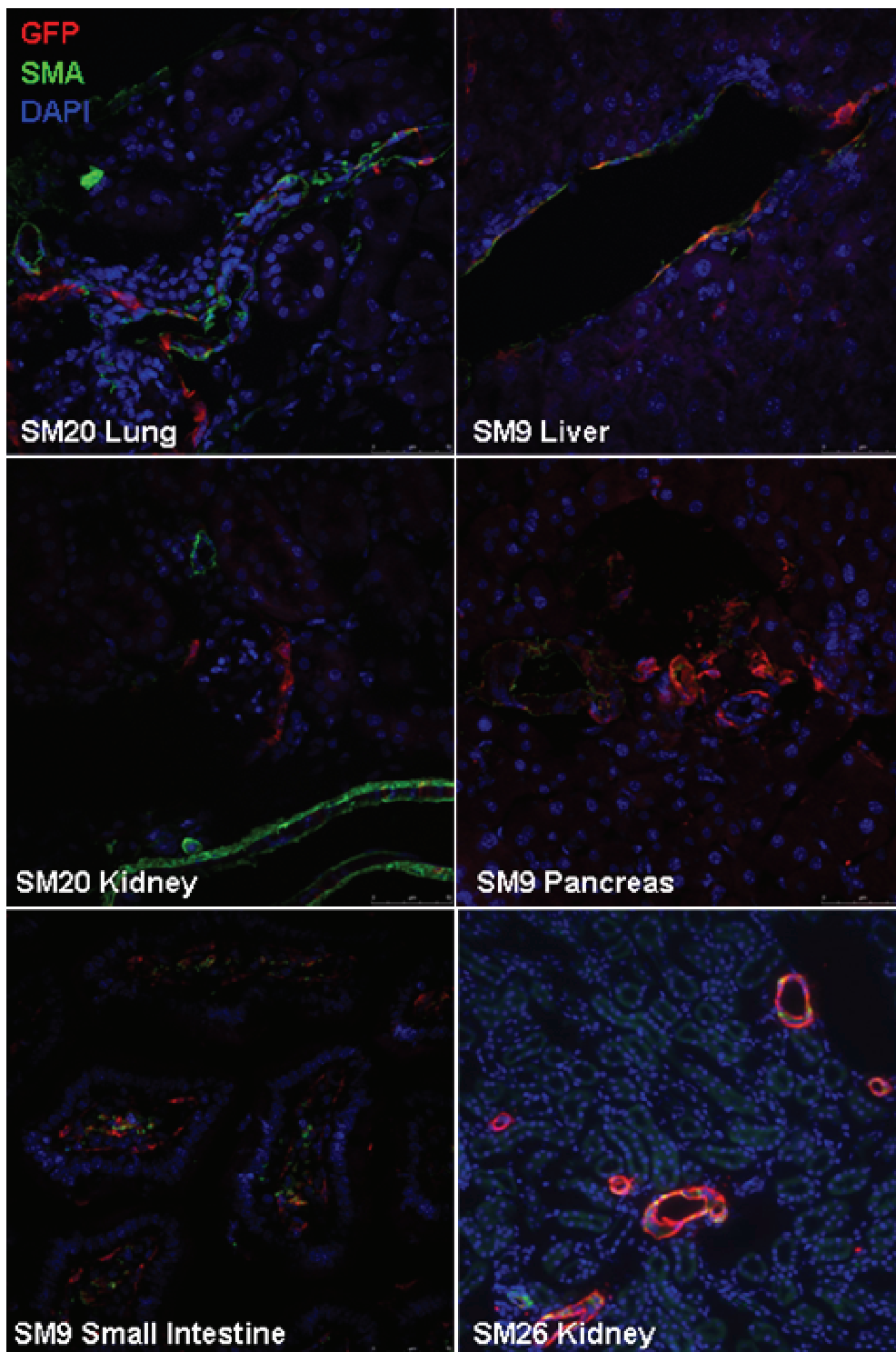
Figure 41. Overlapping GFP and SMA expression across tissues in SMA-RPGFP lines
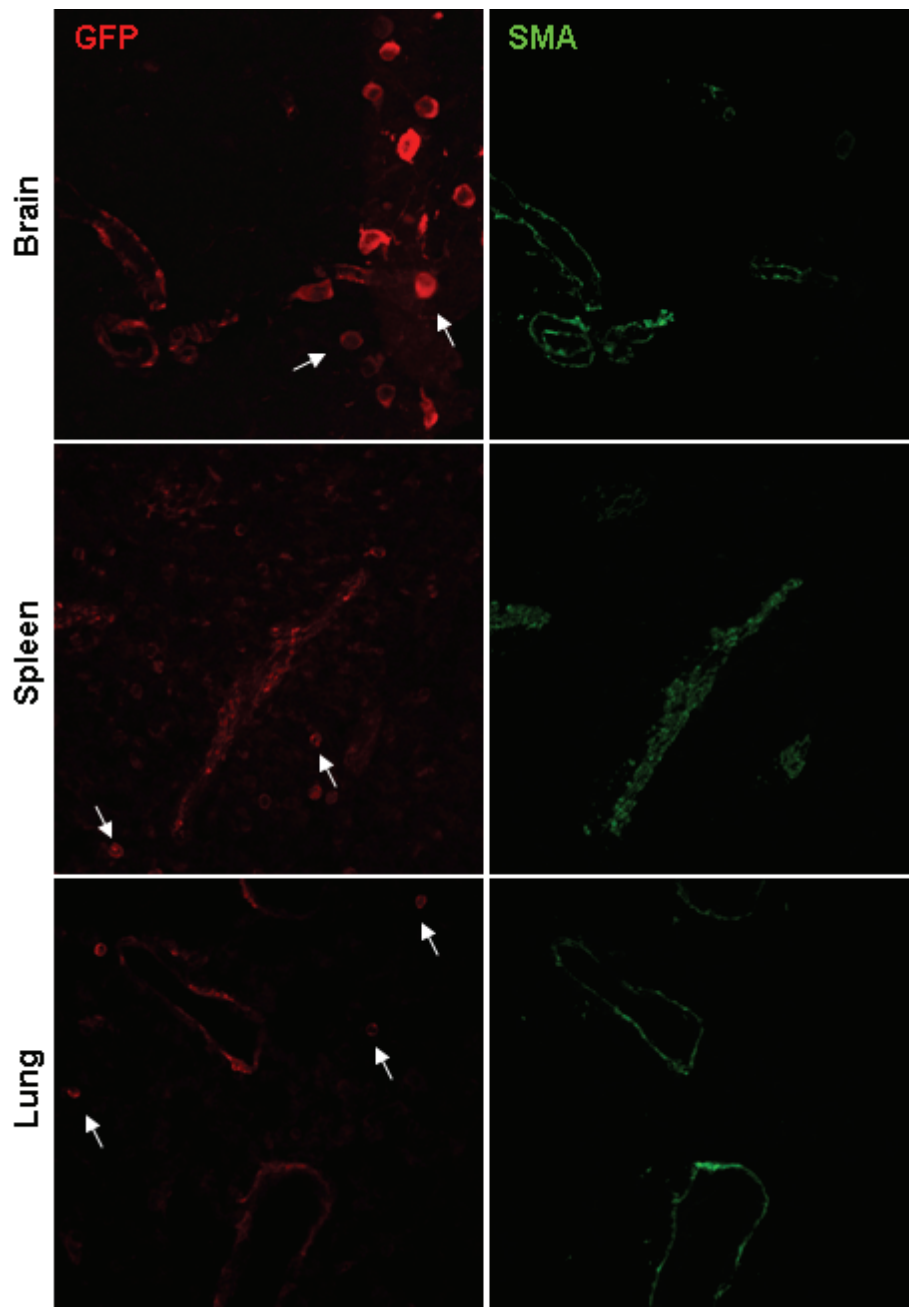
Figure 42. SMA9 expression in SMA+ and SMA- cells
SMA9 expresses in virtually all vessel associated SMA+ cells. However it also expresses in non-SMA+, non-vessel associated cells in some tissues (white arrows), including the brain. On top, a cluster of GFP expressing SMA- cells are situated near GFP expressing SMA+ cells associated with a blood vessel.

To confirm expression in tumors, these mice were crossed with Ntv-a/Ink4a/Arf-/- lines and PDGF-driven brain tumors generated. GFP staining characteristic of SMA expression in glioma perivascular regions was observed in some lines (Fig 43), but only SMA-9 expressed GFP at a high level in these regions (Figure 44). In these tumors in the SMA-9 line, cells that lacked smooth muscle morphology and SMA staining were also noted expressing GFP (Figure 44).
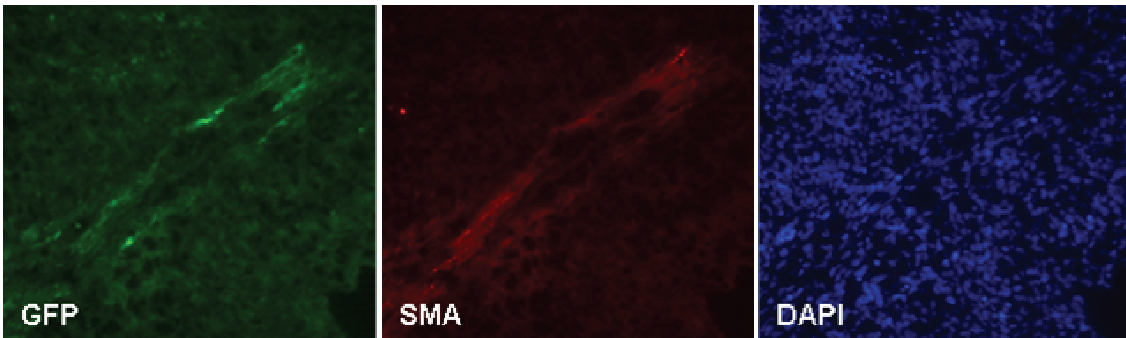
Figure 43. SMA26 shows weak GFP expression in glioma perivascular region
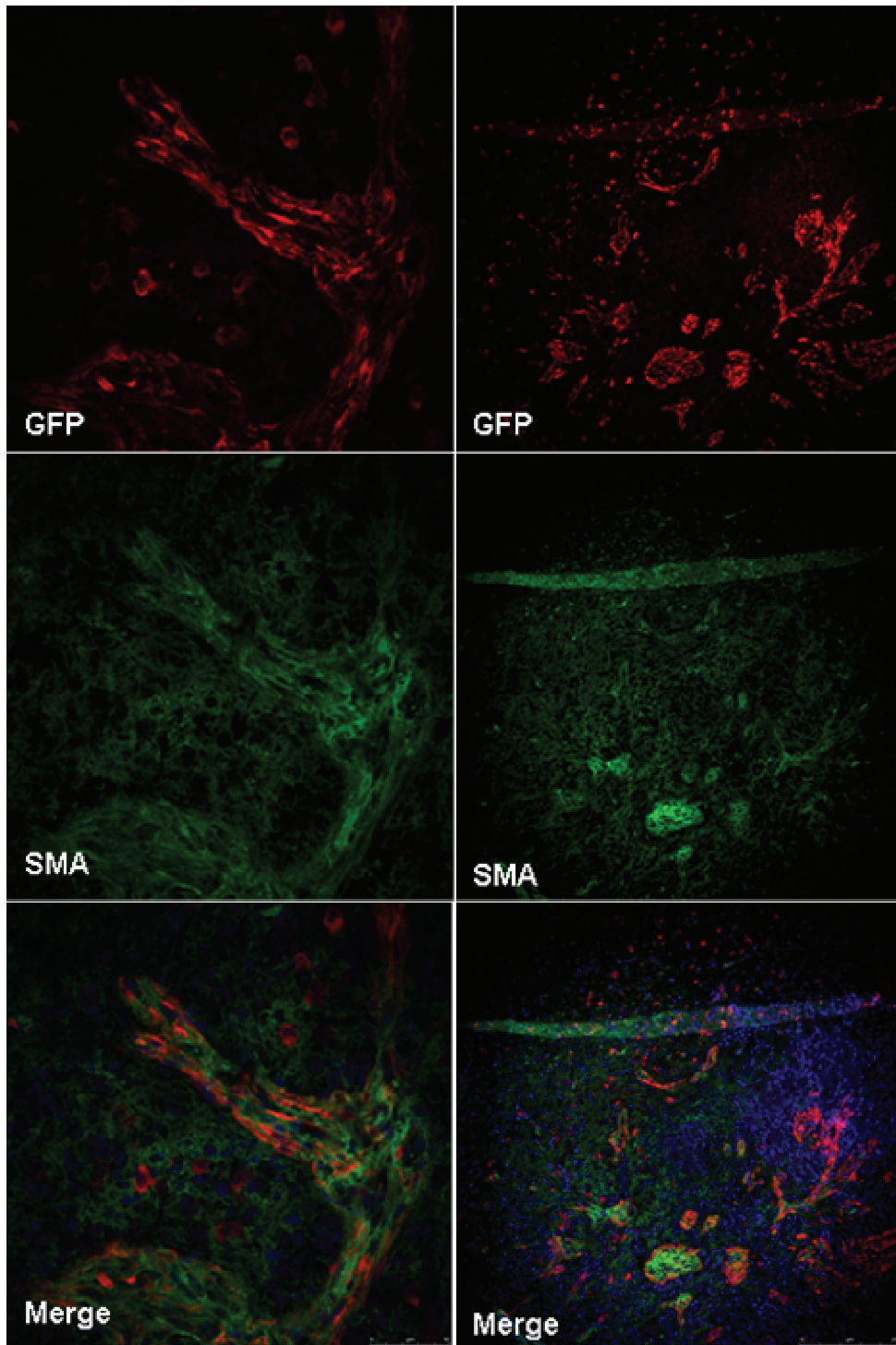
Figure 44. SMA9 expresses at high levels in brain perivascular region and other cells
SMA9 GFP expression in PDGF-driven gliomas. SMA9 expresses strongly in perivsacular regions. Expression also seen in non-vessel associated, apparently SMA- cells. High SMA background in tumor is not unusual.

To determine the yield of TRAP from brain tumors in these mice, and to assess the specificity of the RNA recovered, IP was performed on brain tumors from two lines, SMA9 and SMA20. Macrodissected brain tumor from SMA-9 yielded ~50ng of RNA via TRAP, while SMA20 yielded ~30ng of RNA but with higher background. To assess enrichment of smooth muscle markers, we performed qRT-PCR on immunoprecipitated RNA and input fractions. SMA9 showed high enrichment for SMA, some enrichment for SMMHC, and depletion of CD31, GFAP, and Olig2 (Fig 45). SMA20 showed modest enrichment for SMA, no enrichment for SMMHC, some depletion of GFAP and Olig2, and small enrichment of CD31. Notably, NeuN was enriched in both lines, suggesting that the SMA negative cells seen to express in brain tumors via staining are likely to be neurons. SMMHC amplified poorly in general, and while SMMHC is a general marker of smooth muscle cells, it may not be highly expressed in brain tumor vSMCs. Overall, given that it has stronger expression and yield than the other lines, and demonstrates greater enrichment of smooth muscle markers and depletion of other markers, the SMA9 line seems to be the most useful going forward. However, the issue of misexpression would seem to be a significant drawback for some purposes.

Tumors in SMA lines: IP vs Input (GAPDH/HPRT Normalized)
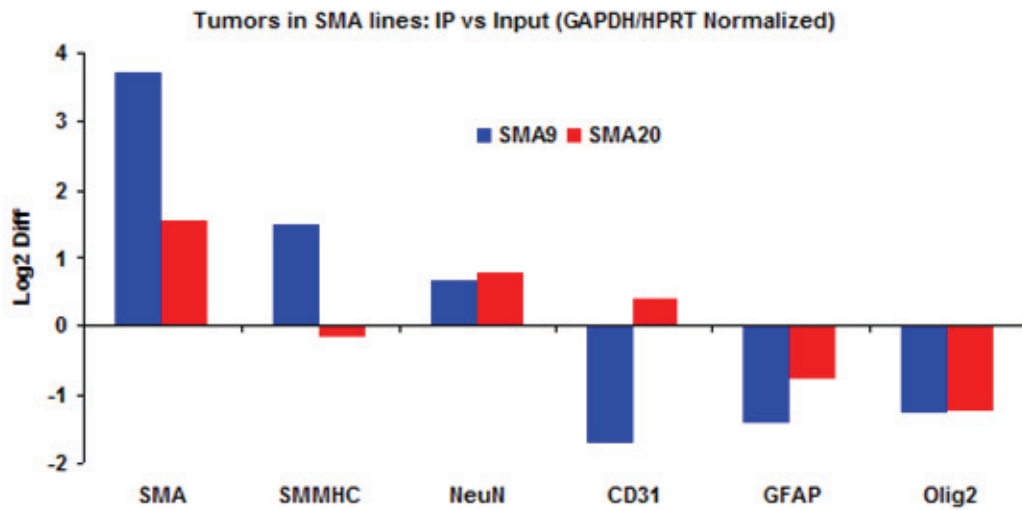
Figure 45. TRAP from PDGF-glioma in SMA lines enriches for vSMC/pericyte markers
qPCR on RCAS-PDGF tumor in SMA9 and SMA20 lines. SMA9 showed high enrichment for SMA, enrichment for SMMHC, and depletion of endothelial, astrocyte, and OPC/tumors markers. SMA20 showed less smooth muscle specific enrichments, with lower enrichment of SMA, no enrichment of SMMHC, no depletion of CD31, and some depletion of GFAP and Olig2. Both lines showed NeuN enrichment, likely indicating that the non-SMA cells seen to stain for GFP in PDGF tumors in these lines were neurons.

Astrocyte Targeted Lines

The GFAP-RPGFP construct was used to generate 17 positive founder mice. Animals with multiple integrants were identified by non-Mendelian inheritance patterns, and positive offspring separated to create sub-lines. 4 lines showing widespread expression were isolated. To improve ability to detect expression, kainic acid (KA) was administered to several lines before collection of brains. Kainic acid triggers excitatoxic damage and widespread gliosis in mice, resulting in upregulated GFAP expression. 2 lines were identified in this way, G64 and G23.

Expression in the G64 line was identified by KA treatment, which induced broad expression (Fig 46), but expression in and around tumors was patchy did not generally overlap well with GFAP staining (Fig 47). The G23 line expressed highly after KA treatment in many astrocytes (Fig 48). G23 expression was low in normal brain, but expression was seen in reactive astrocytes at the periphery of tumors, suggesting that this line may only express in activated astrocytes (Fig 49). G23 did not express in intratumoral astrocytes. Curiously, this line expresses in the purkinje neurons of the cerebellum (Fig 50). Overall, both G64 and G23 did not have high degrees of overlap with GFAP staining in tumors.
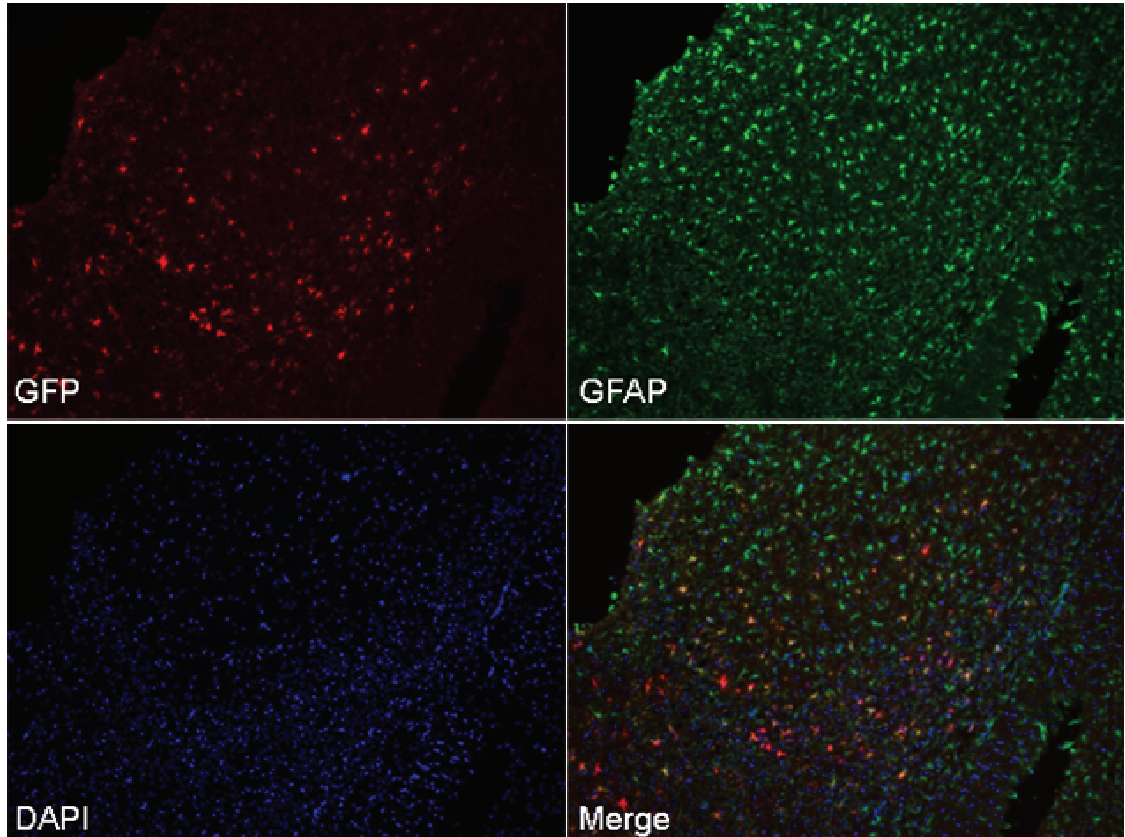
Figure 46. G23-RPGFP line GFP expression after kainic acid induced gliosis
Immunofluorescence of brain sections from mice treated with KA shows GFP expression in numerous reactive astrocytes accompanying widespread gliosis.
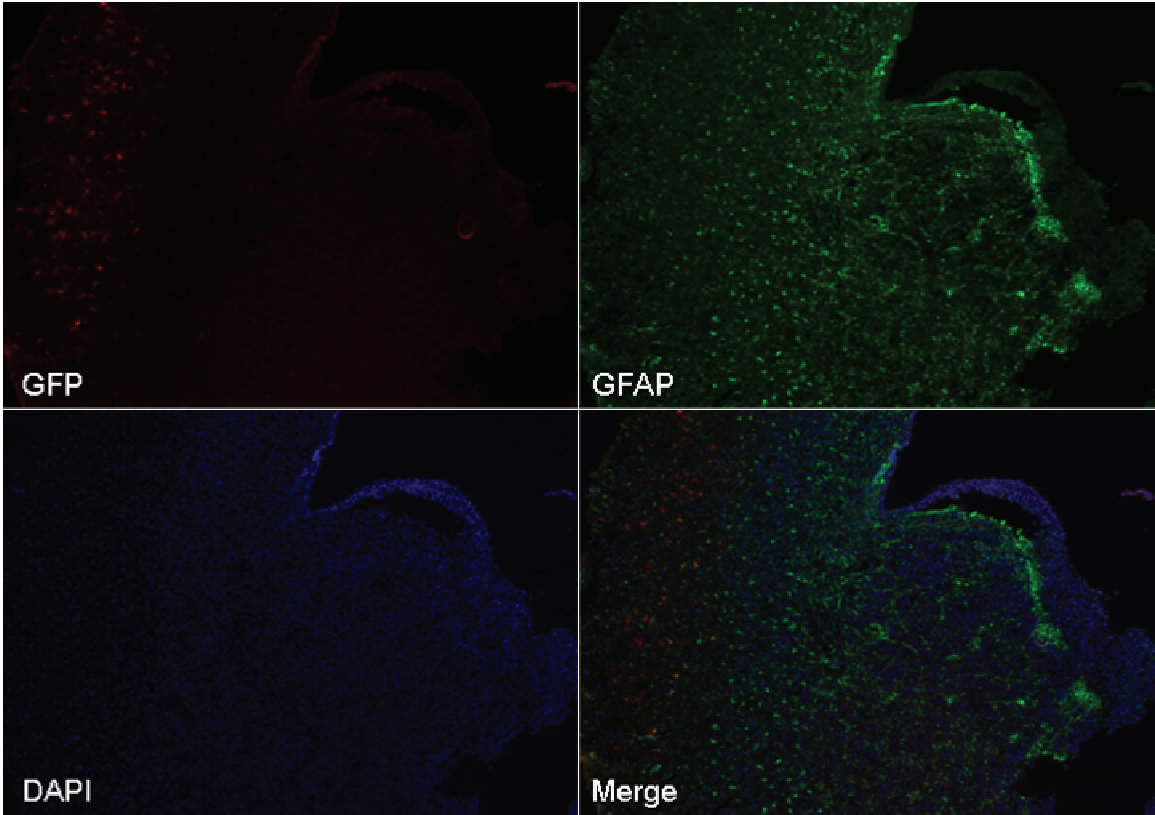
Figure 47. G23-RPGFP GFP Expression in Tumor Associated Astrocytes
Immunofluorescence of PDGF-driven gliomas from G23 line. GFP is expressed in some populations of peritumoral astrocytes at the invasive front of the tumor. G23 does not express in intra-tumoral astrocytes.
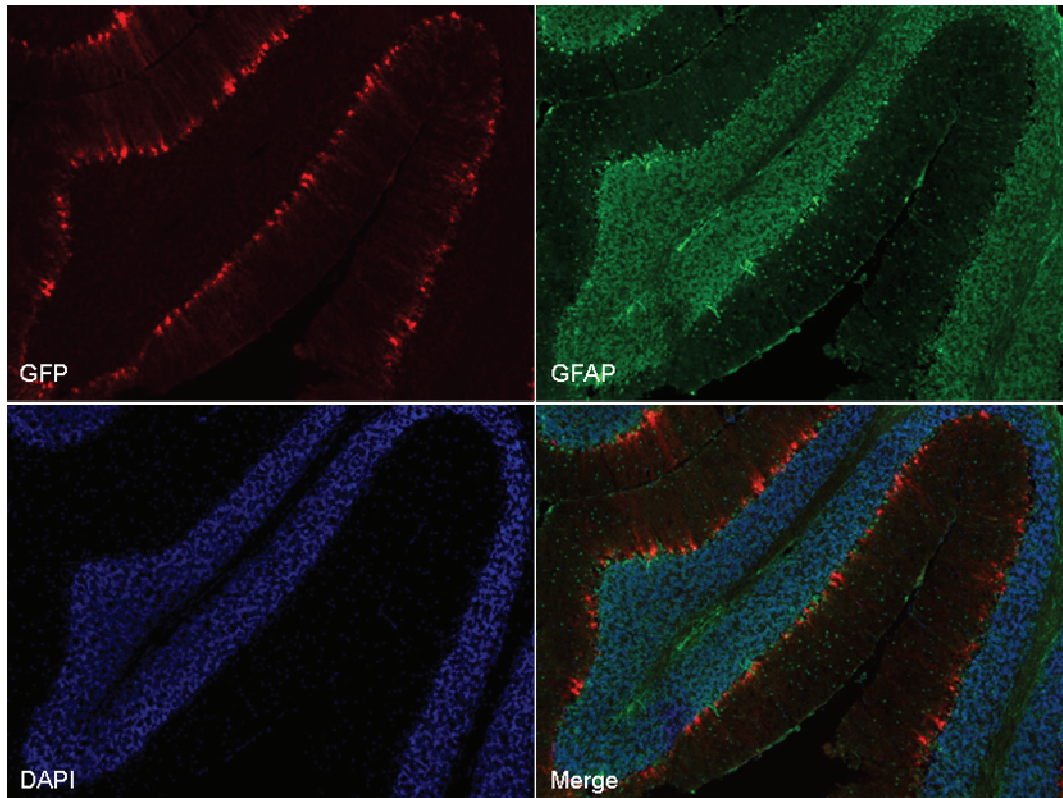
Figure 48. G23-RPGFP Expresses GFP in Purkinje cells of the cerebellum

G49 was identified by staining in the brains of young mice. Interestingly, it seems to express in the subventricular zone of the lateral ventricle, where GFAP+ stem cells reside (Fig 51). In tumor bearing mice, the G49 has the strongest expression of amongst GFAP lines by some margin. At the tumor periphery, regional expression was similar to astrocytes, but while it expressed in some astrocytes (Fig 52), expression was also lacking in a number of reactive astrocytes (Fig 53, 54). It also expressed in some cells that were not GFAP positive (Fig 52). Unfortunately this line appears to expess relatively strongly in the tumor bulk cells of PDGF driven gliomas (Fig 54). There may be some GFAP expression in these tumors which is below the detection threshold to which our antibodies are titrated, but which this strongly expressing line reveals.
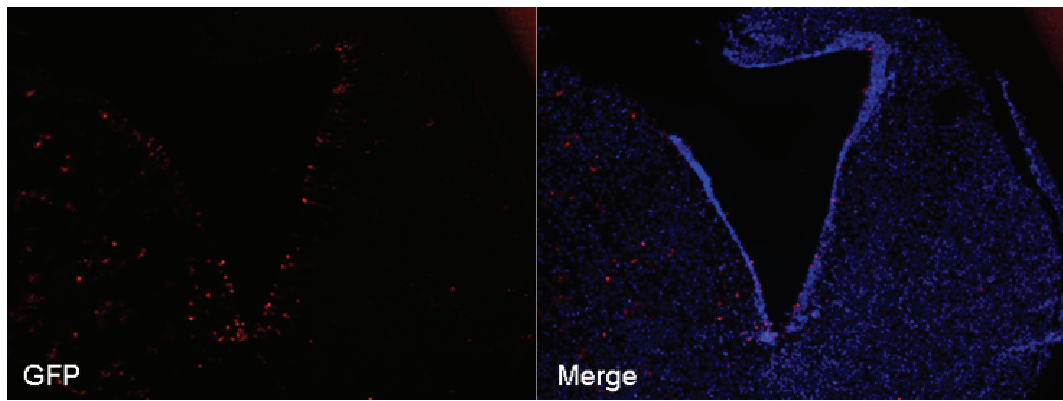
Figure 49. G49-RPGFP line expresses GFP in cells of lateral ventrical in juvenile mice.
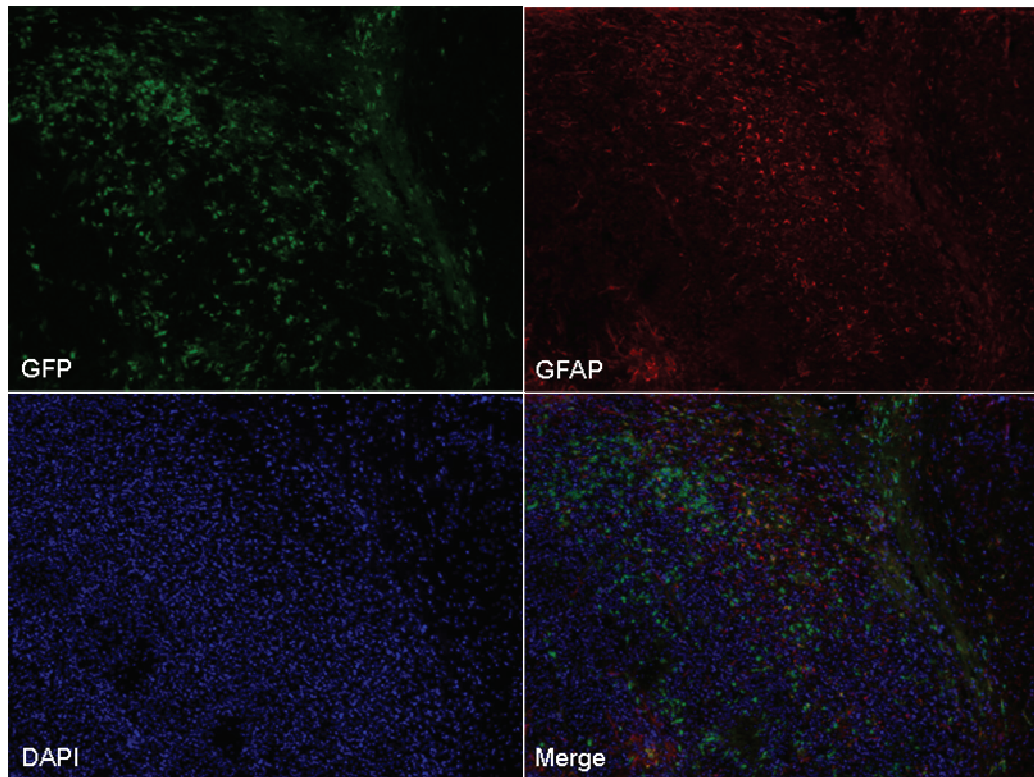
Figure 50. G49-RPGFP expresses in tumor associated astrocytes and some GFAP- cells
G49 GFP expression broadly overlapping with GFAP expression in PDGF-driven glioma. G49 expresses
in many glioma associated cells, including many reactive astrocytes, but also some GFAP- cells.
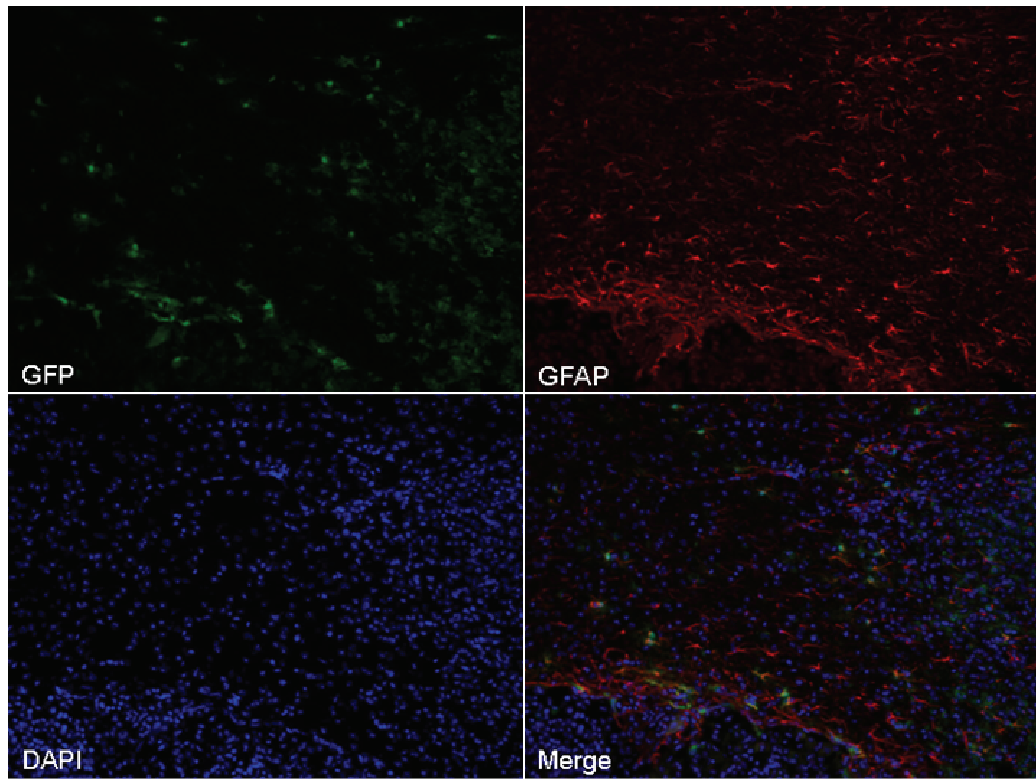
Figure 51. G49-RPGFP expresses in some but not all tumor associated reactive astrocytes
G49 GFP expression broadly overlaps with GFAP expression in PDGF-driven glioma.
Some GFAP+ reactive astrocytes do not express GFP.
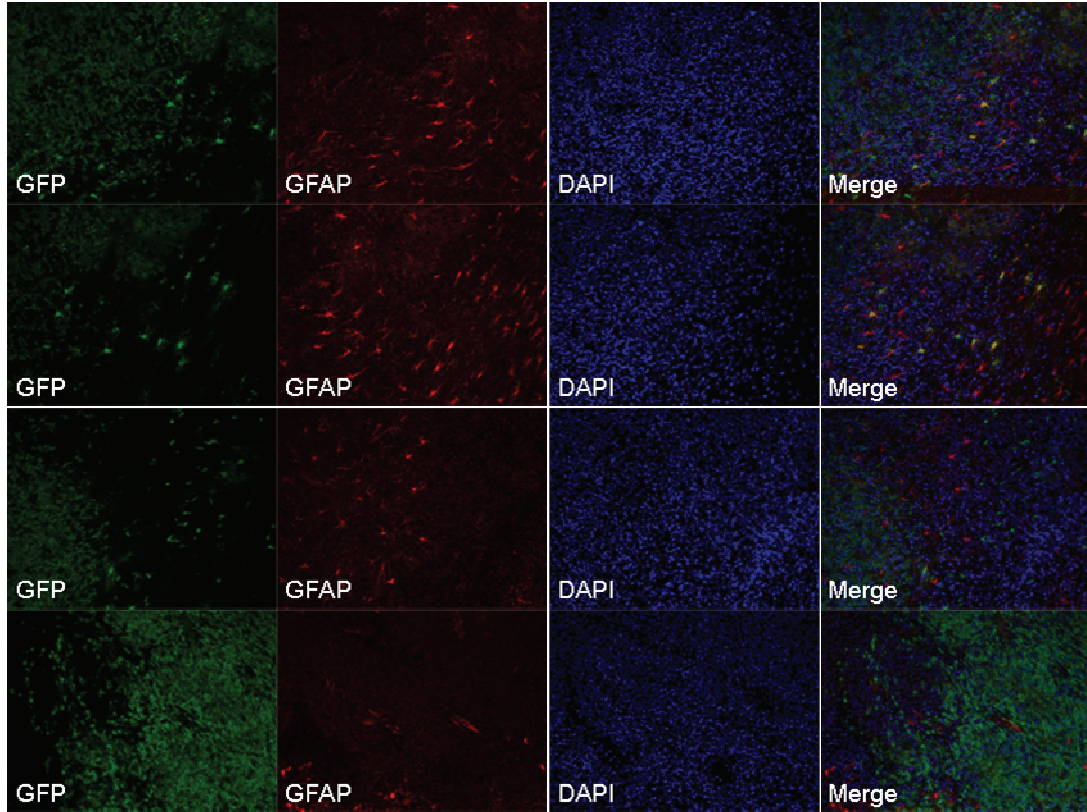
Figure 52. G49-RPGFP expresses GFP in PDGF-glioma tumor bulk
Immunofluorescence for GFP and GFAP shows co-expression in some reactive astrocytes. GFP is expressed on large regions of the tumor bulk.

Aldehyde dehydrogenase (ALDH1L1) was recently characterized as an astrocyte marker that labels astrocytes at least as well as GFAP (151).   An ALDH1L1 BAC promoter driven TRAP mouse has been made, which could potentially label astrocytes without being expressed in the tumor bulk (78). This line was no longer extant, so we had it line re-derived from frozen sperm samples. We characterized its expression in our tumors, and found it does not express in the tumor bulk cells of PDGF-driven gliomas. Furthermore the overlap with GFAP expressing astrocytes was nearly complete, including in the perivascular population of astrocytes (Fig 55). TRAP had previously been performed with this line and validated (78).

Of the 7 transgene positive CD44 lines generated, none expressed were positive for GFP expression. This was not completely surprising, as the construct used had little history and was barely characterized.

Microglia/Macrophage Targeted Lines

The CD11b-RPGFP construct was used to generate 8 transgene positive single integrant founder lines. To date, two of these lines were tested for GFP expression by intraperitoneal lavage, a procedure which is used to recover peritoneal macrophages. FACS analysis of these samples revealed GFP expression in both samples. Co-staining with CD11b antibody revealed overlap of the GFP and CD11b positive populations. Further characterization of these lines is ongoing in collaboration with the laboratory of Johanna Joyce.

146

Discussion

The VECad10a mouse yields usable quantities of RNA from several tissues via TRAP that is enriched for endothelial cell type markers. In tissues such as the lung or kidney, the yield is more than sufficient and these mice will likely prove useful for biological studies in these tissues. The relative overall rarity of these cells in the brain and brain tumors results in background levels that may be too high for some analyses if uncontrolled. However, it remains an option to assay the input samples in parallel to control for background. Methodological improvements may be able to increase the specificity of the RNA obtained and decrease background levels in the brain in these mice. The SMA9 line also yields usable quantities of RNA and expresses well in a variety of tissues. However, unlike the VECad10a line, it expresses aberrantly in non-smooth muscle cells in some tissues. In the brain it appears to express in a population of neurons. This mis-expression cannot be improved upon by protocol improvements short of elaborate transplantation assays, and may limit their usefulness in some organ systems. The GFAP49 mouse line expresses highly and in many reactive astrocytes, but expresses in tumor bulk cells in the de novo PDGF-driven model. This restricts its usefulness in the RCAS model, but it should still be useful in transplantation or xenograft models. The GFAP23 line does not express as broadly as the G49 line, but may label a restricted population of reactive astrocytes, as its expression was much higher in injured or tumor associated brain. The ALDH1L1 mouse likely represents the superior option in the RCAS-PDGF model, as it does not express in tumor bulk cells, yet has high levels of specific expression and good overlap with astrocytes. The characterization of the CD11b

lines is ongoing, but both of the lines tested to date have shown expression in CD11b cells.

Taken together, these lines represent a new resource for cell-type specific studies in the brain and variety of other organ systems in a wide range of mouse models. The VECad10a, GFAP, and ALDH1L1 lines have been shared with collaborators who are using them to study the role of endothelial cells and astrocytes in metastases to the brain and other organs such as the lung. The CD11b lines are being further validated and used by collaborators investigating the role of macrophages in cancer in a variety of organs. The VECadherin, SMA, and astrocyte lines together comprise a suite of tools ideally suited to studying tumor vasculature. Together these lines would be of particular use in deciphering the effects of the new line of anti-angiogenic therapies on glioma progression.

All data shown here was from the standard TRAP protocol using a 30 minute incubation with protein G dynabeads. Several alterations to the TRAP protocol were tested to attempt to improve yield and reduce background in the brain, but none significantly improved over the standard protocol. Biotinylated protein L in conjunction with streptavidin-coated magnetic beads had been suggested to reduce background and allow longer IP times, but in our hands the yield was lower as well, and no timepoint provided either improved enrichment or yield relative to the standard protocol. Direct conjugation of the antibodies to beads via epoxy was also tested, but resulted in very high background. Other techniques such as preclearing the lysate, increasing the lysis volume, and increasing washes were tried, but did not yield any noticeable improvements. Increasing the immunoprecipitation time to 2 hours from 30 minutes improved yields

while maintaining similar levels of enrichment versus background in some cases. Different incubation periods may prove optimal for different tissues, given different levels of RNase activity, yield, and background. There remain other commercially available beads suggested to improve enrichment that may yet reduce background.

In tissues other than brain, levels of RNase pose technical challenges. One potential method for dealing with RNase would be to incorporate some of the older non-specific RNase inhibitors, such as heparin. These have fallen out of favor as a class because they inhibit most downstream enzymatic reactions, such as reverse transcription and PCR, and can be difficult to remove via precipitation. Since RNA is bound to beads which facilitate washing during TRAP, it may be possible to use non-specific RNase inhibitors in the lysate and then eliminate them via washing. We performed pilot experiments with vanadyl ribonuclease complex in the homogenization buffer (152). We found it to have potent RNase inhibitory properties, but it appeared to adhere to the magnetic beads and dramatically increased background.

DISCUSSION AND SUMMARY

The importance of the *in vivo* tumor microenvironment and the differences in tumor cell behavior *in vivo* and *in vitro* has become more and more apparent. Mouse models are increasingly able to reproduce the complex microenvironment seen in human disease. However, tools are still needed to tease out the interactions in the complex systems that these mouse models represent. Previously cell sorting methods such as FACS were the sole method for studying specific cell types within a complex tumor. Cell sorting methods are only feasible when a given tissue can be dissociated in a way that allows recovery of intact individual cells. No previous system allowed *in vivo* translational profiling; only total mRNA profiles could be assessed. Translation is a regulated and important step in determining cellular behavior that is frequently dysregulated in tumors. Translation occurs independently from transcription, and mechanisms and pathways regulating translation represent a separate set of potential therapeutic targets in the disease setting.

Our understanding of the patterns of genomic lesions and expression alterations within gliomas as a class have changed the way this disease is viewed in recent years. High grade gliomas are comprised of distinct subtypes of disease, each characterized by activation of different signaling pathways. This evidence requires a re-evaluation of what constitutes a relevant mouse model of glioma. Mouse models must not just recapitulate the histology of human glioma, but a given molecular profile as well.

Here we present a system that allows the assessment of gene expression changes and regulation at both the transcriptional and translational level in defined cell types *in*

vivo. We used this system in a relevant model of the proneural subtype of glioma to assess the differences in translational regulation between transformed and normal brain oligodendrocyte precursor cells. We found that genes associated with proliferation are translated with increased efficiency in transformed Olig2+ tumor cells when compared to the normal Olig2+ OPCs that they most closely resemble, highlighting the potential importance of translational regulation in disease and the corresponding possibilties for novel therapeutic interventions. We then compared the translatome of PDGF-driven PTEN WT and PTEN deleted tumors. PTEN is frequently deleted in human glioma, and inhibits the PI3K/Akt/mTOR pathway, which is a known regulator of translation. Interestingly, we found that PTEN loss results in downregulation of genes associated with oxidative phosphorylation. PI3K pathway upregulation in tumor cells is associated with a shift from oxidative phosphorylation towards glycolysis, a phenomenon known as the Warburg Effect. These data suggest that there is a previously unappreciated translational component to the induction of the Warburg Effect by PI3K.

We next used our system to examine the response of the proneural glioma model to radiation. Radiation induced transient cell cycle arrest and apoptosis which was restricted to the Olig2+ tumor bulk, again highlighting the need for cell type specificity in profiling studies. Surprisingly, and in contrast with previous results from cell culture (56), alterations in the mRNA content of tumor bulk cells was a greater determinant of changes in translated mRNA than changes in the efficiency with which mRNAs were recruited to the ribosome after irradiation. The overall *in vivo* radiation response appears to be largely driven by the transcription factors p53 and E2F, and indeed the most highly induced genes after irradiation in p53 intact tumors were all sensitive to the knockdown

of p53 activity. Most interestingly, we found that irradiation of PDGF-driven tumors induces a rapid shift in glioma subtype from proneural to mesenchymal. This happened within 6 hours regardless of PTEN status and appears to be insensitive to p53 knockdown. The shift occurs in tumor cells themselves and is not the result of relative enrichment of the more radiation-resistant stroma. Stat3 and CEBPB have been reported as master regulators of a shift towards the mesenchymal subtype, and targets of both were upregulated after irradiation. The rapidity of the shift is surprising and implies that the glioma subtypes are more plastic that previously supposed. This has large implications for ongoing attempts to tailor individual therapy based on subtyping. Optimal adjuvant therapy for a patient undergoing radiotherapy, for instance, might involve targeted inhibition of both proneural and mesenchymal associated pathways.

Much recent work from our lab and others has focused on the important active and passive roles that stromal cell types play in tumorigenesis and tumor development. We sought to extend our in vivo gene expression profiling system to the stromal cells found in gliomas and other tumors. TRAP mice were generated that target endothelial cells, vascular smooth muscle cells, astrocytes, and microglia.

This collection of mice provides a new set of tools for cell type specific studies *in vivo*. In addition to enabling translational studies, these mice provide significant advantages over cell sorting approaches for cell type specific expression profiling. Ribosome-associated RNA on a stand-alone basis better represents the protein production of a given type than total mRNA. There are practical benefits to TRAP isolation of RNA – TRAP does not require expensive capital equipment and can be performed on short

notice. Furthermore, TRAP may represent a superior means to obtaining cell type specific RNA in tissues that are difficult to dissociate.

Further improvements in the TRAP methodology should offer better RNase control in non-brain tissues. Alterations to the immunoprecipitation protocol may be able to improve yield and reduce background. Currently in some tissues where the cell population of interest is relatively rare, background is high relative to the cell-type specific RNA recovered. However, in these cases there remains the option of assaying input samples in parallel to control for background.

There are several limitations of the TRAP method that must be kept in mind. First and foremost, translation of proteins is not necessarily reflective of cellular protein activity; protein folding and maturation, post-translational modification, intracellular location and trafficking, and protein sequestration or degradation all affect the activity of protein after translation. Further, various factors can result in artifacts affecting both TRAP expression profiles and their application in measuring translation. The sensitivity of TRAP in some instances may also be lower than sucrose gradient isolation of polysomes, and techniques should be considered to improve TRAP sensitivity.

Differences between tissues and homogenization conditions have the potential to lead to artifacts in expression signatures. The contribution of background signal from the non-target cells in a tissue will vary depending on the expression profile of other cells in the tissue, the relative prevalence of the target cell type, and the accuracy of dissection. For this reason, the input tissue lysate is a critical control, especially when comparing across tissue types. Additionally, endoplasmic reticulum bound ribosomes and their associated messages must be solubilized utilizing the detergent DHPC. Therefore, the

apparent abundance of transcripts encoding proteins that mature through the secretory pathway may be particularly sensitive to variance in the efficiency of this solubilization step.

There are additional caveats to consider when using TRAP to perform translational studies. FACS and TRAP may differentially enrich different sets of transcripts that are not reflective of differences in translation. As FACS isolation recovers individual cells based on their level of fluorescence, it can be used to recover mRNA only from cells reaching a certain threshold of fluorescence. In contrast, TRAP will recover mRNA from any cells that express the TRAP transgene, regardless of expression level, in proportion to that level of expression. In tissues with abundant cells of interest, the importance of this is likely to be minor, but in tissues with rare cells of interest, low levels of GFP expression in abundant non-target cells could cause significant differences in expression profiles. FACS is also prone to false positives from autofluorescent cells. For instance, various tumor treatments result in an influx of immune cells, which are known to be highly autofluorescent. There is evidence from our tumors that some treatments which result in an influx of immune cells do result in an increase of immune markers in FACS expression profiles but not in TRAP expression profiles. These apparent translational differences may represent false positive immune cell FACS contamination. Lower prevalence of the target cell type will tend to exacerbate both the extent of background from TRAP as well as the fraction of improperly sorted false-positives from FACS.

TRAP may also be less sensitive than other methods of assessing translational regulation. Unlike sucrose gradient centrifugation isolation of polysomes, TRAP

expression profiling translational studies do not provide data on the number of ribosomes present on an mRNA. To the extent that lowly translated transcripts are occupied by few ribosomes rather than none, and to the extent that TRAP is able to recover mRNAs occupied by one ribosome with similar efficiency as mRNAs occupied by many ribosomes, the sensitivity of TRAP to translational regulation alterations may be relatively low.

Translational regulation can be mediated by mRNAs shifting between states of high ribosome occupancy (i.e. polysomes) and being unoccupied, in which case TRAP should be sensitive to changes in translational regulation. However, if translational regulation involves shifting between high and low ribosome occupancy (i.e. monosomes), it may be difficult to distinguish between high and low levels of translation with TRAP. In many sucrose gradient studies of translation, the RNA content of the unbound fraction or fractions is not clearly reported. However, it is clear that many stresses and treatments that inhibit translation result in a great increase in the monosome fraction which could account for a considerable portion of the decrease in the polysome fraction (153-155).

The ability of TRAP to recover mRNAs this monosome fraction depends both on the affinity of the anti-GFP antibody used and the percentage of ribosomes that contain the tagged L10a subunit. TRAP utilizes a pair of relatively high affinity anti-GFP monoclonal antibodies in order to generate usable yields of mRNA from rare cell types. Similarly, highly expressing mouse lines have been selected for the purposes of obtaining usable yields of mRNA. Higher transgene expression increases the percentage of ribosomes containing the GFP tagged L10a subunit. This combination of high transgene expression and high affinity antibodies may result in relatively efficient recovery of even

transcripts bound by a single ribosome. Thus, it is possible that in some contexts, translational regulation causes mRNAs to shift from high and low ribosome occupancy, but those mRNAs will nevertheless be efficiently recovered by TRAP, resulting in understated measures of translational regulation. However, in the initial report of the TRAP method, Heiman et al. reported comparable (albeit smaller) measurements of translational regulation from TRAP as compared to sucrose gradient measures in an *in vitro* ferritin translational system (82). Preliminary *in vitro* studies in our hands have given similar results.

A highly specific yet lower affinity anti-GFP antibody might result in preferential isolation of transcripts bound by multiple ribosomes due to cooperative binding effects. This would result in a lower yield of translating RNA, so the overall usefulness of such an approach is unclear, and would depend on the specifics of the antibody and the organ system and cell type being assayed. Similarly, transgenic lines with lower levels of transgene expression may reduce levels of transgene incorporation into ribosomes, thereby reducing monsome recovery relative to polysome recovery. However, this would also negatively impact on the RNA yields.

One potential means to increasing the sensitivity of translational measure obtained via TRAP would be to incorporate recently described ribosome footprinting techniques (156, 157). These techniques utilize the ability of the ribosome to protect bound mRNA from RNase digestion. Polysomes are typically isolated via sucrose gradient centrifugation, followed by digestion with RNAse. RNA fragments corresponding to the "footprint" of one ribosome are isolated and subjected to RNA-Seq to determine the sequence of mRNA to which the ribosome was bound. In this way, whole transcriptome

ribosome occupancy rates can be determined, offering extremely granular, transcript-specific information on translation states. These methods have been developed for *in vitro* use and currently require large amounts of input RNA.

It may be possible to adapt this method for use with mRNA isolated via TRAP rather than sucrose gradient. High affinity antibodies could be used to maximize ribosome-bound mRNA isolation, with the footprinting method then used to asses ribosome occupancy. This combined method would give much more sensitive measures of translational regulation, as well as additional information about ribosome density and location on transcripts. The principal hurdle to this method is the amount of input RNA currently required. This method would also be highly sensitive to any residual RNase activity during the immunoprecipitation procedure. Higher RNase activity would cause increased degradation of the intervening mRNA sequence between ribosomes, resulting in the loss of any ribosomes not bound directly to anti-GFP antibodies during washing. This loss of bound ribosomes could then be interpreted as decreased translational activity.

Going forward, these mice can be used to study the response of tumor and stromal cell types to other current and potential treatments. The effects of various potential pharmaceutical interventions on important translationally regulated transcripts in tumor cells can be studied *in vivo*. Furthermore, we can use these datasets to begin to identify important *in vivo* regulators of translation. Transcript specific regulation of translation can occur through various mechanisms, including miRNA binding, RNA binding proteins, and structured regions of the UTRs. Enrichment of miRNA and protein binding sites and predicted mRNA secondary structures amongst translationally regulated transcripts can be used to generate candidate *in vivo* translational regulators for further

study. The TRAP system can then provide an *in vivo* method to assess perturbations of these candidate regulatory mechanisms. In the cancer setting, validated translational regulators may represent desirable drug targets, and translational effects of candidate drugs could be assessed *in vivo* via the TRAP system. More broadly, this set of mice will allow investigators to perform comprehensive transcriptional and translational profiling in a wide range of organ and disease systems; already these mice are being used by collaborators to study the role of these cells types in metastasis to various organs.

BIBLIOGRAPHY

1. Wen PY, Kesari S (2008) Malignant gliomas in adults. *N Engl J Med* 359:492-507.

2. Huse JT, Holland EC (2010) Targeting brain cancer: advances in the molecular pathology of malignant glioma and medulloblastoma. *Nat Rev Cancer* 10:319-331.

3. Louis DN, et al. (2007) The 2007 WHO classification of tumours of the central nervous system. *Acta Neuropathol* 114:97-109.

4. Rong Y, Durden DL, Van Meir EG, Brat DJ (2006) 'Pseudopalisading' necrosis in glioblastoma: a familiar morphologic feature that links vascular pathology, hypoxia, and angiogenesis. *J Neuropathol Exp Neurol* 65:529-539.

5. Anonymous (2008) Comprehensive genomic characterization defines human glioblastoma genes and core pathways. *Nature* 455:1061-1068.

6. Parsons DW, et al. (2008) An integrated genomic analysis of human glioblastoma multiforme. *Science* 321:1807-1812.

7. Efeyan A, Serrano M (2007) p53: Guardian of the Genome and Policeman of the Oncogenes. *Cell Cycle* 6:1006-1010.

8. Zilfou JT, Lowe SW (2009) Tumor suppressive functions of p53. *Cold Spring Harb Perspect Biol* 1:a001883.

9. Yan H, et al. (2009) IDH1 and IDH2 mutations in gliomas. *N Engl J Med* 360:765-773.

10. Dang L, et al. (2009) Cancer-associated IDH1 mutations produce 2-hydroxyglutarate. *Nature* 462:739-744.

11. Noushmehr H, et al. (2010) Identification of a CpG island methylator phenotype that defines a distinct subgroup of glioma. *Cancer Cell* 17:510-522.

12. Turcan S, et al. (2012) IDH1 mutation is sufficient to establish the glioma hypermethylator phenotype. *Nature* 483:479-483.

13. Phillips HS, et al. (2006) Molecular subclasses of high-grade glioma predict prognosis, delineate a pattern of disease progression, and resemble stages in neurogenesis. *Cancer Cell* 9:157-173.

14. Verhaak RG, et al. (2010) Integrated genomic analysis identifies clinically relevant subtypes of glioblastoma characterized by abnormalities in PDGFRA, IDH1, EGFR, and NF1. *Cancer Cell* 17:98-110.

15. Brennan C, et al. (2009) Glioblastoma subclasses can be defined by activity among signal transduction pathways and associated genomic alterations. *PLoS One* 4:e7752.

16. Kinzler KW, Vogelstein B (1998) Landscaping the cancer terrain. *Science* 280:1036-1037.

17. Skobe M, Fusenig NE (1998) Tumorigenic conversion of immortal human keratinocytes through stromal cell activation. *Proc Natl Acad Sci U S A* 95:1050-1055.

18. Hanahan D, Folkman J (1996) Patterns and emerging mechanisms of the angiogenic switch during tumorigenesis. *Cell* 86:353-364.

19. Hanahan D, Weinberg RA (2000) The hallmarks of cancer. *Cell* 100:57-70.
20. Wesseling P, et al. (1995) Early and extensive contribution of pericytes/vascular smooth muscle cells to microvascular proliferation in glioblastoma multiforme: an immuno-light and immuno-electron microscopic study. *J Neuropathol Exp Neurol* 54:304-310.
21. Charles NA, Holland EC, Gilbertson R, Glass R, Kettenmann H (2012) The brain tumor microenvironment. *Glia* 60:502-514.
22. Tate M, Aghi M (2009) Biology of angiogenesis and invasion in glioma. *Neurotherapeutics* 6:447-457.
23. Kerbel RS (2008) Tumor angiogenesis. *N Engl J Med* 358:2039-2049.
24. Norden AD, Drappatz J, Wen PY (2009) Antiangiogenic therapies for high-grade glioma. *Nat Rev Neurol* 5:610-620.
25. Ferrara N (2004) Vascular Endothelial Growth Factor: Basic Science and Clinical Progress. *Endocr Rev* 25:581-611.
26. Plate KH, Breier G, Weich HA, Risau W (1992) Vascular endothelial growth factor is a potential tumour angiogenesis factor in human gliomas in vivo. *Nature* 359:845-848.
27. Ferrara N, Kerbel RS (2005) Angiogenesis as a therapeutic target. *Nature* 438:967-974.
28. Charles N, et al. (2010) Perivascular nitric oxide activates notch signaling and promotes stem-like character in PDGF-induced glioma cells. *Cell Stem Cell* 6:141-152.
29. Hellstrom M, Kalen M, Lindahl P, Abramsson A, Betsholtz C (1999) Role of PDGF-B and PDGFR-beta in recruitment of vascular smooth muscle cells and pericytes during embryonic blood vessel formation in the mouse. *Development* 126:3047-3055.
30. Benjamin LE, Golijanin D, Itin A, Pode D, Keshet E (1999) Selective ablation of immature blood vessels in established human tumors follows vascular endothelial growth factor withdrawal. *J Clin Invest* 103:159-165.
31. Armulik A, et al. (2010) Pericytes regulate the blood-brain barrier. *Nature* 468:557-561.
32. Song S, Ewald AJ, Stallcup W, Werb Z, Bergers G (2005) PDGFRbeta+ perivascular progenitor cells in tumours regulate pericyte differentiation and vascular survival. *Nat Cell Biol* 7:870-879.
33. Morikawa S, et al. (2002) Abnormalities in pericytes on blood vessels and endothelial sprouts in tumors. *Am J Pathol* 160:985-1000.
34. Calabrese C, et al. (2007) A perivascular niche for brain tumor stem cells. *Cancer Cell* 11:69-82.
35. Watters JJ, Schartner JM, Badie B (2005) Microglia function in brain tumors. *J Neurosci Res* 81:447-455.
36. Halliday JJ, Holland EC (2011) Connective tissue growth factor and the parallels between brain injury and brain tumors. *J Natl Cancer Inst* 103:1141-1143.
37. Charles N, Holland EC (2010) The perivascular niche microenvironment in brain tumor progression. *Cell Cycle* 9:3012-3021.
38. Markovic DS, et al. (2009) Gliomas induce and exploit microglial MT1-MMP expression for tumor expansion. *Proc Natl Acad Sci U S A* 106:12530-12535.

39.   Lewis CE, Pollard JW (2006) Distinct role of macrophages in different tumor microenvironments. *Cancer Res* 66:605-612.

40.   Katz AM, et al. (2012) Astrocyte-specific expression patterns associated with the PDGF-induced glioma microenvironment. *PLoS One* 7:e32453.

41.   Amankulor NM, et al. (2009) Sonic hedgehog pathway activation is induced by acute brain injury and regulated by injury-related inflammation. *J Neurosci* 29:10299-10308.

42.   Becher OJ, et al. (2008) Gli activity correlates with tumor grade in platelet-derived growth factor-induced gliomas. *Cancer Res* 68:2241-2249.

43.   Ohka F, Natsume A, Wakabayashi T (2012) Current trends in targeted therapies for glioblastoma multiforme. *Neurol Res Int* 2012:878425.

44.   Jelsma R, Bucy PC (1967) The treatment of glioblastoma multiforme of the brain. *J Neurosurg* 27:388-400.

45.   Walker MD, Strike TA, Sheline GE (1979) An analysis of dose-effect relationship in the radiotherapy of malignant gliomas. *Int J Radiat Oncol Biol Phys* 5:1725-1731.

46.   Walker MD, et al. (1980) Randomized comparisons of radiotherapy and nitrosoureas for the treatment of malignant glioma after surgery. *N Engl J Med* 303:1323-1329.

47.   Stupp R, et al. (2009) Effects of radiotherapy with concomitant and adjuvant temozolomide versus radiotherapy alone on survival in glioblastoma in a randomised phase III study: 5-year analysis of the EORTC-NCIC trial. *The Lancet Oncology* 10:459-466.

48.   Uhm JH, et al. (2011) Phase II evaluation of gefitinib in patients with newly diagnosed Grade 4 astrocytoma: Mayo/North Central Cancer Treatment Group Study N0074. *Int J Radiat Oncol Biol Phys* 80:347-353.

49.   Friedman HS, et al. (2009) Bevacizumab alone and in combination with irinotecan in recurrent glioblastoma. *J Clin Oncol* 27:4733-4740.

50.   Chinot OL, et al. (2011) AVAglio: Phase 3 trial of bevacizumab plus temozolomide and radiotherapy in newly diagnosed glioblastoma multiforme. *Adv Ther* 28:334-340.

51.   Keunen O, et al. (2011) Anti-VEGF treatment reduces blood supply and increases tumor cell invasion in glioblastoma. *Proc Natl Acad Sci U S A* 108:3749-3754.

52.   Fomchenko EI, Holland EC (2006) Mouse Models of Brain Tumors and Their Applications in Preclinical Trials. *Clinical Cancer Research* 12:5288-5297.

53.   Reynolds BA, Weiss S (1992) Generation of neurons and astrocytes from isolated cells of the adult mammalian central nervous system. *Science* 255:1707-1710.

54.   Galli R, et al. (2004) Isolation and Characterization of Tumorigenic, Stem-like Neural Precursors from Human Glioblastoma. *Cancer Research* 64:7011-7021.

55.   Lee J, et al. (2006) Tumor stem cells derived from glioblastomas cultured in bFGF and EGF more closely mirror the phenotype and genotype of primary tumors than do serum-cultured cell lines. *Cancer Cell* 9:391-403.

56.   Jamal M, Rath BH, Williams ES, Camphausen K, Tofilon PJ (2010) Microenvironmental regulation of glioblastoma radioresponse. *Clin Cancer Res* 16:6049-6059.

57. Huse JT, Holland EC (2009) Genetically engineered mouse models of brain cancer and the promise of preclinical testing. *Brain Pathol* 19:132-143.

58. Reilly KM, Loisel DA, Bronson RT, McLaughlin ME, Jacks T (2000) Nf1;Trp53 mutant mice develop glioblastoma with evidence of strain-specific effects. *Nat Genet* 26:109-113.

59. Zhu Y, et al. (2005) Early inactivation of p53 tumor suppressor gene cooperating with NF1 loss induces malignant astrocytoma. *Cancer Cell* 8:119-130.

60. Ding H, et al. (2001) Astrocyte-specific expression of activated p21-ras results in malignant astrocytoma formation in a transgenic mouse model of human gliomas. *Cancer Res* 61:3826-3836.

61. Xiao A, Wu H, Pandolfi PP, Louis DN, Van Dyke T (2002) Astrocyte inactivation of the pRb pathway predisposes mice to malignant astrocytoma development that is accelerated by PTEN mutation. *Cancer Cell* 1:157-168.

62. Uhrbom L, Hesselager G, Nister M, Westermark B (1998) Induction of brain tumors in mice using a recombinant platelet-derived growth factor B-chain retrovirus. *Cancer Res* 58:5275-5279.

63. Hughes SH, Greenhouse JJ, Petropoulos CJ, Sutrave P (1987) Adaptor plasmids simplify the insertion of foreign DNA into helper-independent retroviral vectors. *Journal of Virology* 61:3004-3012.

64. Bates P, Young JA, Varmus HE (1993) A receptor for subgroup A Rous sarcoma virus is related to the low density lipoprotein receptor. *Cell* 74:1043-1051.

65. Young JA, Bates P, Varmus HE (1993) Isolation of a chicken gene that confers susceptibility to infection by subgroup A avian leukosis and sarcoma viruses. *J Virol* 67:1811-1816.

66. Holland EC, Hively WP, DePinho RA, Varmus HE (1998) A constitutively active epidermal growth factor receptor cooperates with disruption of G1 cell-cycle arrest pathways to induce glioma-like lesions in mice. *Genes Dev* 12:3675-3685.

67. Holland EC, Hively WP, Gallo V, Varmus HE (1998) Modeling mutations in the G1 arrest pathway in human gliomas: overexpression of CDK4 but not loss of INK4a-ARF induces hyperploidy in cultured mouse astrocytes. *Genes Dev* 12:3644-3649.

68. Holland EC, et al. (2000) Combined activation of Ras and Akt in neural progenitors induces glioblastoma formation in mice. *Nat Genet* 25:55-57.

69. Shih AH, et al. (2004) Dose-dependent effects of platelet-derived growth factor-B on glial tumorigenesis. *Cancer Res* 64:4783-4789.

70. Marumoto T, et al. (2009) Development of a novel mouse glioma model using lentiviral vectors. *Nat Med* 15:110-116.

71. de Vries NA, et al. (2010) Rapid and Robust Transgenic High-Grade Glioma Mouse Models for Therapy Intervention Studies. *Clinical Cancer Research* 16:3431-3441.

72. Fomchenko EI, et al. (2011) Recruited cells can become transformed and overtake PDGF-induced murine gliomas in vivo during tumor progression. *PLoS One* 6:e20605.

73. Spriggs KA, Bushell M, Willis AE (2010) Translational Regulation of Gene Expression during Conditions of Cell Stress. *Molecular Cell* 40:228-237.

74. Sonenberg N, Hinnebusch AG (2009) Regulation of translation initiation in eukaryotes: mechanisms and biological targets. *Cell* 136:731-745.

75. Jackson RJ, Hellen CU, Pestova TV (2010) The mechanism of eukaryotic translation initiation and principles of its regulation. *Nat Rev Mol Cell Biol* 11:113-127.

76. Lu X, de la Pena L, Barker C, Camphausen K, Tofilon PJ (2006) Radiation-induced changes in gene expression involve recruitment of existing messenger RNAs to and away from polysomes. *Cancer Res* 66:1052-1061.

77. Hu X, et al. (2005) mTOR promotes survival and astrocytic characteristics induced by Pten/AKT signaling in glioblastoma. *Neoplasia* 7:356-368.

78. Doyle JP, et al. (2008) Application of a translational profiling approach for the comparative analysis of CNS cell types. *Cell* 135:749-762.

79. Pitter KL, et al. (2011) Perifosine and CCI 779 co-operate to induce cell death and decrease proliferation in PTEN-intact and PTEN-deficient PDGF-driven murine glioblastoma. *PLoS One* 6:e14545.

80. Squatrito M, et al. (2010) Loss of ATM/Chk2/p53 pathway components accelerates tumor development and contributes to radiation resistance in gliomas. *Cancer Cell* 18:619-629.

81. Bleau AM, et al. (2009) PTEN/PI3K/Akt pathway regulates the side population phenotype and ABCG2 activity in glioma tumor stem-like cells. *Cell Stem Cell* 4:226-235.

82. Heiman M, et al. (2008) A translational profiling approach for the molecular characterization of CNS cell types. *Cell* 135:738-748.

83. Hambardzumyan D, Amankulor NM, Helmy KY, Becher OJ, Holland EC (2009) Modeling Adult Gliomas Using RCAS/t-va Technology. *Transl Oncol* 2:89-95.

84. Becher OJ, et al. (2010) Preclinical evaluation of radiation and perifosine in a genetically and histologically accurate model of brainstem glioma. *Cancer Res* 70:2548-2557.

85. Hambardzumyan D, et al. (2008) PI3K pathway regulates survival of cancer stem cells residing in the perivascular niche following radiation in medulloblastoma in vivo. *Genes Dev* 22:436-448.

86. Subramanian A, et al. (2005) Gene set enrichment analysis: a knowledge-based approach for interpreting genome-wide expression profiles. *Proc Natl Acad Sci U S A* 102:15545-15550.

87. Eden E, Navon R, Steinfeld I, Lipson D, Yakhini Z (2009) GOrilla: a tool for discovery and visualization of enriched GO terms in ranked gene lists. *BMC Bioinformatics* 10:48.

88. Helmy K, et al. (2012) Identification of global alteration of translational regulation in glioma in vivo. *PLoS One* 7:e46965.

89. Le Quesne JP, Spriggs KA, Bushell M, Willis AE (2010) Dysregulation of protein synthesis and disease. *J Pathol* 220:140-151.

90. Rajasekhar VK, Holland EC (2004) Postgenomic global analysis of translational control induced by oncogenic signaling. *Oncogene* 23:3248-3264.

91. Holland EC, Sonenberg N, Pandolfi PP, Thomas G (2004) Signaling control of mRNA translation in cancer pathogenesis. *Oncogene* 23:3138-3144.

92. Rajasekhar VK, et al. (2003) Oncogenic Ras and Akt signaling contribute to glioblastoma formation by differential recruitment of existing mRNAs to polysomes. *Mol Cell* 12:889-901.

93. Balagopal V, Parker R (2009) Polysomes, P bodies and stress granules: states and fates of eukaryotic mRNAs. *Curr Opin Cell Biol* 21:403-408.

94. Melamed D, Eliyahu E, Arava Y (2009) Exploring translation regulation by global analysis of ribosomal association. *Methods* 48:301-305.

95. Jones RG, Thompson CB (2009) Tumor suppressors and cell metabolism: a recipe for cancer growth. *Genes Dev* 23:537-548.

96. Kaelin WG, Jr., Thompson CB (2010) Q&A: Cancer: clues from cell metabolism. *Nature* 465:562-564.

97. Plas DR, Thompson CB (2005) Akt-dependent transformation: there is more to growth than just surviving. *Oncogene* 24:7435-7442.

98. Dai C, et al. (2001) PDGF autocrine stimulation dedifferentiates cultured astrocytes and induces oligodendrogliomas and oligoastrocytomas from neural progenitors and astrocytes in vivo. *Genes Dev* 15:1913-1925.

99. Dai C, et al. (2005) The characteristics of astrocytomas and oligodendrogliomas are caused by two distinct and interchangeable signaling formats. *Neoplasia* 7:397-406.

100. Lei L, et al. (Glioblastoma models reveal the connection between adult glial progenitors and the proneural phenotype. *PLoS One* 6:e20041.

101. Ng K, Pullirsch D, Leeb M, Wutz A (2007) Xist and the order of silencing. *EMBO Rep* 8:34-39.

102. Ashburner M, et al. (2000) Gene ontology: tool for the unification of biology. The Gene Ontology Consortium. *Nat Genet* 25:25-29.

103. Ingolia NT, Ghaemmaghami S, Newman JR, Weissman JS (2009) Genome-wide analysis in vivo of translation with nucleotide resolution using ribosome profiling. *Science* 324:218-223.

104. Appolloni I, et al. (2009) PDGF-B induces a homogeneous class of oligodendrogliomas from embryonic neural progenitors. *Int J Cancer* 124:2251-2259.

105. Rivers LE, et al. (2008) PDGFRA/NG2 glia generate myelinating oligodendrocytes and piriform projection neurons in adult mice. *Nat Neurosci* 11:1392-1401.

106. Guo F, Ma J, McCauley E, Bannerman P, Pleasure D (2009) Early postnatal proteolipid promoter-expressing progenitors produce multilineage cells in vivo. *J Neurosci* 29:7256-7270.

107. Vivanco I, Sawyers CL (2002) The phosphatidylinositol 3-Kinase AKT pathway in human cancer. *Nat Rev Cancer* 2:489-501.

108. Ma XM, Blenis J (2009) Molecular mechanisms of mTOR-mediated translational control. *Nat Rev Mol Cell Biol* 10:307-318.

109. Huse JT, et al. (2009) The PTEN-regulating microRNA miR-26a is amplified in high-grade glioma and facilitates gliomagenesis in vivo. *Genes Dev* 23:1327-1337.

110. Weber GL, Parat MO, Binder ZA, Gallia GL, Riggins GJ (Abrogation of PIK3CA or PIK3R1 reduces proliferation, migration, and invasion in glioblastoma multiforme cells. *Oncotarget* 2:833-849.

111. Vander Heiden MG, Cantley LC, Thompson CB (2009) Understanding the Warburg effect: the metabolic requirements of cell proliferation. *Science* 324:1029-1033.

112. Zid BM, et al. (2009) 4E-BP extends lifespan upon dietary restriction by enhancing mitochondrial activity in Drosophila. *Cell* 139:149-160.

113. Zoncu R, Efeyan A, Sabatini DM (2011) mTOR: from growth signal integration to cancer, diabetes and ageing. *Nat Rev Mol Cell Biol* 12:21-35.

114. Fuster MM, Esko JD (2005) The sweet and sour of cancer: glycans as novel therapeutic targets. *Nat Rev Cancer* 5:526-542.

115. Yuan K, et al. (2008) Alterations in human breast cancer adhesion-motility in response to changes in cell surface glycoproteins displaying alpha-L-fucose moieties. *Int J Oncol* 32:797-807.

116. Hakomori S (1996) Tumor malignancy defined by aberrant glycosylation and sphingo(glyco)lipid metabolism. *Cancer Res* 56:5309-5318.

117. Pochec E, Litynska A, Amoresano A, Casbarra A (2003) Glycosylation profile of integrin alpha 3 beta 1 changes with melanoma progression. *Biochim Biophys Acta* 1643:113-123.

118. Spriggs KA, Bushell M, Willis AE (2010) Translational regulation of gene expression during conditions of cell stress. *Mol Cell* 40:228-237.

119. Lee SW, et al. (1999) Patterns of failure following high-dose 3-D conformal radiotherapy for high-grade astrocytomas: a quantitative dosimetric study. *Int J Radiat Oncol Biol Phys* 43:79-88.

120. Chan JL, et al. (2002) Survival and failure patterns of high-grade gliomas after three-dimensional conformal radiotherapy. *J Clin Oncol* 20:1635-1642.

121. Davis LW (1989) Malignant glioma--a nemesis which requires clinical and basic investigation in radiation oncology. *Int J Radiat Oncol Biol Phys* 16:1355-1365.

122. Amberger-Murphy V (2009) Hypoxia helps glioma to fight therapy. *Curr Cancer Drug Targets* 9:381-390.

123. Barcellos-Hoff MH, Newcomb EW, Zagzag D, Narayana A (2009) Therapeutic targets in malignant glioblastoma microenvironment. *Semin Radiat Oncol* 19:163-170.

124. Bao S, et al. (2006) Glioma stem cells promote radioresistance by preferential activation of the DNA damage response. *Nature* 444:756-760.

125. Braunstein S, Badura ML, Xi Q, Formenti SC, Schneider RJ (2009) Regulation of protein synthesis by ionizing radiation. *Mol Cell Biol* 29:5645-5656.

126. Powley IR, et al. (2009) Translational reprogramming following UVB irradiation is mediated by DNA-PKcs and allows selective recruitment to the polysomes of mRNAs encoding DNA repair enzymes. *Genes Dev* 23:1207-1220.

127. Dougherty JD, et al. (2012) Candidate pathways for promoting differentiation or quiescence of oligodendrocyte progenitor-like cells in glioma. *Cancer Res* 72:4856-4868.

128. Dornan D, et al. (2004) Interferon regulatory factor 1 binding to p300 stimulates DNA-dependent acetylation of p53. *Mol Cell Biol* 24:10083-10098.

129. Cerami E, et al. (2012) The cBio cancer genomics portal: an open platform for exploring multidimensional cancer genomics data. *Cancer Discov* 2:401-404.

130. Carro MS, et al. (2010) The transcriptional network for mesenchymal transformation of brain tumours. *Nature* 463:318-325.

131. Hirai H, Karian P, Kikyo N (2011) Regulation of embryonic stem cell self-renewal and pluripotency by leukaemia inhibitory factor. *Biochem J* 438:11-23.

132. Demoulin JB, Renauld JC (1998) Signalling by cytokines interacting with the interleukin-2 receptor gamma chain. *Cytokines Cell Mol Ther* 4:243-256.

133. Jain RK (2005) Normalization of tumor vasculature: an emerging concept in antiangiogenic therapy. *Science* 307:58-62.

134. Straume O, et al. (2002) Prognostic Importance of Glomeruloid Microvascular Proliferation Indicates an Aggressive Angiogenic Phenotype in Human Cancers. *Cancer Research* 62:6808-6811.

135. Peddinti R, et al. (2007) Prominent Microvascular Proliferation in Clinically Aggressive Neuroblastoma. *Clinical Cancer Research* 13:3499-3506.

136. Routray C, et al. (2011) Protein kinase G signaling disrupts Rac1-dependent focal adhesion assembly in liver specific pericytes. *American Journal of Physiology - Cell Physiolog* 301:C66-C74.

137. Clement V, Sanchez P, de Tribolet N, Radovanovic I, Ruiz i Altaba A (2007) HEDGEHOG-GLI1 signaling regulates human glioma growth, cancer stem cell self-renewal, and tumorigenicity. *Curr Biol* 17:165-172.

138. De Palma M, et al. (2005) Tie2 identifies a hematopoietic lineage of proangiogenic monocytes required for tumor vessel formation and a mesenchymal population of pericyte progenitors. *Cancer Cell* 8:211-226.

139. Gory S, et al. (1999) The vascular endothelial-cadherin promoter directs endothelial-specific expression in transgenic mice. *Blood* 93:184-192.

140. Hisatsune H, et al. (2005) High level of endothelial cell-specific gene expression by a combination of the 5' flanking region and the 5' half of the first intron of the VE-cadherin gene. *Blood* 105:4657-4663.

141. Mack CP, Owens GK (1999) Regulation of smooth muscle alpha-actin expression in vivo is dependent on CArG elements within the 5' and first intron promoter regions. *Circ Res* 84:852-861.

142. Gan Q, Yoshida T, Li J, Owens GK (2007) Smooth muscle cells and myofibroblasts use distinct transcriptional mechanisms for smooth muscle alpha-actin expression. *Circ Res* 101:883-892.

143. Brenner M, Kisseberth WC, Su Y, Besnard F, Messing A (1994) GFAP promoter directs astrocyte-specific expression in transgenic mice. *J Neurosci* 14:1030-1037.

144. Zhuo L, et al. (1997) Live Astrocytes Visualized by Green Fluorescent Protein in Transgenic Mice. *Developmental Biology* 187:36-42.

145. Holland EC, Varmus HE (1998) Basic fibroblast growth factor induces cell migration and proliferation after glia-specific gene transfer in mice. *Proc Natl Acad Sci U S A* 95:1218-1223.

146. Sarthy V, Hoshi H, Mills S, Dudley VJ (2007) Characterization of green fluorescent protein-expressing retinal cells in CD 44-transgenic mice. *Neuroscience* 144:1087-1093.

147. Dziennis S, et al. (1995) The CD11b promoter directs high-level expression of reporter genes in macrophages in transgenic mice. *Blood* 85:319-329.
148. Cailhier JF, et al. (2005) Conditional macrophage ablation demonstrates that resident macrophages initiate acute peritoneal inflammation. *J Immunol* 174:2336-2342.
149. Ferron M, Vacher J (2005) Targeted expression of Cre recombinase in macrophages and osteoclasts in transgenic mice. *Genesis* 41:138-145.
150. Gowing G, Vallieres L, Julien JP (2006) Mouse model for ablation of proliferating microglia in acute CNS injuries. *Glia* 53:331-337.
151. Cahoy JD, et al. (2008) A Transcriptome Database for Astrocytes, Neurons, and Oligodendrocytes: A New Resource for Understanding Brain Development and Function. *The Journal of Neuroscience* 28:264-278.
152. del Prete MJ, Vernal R, Dolznig H, Mullner EW, Garcia-Sanz JA (2007) Isolation of polysome-bound mRNA from solid tissues amenable for RT-PCR and profiling experiments. *RNA* 13:414-421.
153. Smirnova JB, et al. (2005) Global gene expression profiling reveals widespread yet distinctive translational responses to different eukaryotic translation initiation factor 2B-targeting stress pathways. *Mol Cell Biol* 25:9340-9349.
154. Fringer JM, Acker MG, Fekete CA, Lorsch JR, Dever TE (2007) Coupled release of eukaryotic translation initiation factors 5B and 1A from 80S ribosomes following subunit joining. *Mol Cell Biol* 27:2384-2397.
155. Ashe MP, Slaven JW, De Long SK, Ibrahimo S, Sachs AB (2001) A novel eIF2B-dependent mechanism of translational control in yeast as a response to fusel alcohols. *EMBO J* 20:6464-6474.
156. Ingolia NT, Ghaemmaghami S, Newman JRS, Weissman JS (2009) Genome-Wide Analysis in Vivo of Translation with Nucleotide Resolution Using Ribosome Profiling. *Science* 324:218-223.
157. Hsieh AC, et al. (2012) The translational landscape of mTOR signalling steers cancer initiation and metastasis. *Nature* 485:55-61.